LARGE AXISYMMETRIC DEFORMATION OF THIN SHELLS OF REVOLUTION

by

G. Wayne Brodland

A Thesis

Submitted to the Faculty of Graduate Studies

in Partial Fulfillment of the Requirements for the Degree

of Doctor of Philosophy

The University of Manitoba

Department of Civil Engineering

Winnipeg, Manitoba

November, 1985

LARGE AXISYMMETRIC DEFORMATION OF THIN SHELLS OF REVOLUTION

BY

G. WAYNE BRODLAND

A thesis submitted to the Faculty of Graduate Studies of
the University of Manitoba in partial fulfillment of the requirements
of the degree of

DOCTOR OF PHILOSOPHY

ABSTRACT

A survey of the literature associated with the title problem indicates a considerable dearth of solution techniques for severely deformed axisymmetric shells of arbitrary shape. An efficient, numerical, energy minimization scheme which permits unlimited meridian displacement and rotation and essentially unlimited middle surface extension, is presented. Homogeneous, isotropic, incompressible materials satisfying the nonlinear Mooney-Rivlin constitutive law are assumed. Analytical expressions for the strain field and total strain energy through the thickness of the shell are derived. The strain energy of each element is determined by integrating the above analytical expression over the surface of the element using Gaussian quadrature. Local potential energy minima represent solutions, and are found using a sequential descent method which utilizes the gradient and Hessian of the energy hypersurface, and which incorporates a line search technique to accelerate convergence. Displacements and stresses within $\frac{1}{2}\%$ and 2% respectively, of comparable linear and nonlinear analytical solutions are often possible using as few as 8 elements.

The method is then used to do an extensive analysis of uniformly loaded circular plates, point loaded spherical caps and edge loaded cylinders. Interesting and previously unpublished phenomena are identified in each of these problems as a result of studying the effect of each of their dimensionless parameters. The analysis showed for example, that the behavior of plates depends on the actual thickness to radius ratio even for plates which have classically been called thin. Since this ratio does not appear in any of the analytical solutions, its

effect must be determined numerically. The snapping of a spherical cap as it is everted and again as it is returned to its initial configuration is studied. It is shown that some of the meridian contours produced by eversion are different from those produced on the return to the initial configuration. An experimental demonstration done to verify the numerical results is included. The domains of long, intermediate and short cylinder behavior both for linear and nonlinear deflections are identified.

DEDICATION

"Dem hochsten Gott allein zu Ehren,

Dem Nechsten, draus sich zu belehren".

J.S. Bach, Orgelbuchlein, 1723.

(To the honor of the Supreme God alone,

For the instruction of my neighbor.)

ACKNOWLEDGEMENTS

The author wishes to thank Dr. Harley Cohen for suggesting the research topic, and for his timely comments and suggestions during the course of the work. Thanks are also due to my wife, Heather, for tolerating the long and sometimes irregular hours it was necessary for the author to put in, and to my brother, Dale, for help with many details. The careful typing of text and equations by Mrs. Valerie Ring is sincerely appreciated. Finally, the author wishes to acknowledge the support of NSERC during the first two years of this research, and of the University of Manitoba during the final year.

TABLE OF CONTENTS

LIST OF FIGURES

NOMENCLATURE

Below is a list of the principal symbols used in this thesis. In order to use those symbols which are conventional in each of the several fields upon which this work draws, it has been necessary to use certain symbols to represent two or more unrelated quantities. All symbols are defined as they arise in the text, and confusion as to the intended meaning of any particular symbol is unlikely.

Corresponding upper and lower case letters are used to denote quantities in the undeformed and deformed configurations, respectively. Vectors, matrices and tensors are represented by bold-face symbols.

Operators and Special Symbols:

$\simeq$	Approximately equal
$\approx$	Proportional
$\equiv$	Identically equal
$\lvert \cdot \rvert$	Absolute value of a scalar, or determinant of a matrix
$\lVert \cdot \rVert$	A suitable norm
δ	Variation of a quantity
$A \subset B$	A is a subset of B
$A \rightarrow B$	A approaches B
$A \Rightarrow B$	A implies B
$\cdot$	Dot product of vectors
x	Cross product of vectors
$\mathbf{Q}^{-1}$	Inverse of matrix $\mathbf{Q}$
$\mathbf{Q}^{T}$	Transpose of matrix $\mathbf{Q}$
∇^2	Laplacian operator
$X=[a,b]$	Represents the closed interval $a \leq X \leq b$

/ Division. All quantities to the left of the symbol are in the numerator and those on its right are in the denominator, thus $qa^4/Dh \equiv \frac{qa^4}{Dh}$

Indices:

The index denoted below by i may, in general, qualify the quantity of which it is a subscript as being in the:

1 - meridial direction,

2 - parallel direction,

r - radial direction, or

θ - hoop direction.

Nomenclature:

a — a characterisitic dimension giving the intial
- radius of a circular plate
- radius of curvature of a spherical cap
- radius of a cylindrical shell

C_1, C_2 — Mooney-Rivlin material constants

C — Right Cauchy-Green deformation tensor

D — flexural stiffness of a plate or shell $= \frac{Eh^3}{12(1-\nu^2)}$

e — Napier's constant, approximately equal to 2.7183

E — Young's modulus

E, E_{jk} — Lagrangian finite-strain tensor

F — deformation gradient tensor

G — material shear modulus

h — shell or plate initial thickness

I_1, I_2, I_3 — strain invariants

K_i principal radii of shell middle surface in initial state

k_i principal radii of shell middle surface in current (deformed) state

ℓ a characteristic dimension giving the

- deformed length of a finite element
- initial length of a cylindrical shell

M applied moment load

M_i bending stress resultant

N_i membrane stress resultant

N,n local coordinate normal to middle surface

Q applied shear load

Q_i shear stress resultant

q magnitude of distributed load

r radial coordinate of polar or cylindrical coordinate system

S,s parameterization of meridian

T undeformed shell thickness

$\mathbf{T},T_{jk}$ second Piola-Kirchoff stress tensor

$\bar{U}$ total potential energy

u radial component of displacement

v transverse component of displacement

w axial component of displacement

$w(),w'(),w''()$: strain per unit volume

W strain energy per unit of middle surface area

$\bar{W}$ total strain energy of a shell or segment thereof

$\mathbf{X},X_j$ generalized coordinates

z axial coordinate of cylindrical coordinate system

ε_i strain component in the i- direction

θ transverse coordinate of polar or cylindrical coordinate system

λ a characteristic quantity given by

$$\lambda = [12(1-\nu^2)]^{\frac{1}{4}}\sqrt{\frac{a}{h}}\sin\xi_o \quad \text{for a spherical cap, and by}$$

$$\lambda = \left(\frac{3(1-\nu^2)}{a^2h^2}\right)^{1/4} \quad \text{for a cylinder}$$

λ_i principal extensions of shell middle surface

ν Poisson's ratio

π constant, approximately equal to 3.1416

σ stress

σ^m membrane stress

σ^b bending stress

CHAPTER 1

INTRODUCTION

1.1 PROLOGUE

Research in solid mechanics can be grouped into three main classifications: experimental, analytical and numerical. Work in each of these areas compliments research in the other two. Experimental work frequently provides an understanding of the fundamental behavior of a body and often suggests a basis upon which an analytical model can be built. Analytical research, on the other hand, varies from highly theoretical research concerned with existence and uniqueness of solutions [2,85] to calculation of solutions to specific problems [5,7,9 et cetera]. While analytical solutions often provide the best overall understanding of a problem, they are generally possible only for relatively simple geometries and material responses. Numerical solution techniques, which have become important in the last few decades, permit solution of problems with highly complex geometries and material responses. However, numerical solutions, like experimental results, do not give direct evidence of the parameters governing the problem, nor of their effect.

The research presented here includes a new numerical method allowing large strains, displacements and rotations for analysis of thin axisymmetric shells, and an in-depth analysis of uniformly loaded plates, point loaded spherical caps and edge loaded cylinders. Significant and previously unpublished phenomena are identified in each of these problems. A simple experimental demonstration of the bi-directional snapping of a spherical cap is also included, as the numerical results obtained here are significantly different from previously published experimental [18], analytical [5,9 et cetera] and numerical [47] research.

The mechanical behavior of a solid body is governed by the properties of its material as embodied in constitutive equations, equations describing local translational and rotational equilibrium, and equations which ensure the compatibility of the strain and displacement fields. Finding its response to applied load requires simultaneous solution of the above differential equations, either directly or by finding extrema of an objective functional, such as total potential energy, which embodies the separate equations.

These equations can be simplified considerably from their general form since we limit our attention to homogeneous isotropic materials - that is materials whose properties do not vary from place to place within the body, and whose properties are independent of the orientation of the material. Metals and many polymers such as rubber are modelled well under these assumptions. We also assume that the material is incompressible, as rubber and natural biological materials are. Exact numerical solutions to these equations are in general very difficult to find. Nonlinear solutions are known, however, for cases of homogeneous strain (see for example [26, Chapter 2]), and linear solutions for linear homogeneous isotropic materials are known for bodies bounded on all sides by suitable coordinate surfaces. Linear solutions often take the form of triple summations of Sturm-Liouville series whose constants are determined by integration. Few other exact solutions exist.

Very good approximate solutions can be found easily for certain classes of three-dimensional bodies. These solutions are possible because all material in the body is close to a simple generator, such as a line or surface. The strain field over the entire body can then be expressed quite accurately in terms of the strain of this generator, by using suitable assumptions. (For example, it is often assumed that fibers initially normal to the generator remain normal to it during deformation). The local rigidity of the body can be expressed in terms of the generator and

consequently the generator can be endowed with the physical properties of the body. The original problem is thus reduced in complexity and sometimes also in dimension. A wide variety of particular approaches exist for this simplification. (See for example, References [12,14,52,53,69 and 72]).

The first class of three-dimensional bodies which are easily simplified, is rods. They may be thought of as the physical realization of a mathematical curve. The only restrictions on the cross-section of the realization are that its centroid lie on the generating curve, that its dimensions be small compared with the local curvature of the generating curve, and that its cross-section not vary too quickly along the length of the generator. Beams, columns and arches are the most common types of rods. When the cross-section is very small, bending stress resultants, which vary roughly as the square of the area, become insignificant compared with the axial resultant, which varies linearly with the area. Cables and chains are structures of this type.

The classes of three-dimensional bodies which are of particular interest here, are plates and shells; which are physical realizations of planes and surfaces, respectively. Here, the generating or middle surface is realized by introduction of material to an equal distance from each of its sides. (Note that in general this is not quite the same as introduction of an equal volume of material on each side). Mild restrictions apply to the shell thickness and its variation over the surface. Important shell structures include curved concrete roofs; boat hulls; most sheet metal automotive components, including many body parts; submarine hulls; igloos; and the petals of most flowers. When the thickness of these structures is very small, bending resultants which vary as the thickness cubed, become negligible compared with membrane resultants which vary linearly with thickness. Such structures are known as membranes and the in-plane tensile resultants and stresses are known, respectively, as membrane resultants and membrane stresses.

Automotive door skins, aircraft coverings and inflatable structures are common examples of membrane structures. It is often possible for purposes of stress and deflection analysis to treat shells as if they were membranes, by neglecting bending stresses and resultants. This common approach gives rise to the so-called membrane theory of shells.

A truss is almost always much stronger and more rigid than an equally well designed beam of similar weight and span, because of its shape. It is deeper in the direction of the applied load, and load is carried largely by tensile stresses, rather than being carried exclusively by relatively inefficient bending stresses. It is the curved shape of shell structures which enables them to utilize relatively efficient membrane effects and thereby provides their exceptional strength and rigidity compared to flat plates which like beams can only utilize bending mechanisms.

This shape effect can be dramatically illustrated by comparing the rigidity of a small flat piece of heavy tinfoil or paper when transversely loaded, with a similar one which has been slightly crumpled up and then almost straightened out. The crumpled sheet is a very poor shell design, but even so, is generally much more rigid and less highly stressed than the flat sheet for a given load. In the crumpled sheet, the load is carried largely by highly efficient membrane mechanisms which are not found in flat plates.

Shells are further classified as either thin, if the minimum local radius of curvature is at least ten times the local thickness; or thick, if it is not. Thin shells are of greater practical importance because of their frequent use. Fortunately, they are also more easily analysed than thick shells, as certain second order effects which are important in thick shells, can be neglected. We restrict further attention to thin shells, but note here that many thin shell results hold at least approximately for thick shells.

One further criterion is usually used to classify shells for analysis. If significant deflection is confined to a region of the shell whose height with respect to a reference plane, is everywhere less than about six times the smallest base dimension of this region, it is classed as a shallow shell. Many shells, such as those typically used for roofs of buildings, satisfy this criteria. Linear analysis of shells in this class is greatly simplified, as the thirteen governing differential equations given in Section 2.4, can be combined to yield two simultaneous fourth-order differential equations [20, Chapter 7] similar to the von Karman equations given in Section 4.2. Shells which are not shallow are called deep and must usually be analyzed numerically. The behavior of such shells however, is often governed by a small shallow region near the load application point which is described adequately by the shallow shell equations.

That the deflection of thin beams is primarily due to bending strains rather than shearing strains, was recognized and applied by Navier, Bernoulli and Euler. It was Kirchoff however, who made the important realization in 1850 during his study of thin plates that fibers normal to the middle surface remain approximately straight, unchanged in length and normal to it after deformation, and for purposes of analysis may be assumed to possess these three properties. This in turn provided a justification for the Bernoulli-Euler equation of beam bending. In 1888 Love applied these three assumptions to thin shells. Collectively, the three assumptions are known as the Kirchoff-Love hypothesis. They are generally only valid when the body is thin - that is when its thickness is small compared both with its local radius of curvature and its overall dimensions.

The assumption that fibers initially normal to the middle surface remain straight and normal to it is the fundamental assumption which makes shell and plate analysis tractable. Under this assumption, the local strain state through the thickness of the plate is completely governed by the local deformation of

the middle surface. This assumption of fiber normality precludes the possibility of shear strain. Without this assumption, or perhaps some less restrictive assumption providing a suitable local shear strain measure, the analysis of plates based on the response of the middle surface would not be practical. Figure 1.1(a) shows normal fibers on an undeformed beam, while Figures 1.1(b) and (c) show deformations possible naturally and under the Kirchoff-Love hypothesis, respectively. The assumption of fiber normality suppresses the shear strain field, which would otherwise co-exist with extensional and bending strains. Consequently, shear stresses between imaginary layers parallel to the middle surface are also neglected. Since transverse deflections due to bending far exceed those due to shearing when the dimensions of the plate are large compared with its thickness, the so-called Kirchoff-Love hypothesis is justified.

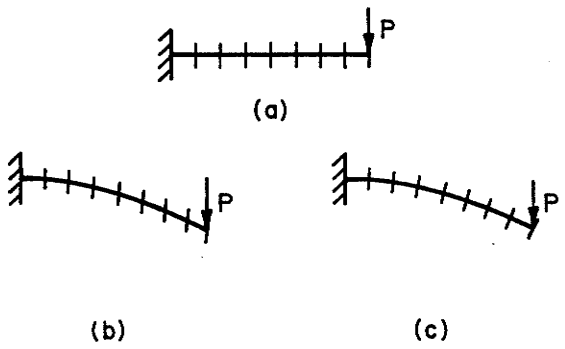

Figure 1.1 The Kirchoff-Love Hypothesis

The Kirchoff-Love hypothesis also includes the concept that stresses and strains normal to the middle surface are negligible. Hence, normal fibers do not change length. When the assumption of normal fiber inextensibility is not made, a relaxed Kirchoff-Love hypothesis is said to be in effect. The relaxed hypothesis

must be used when membrane strains are large and resulting normal strains are no longer negligible. When thick plates are analyzed or when deflections are large, more complex shell theories which incorporate additional strain measures may be required.

A number of phenomena which are not important or do not occur when deflections are small and linear are important when deflections are large or nonlinear. The most important of these are discussed briefly here.

Consider the symmetrically loaded arch shown in Figure 1.2(a). When strains and deflections are sufficiently small that load and deflection are linearly related, the deflection will be symmetrical. This is a well known engineering principle. It is less well known [76] that even if the load and apex of the shell are horizontally restrained, the arch may deform asymmetrically as shown in Figure 1.2(c), rather than deforming symmetrically, as shown in Figure 1.2(b). This phenomenon is due to geometric and/or material nonlinearities which will be discussed forthwith. A full set of symmetric deformation states exist for any given load. As indicated in Thompson and Hunt [76] the symmetric equilibrium states are, in general, stable only over a certain range of load and deflection. Beyond this range, the symmetric

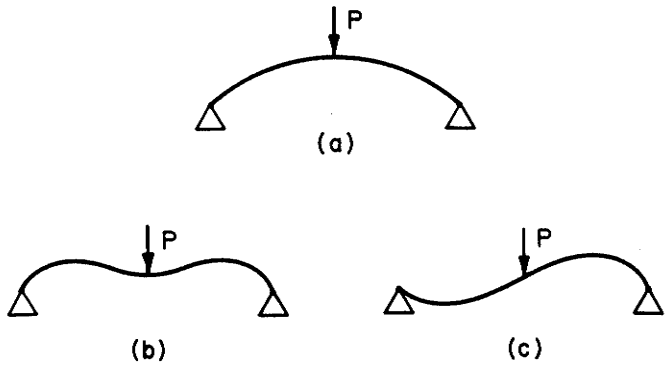

Figure 1.2 Symmetrically Loaded Arch

states do not occur naturally, as asymmetric states of lower energy are easily reached and hence are preferred. The transition from symmetric to asymmetric deformation is in general highly sensitive to imperfections in the arch or body under considerations. From this simple example, it is clear that symmetrical initial geometry and symmetrical loading are not sufficient to ensure that the deformed state is symmetric when nonlinear effects are present. Solutions found under the assumption of symmetry may or may not be stable. Hence, care must be taken to limit the range of load and deformation allowed, or to consider inherently stable geometries such as shown in Figure 1.3 below.

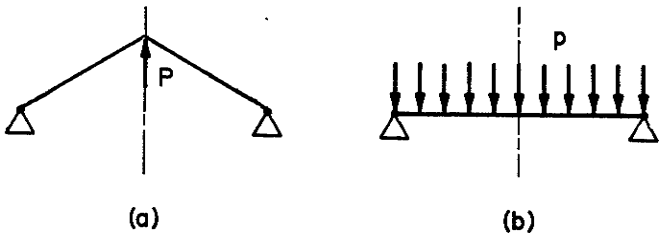

Figure 1.3 Stable Geometries

Most nonlinear behavior in shells is caused by nonlinear material response and by geometric nonlinearities resulting from the structure changing shape as it is loaded. See Ashwell [6] for a discussion of these, as well as other types of nonlinearity. When the stress-strain relations of an elastic material are not adequately described by Hooke's Law, the material response is said to be nonlinear. These so-called material nonlinearities are typically associated with large strain. Steel and wood, for example, obey Hooke's Law for small strains, while concrete and polymers do not. A good body of theory exists to deal with nonlinear constitutive relations, [40]. However, analytical solutions for structures made

of nonlinear materials exist only for simple geometries with homogeneous strain such as uniaxially loaded bars, and for simple nonlinear constitutive relations - bending of beams. Problems which include material nonlinearities must normally be solved numerically. Traditionally, nonlinear behavior in engineering structures has been the result of material nonlinearities.

Geometric nonlinearities are becoming increasingly important as very flexible and highly deformed components and structures are finding greater use. The common engineering assumption that deflections are infinitesimal and that no shape change occurs cannot be used. Geometric nonlinearities, which result from a body changing shape under load, become important.

Note, that it is entirely possible for significant changes in shape to occur while strains are very small. An example of this is a thin cantilever beam, or elastica as shown in Figure 1.4(a), subjected to an end moment. For small moments, the transverse end deflection δ is linearly related to the applied moment M by the relationship

$$\delta = \frac{ML^2}{zEI} \tag{1.1}$$

governing a cantilever beam with an end moment, where L is the elastica length, and EI is its bending rigidity. As a result of the applied moment, the elastica will have a uniform curvature of radius

$$r_c = \frac{EI}{M} \tag{1.2}$$

When deflections are large, the exact relationship

$$\delta = \frac{EI}{M}\left(1 - \cos\frac{ML}{EI}\right) \tag{1.3}$$

must be used. The beam equation (1.1) is a special case of this more general equation. Clearly the end displacement is nonlinearly related to the applied load. However, the strain ε, at any point on the hoop is given by

$$\varepsilon = \frac{Mz}{EI} \tag{1.4}$$

where z is the distance of the point from the neutral axis of the elastica. This strain can be made small enough that Hooke's Law applies by making the elastica sufficiently thin - while keeping (EI) constant - that z is sufficiently small.

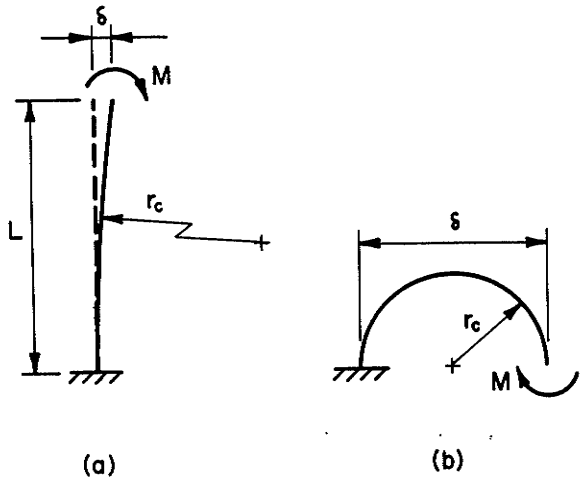

Figure 1.4 Flexible Cantilever

Geometries such as the cantilever elastica and transversely loaded plate, which give rise to bending, tend to exhibit geometrically linear behavior for small loads. Structures need not, however, exhibit an initially linear response. Consider the hinged strut shown in Figure 1.5. Its center deflection δ, is related to the load P, by [22, p. 3; 83, pp. 81,82]

$$\delta = \frac{L}{2}\left(\frac{P}{AE}\right)^{1/3} \tag{1.5}$$

where L is the total strut length,

A is the strut cross-sectional area, and

E is its Young's modulus.

Like Hencky's solution [30] for a circular membrane with a uniform transverse

load, discussed in Section 4.3, the strut does not exhibit even initially linear behavior.

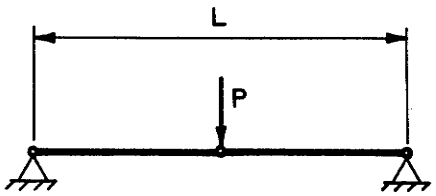

Figure 1.5 Hinged Strut

Geometric nonlinearity can induce coupling effects as seen in a significantly deflected beam subjected to both transverse loads and axial end load, such as shown in Figure 1.6. If the end loads are tensile, the transverse beam deflections will be reduced by the end loads tending to pull the beam straight. Similar coupling effects occur in shells, and in plates as shown by the von Karman equations (4.37 and 4.40-4.44) discussed in Section 4.2.

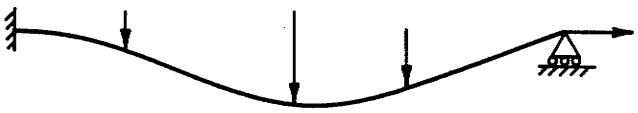

Figure 1.6 Axially Loaded Beam

A number of interesting stability problems arise because of geometric nonlinearity. These are problems for which multiple solutions exist for a particular load, and problems in which large changes in the solution occur for small changes in the load. Both of these effects can be observed in the inextensible, axially loaded column shown in Figure 1.7.

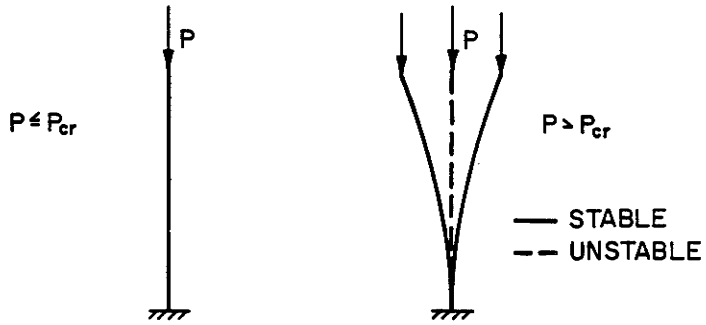

Figure 1.7 Cantilever Column

The maximum load P_{cr}, that a column of length L can support according to the linear analysis of Euler is

$$P_{cr} = \frac{\pi^2 EI}{4L^2} \tag{1.6}$$

For loads less than P_{cr}, the column remains straight. Loads even slightly greater than P_{cr} produce deflections which cannot be determined using linear theory, as the linear analysis considers only small transverse deflections and completely ignores vertical deflections. The deflection of the column for loads even slightly in excess of P_{cr} can only be predicted when a second order analysis accommodating large transverse deflections as well vertical deflections is used. Such an analysis [78,p.2] shows that two stable solutions which are mirror images of each other exist. The governing equations are also satisfied by zero deflection, but this solution is called an unstable equilibrium as any perturbation to it causes the column to move to one of the two stable states. The axially loaded column exhibits both multiple solutions for a given load and solutions significantly different for slight changes in load.

Changes in geometry can also cause significant changes in follower loads.

This effect is clearly seen in a circular membrane subjected to pressure loading such as shown in Figure 1.8.. Not only does the direction of the load at any point change as the membrane deforms, but its total magnitude increases with the increasing area of the membrane. It is this same effect in conjunction with the nonlinear behavior of rubber which causes a cylindrical balloon to exhibit two discrete diameters as it is inflated.

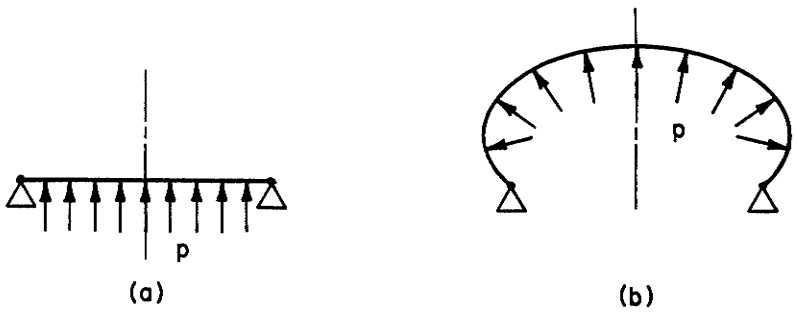

Figure 1.8 Circular Membrane With Pressure Loading

Analytical solutions to various geometrically nonlinear problems with linear material behavior abound. Only a few analytical solutions exist for problems incorporating both geometric and material nonlinearities. For example, solutions exist for the inflation of spherical [27] and cylindrical [88, Section 5.2.2(ii)] balloons.

In a geometrically and materially linear problem, proportionality ($\approx$) exists between

$$\text{load} \approx \text{stress} \approx \text{strain} \approx \text{deflection}.$$

In a materially nonlinear problem, the stress-strain relationship becomes nonlinear. Load-stress and strain-deflection relationships may however, still be linear. Typically, both load-stress and strain-deflection relationships become nonlinear in a geometrically nonlinear problem, even though stress and strain may be linearly related. In a problem which is both geometrically and materially nonlinear, none

of load, stress, strain or deflection may be linearly related to any of the others.

1.2 PROBLEM STATEMENT AND MAIN RESULTS

Though many numerical schemes exist for analysis of shells, it was clear that a more efficient scheme for analysis of highly nonlinear shells was possible. There is at present a particular dearth of programs for analysis of shells having large membrane strains and for shells undergoing significant geometric changes. A new method for the analysis of axisymmetric shells is presented herein. It is carefully designed to accommodate virtually unlimited membrane strains and unlimited middle surface displacements and rotations. Since a relaxed Kirchoff hypothesis is used, together with assumed volume constancy to establish the strain field through the shell thickness from the middle surface deformation, the analysis is accurate only for thin shells. Hyperelastic materials are assumed, to make problem solution using energy techniques possible. For simplicity, the material is also assumed to be homogeneous and isotropic. The method is illustrated for a general Mooney-Rivlin material. In order to maximize computational efficiency, a closed form analytical expression for energy per unit of undeformed middle surface is derived.

The shell meridian is broken into a series of discrete elements and the strain energy within each element is calculated using Gaussian quadrature to integrate the closed form energy expression over the area of the element. The total strain energy and hence the total potential energy of the shell are then calculated in terms of the positions of the element nodes. Problem solutions are determined by finding the nodal positions which, at least locally, minimize the total potential energy. Positions of minimum energy are found using a sequential descent method which utilizes the gradient and Hessian of the energy hypersurface, and which incorporates a line search technique to accelerate convergence. The numerical

scheme is then used to study three problems - uniformly loaded circular plates, point loaded spherical caps and edge loaded cylinders - which collectively cover the full spectrum of problems shown in Figure 1.9, and which are important specializations of the general nonlinear shell problem. The reader is referred to Chapters 4 to 6 for explanations of the justification for each specialization.

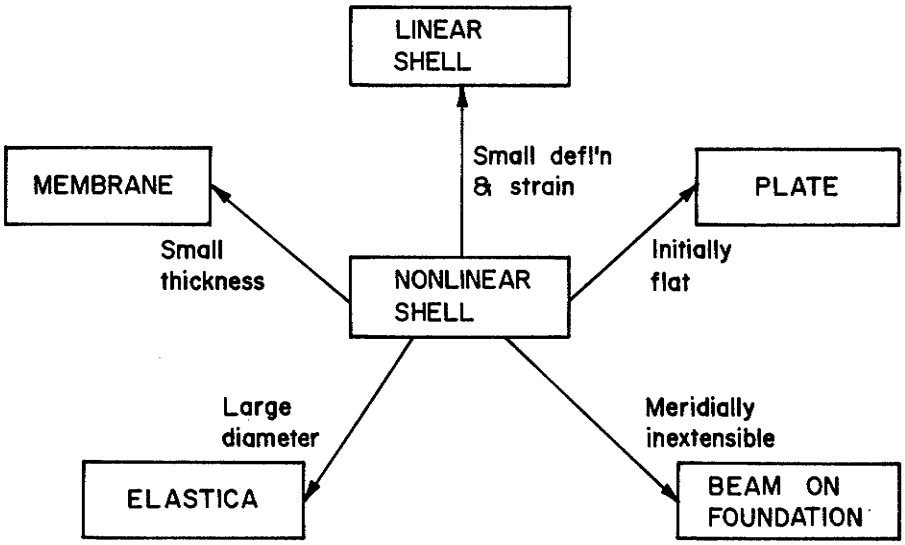

Figure 1.9 Special Nonlinear Shells

The problem considered in Chapter 4 is the uniformly loaded circular plate. Many approximate nonlinear analytical solutions to this problem exist [7,25,87, et cetera] and provide useful comparisons for numerically calculated stresses, strains and deflections. For large deflections produced by correspondingly large loads, the circular plate behaves essentially like a circular membrane for which an analytical solution [30] also exists. This problem served also to ascertain the accuracy of the numerical solutions, since a number of comparable nonlinear analytical solutions exist. Displacements and stresses within 1/2% and 2% respectively, of analytical solutions are easily possible using only 8 elements.

Existing solutions for the uniformly loaded plate are valid only over particular load ranges. It has been possible here, to study the plate under a load range of five magnitudes - from linear behavior to membrane behavior - and to give previously unavailable complete load-deflection and load-stress curves. A careful analysis of the problem to determine the influence of all dimensionless parameters revealed a surprising dependence of the solution on the ratio a/h of the plate radius a to its thickness h even for relatively thin plates. Analytical solutions are independent of this ratio as a result of simplifications used in their derivations. Various stress and displacement contours are also included, and where possible, are compared with analytical solutions.

Chapter 5 considers the behavior of point loaded spherical caps of half angle 5°, 22.5° and 90° and various thicknesses. Load-center deflection curves and meridian contours are given. Again, the effect of all dimensionless parameters is studied. Shells of half angles 5° and 22.5° are shallow and have load-deflection curves which are very similar to each other, but which are somewhat different from those of hemispheres (half angle of 90°). All sufficiently thin shells exhibit snapthrough behavior in proceeding to eversion and exhibit snapthrough again in returning to their initial state. Certain of the meridian contours which are thus produced depend on the direction of the load. Since the load-deflection curves produced here do not agree well with published analytical, numerical and experimental results and since bidirectional snapping had not been identified before, a simple experiment was done on a hollow rubber hemisphere. The experimental observations agreed extremely well with the numerical results and verified that new phenomena had indeed been identified.

Chapter 6 considers the deformation of a cylinder which is clamped at one end and subjected to radial and moment loads uniformly distributed around its other end. The effects of all dimensionless parameters are studied. The domains

of short, intermediate and long cylinder behavior under a wide range of loads are identified. Various types of previously unpublished nonlinear behavior are identified. Short cylinders behave like elasticae and show the effectiveness of the numerical method developed herein for solving problems involving gross deformations.

CHAPTER 2

THEORY

2.1 SURFACE GEOMETRY

The argument given in Section 1.1 shows that for purposes of analysis, we may reduce a shell to a surface. This surface is the middle surface of the shell and is endowed with the shell's extensional and flexural properties.

From the theory of surfaces, it is known that this surface can be defined using two independent parameters ξ_1 and ξ_2. See for example Saada [68, Section 18.3] for a more complete discussion of the theory of surfaces. These parameters form a Gaussian coordinate system (ξ_1, ξ_2) covering the surface, as shown in Figure 2.1. Further, this two-dimensional surface can be imbedded in a three-dimensional space by

$$\begin{aligned} r &= r(\xi_1, \xi_2) \ , \\ z &= z(\xi_1, \xi_2) \ , \\ \theta &= \theta(\xi_1, \xi_2) \end{aligned} \tag{2.1}$$

where r, θ and z constitute a cylindrical coordinate system. Alternatively, one can write the position vector $\mathbf{r}$ as

$$\mathbf{r} = \mathbf{r}(\xi_1, \xi_2) \tag{2.2}$$

as shown in Figure 2.1.

Consider the differential $d\mathbf{r}$ of the position vector $\mathbf{r}(\xi_1, \xi_2)$ of a generic point P on the middle surface of the shell

$$d\mathbf{r} = \frac{\partial \mathbf{r}}{\partial \xi_1} d\xi_1 + \frac{\partial \mathbf{r}}{\partial \xi_2} d\xi_2 \tag{2.3}$$

The partial derivatives $\partial \mathbf{r}/\partial \xi_1$ and $\partial \mathbf{r}/\partial \xi_2$ form a basis $(\mathbf{a}_1, \mathbf{a}_2)$ at P, where

$$\mathbf{a}_1 = \frac{\partial \mathbf{r}}{\partial \xi_1}$$

and

$$\mathbf{a}_2 = \frac{\partial \mathbf{r}}{\partial \xi_2} \tag{2.4}$$

Hence,

$$d\mathbf{r} = \mathbf{a}_1 \, d\xi_1 + \mathbf{a}_2 \, d\xi_2 \ . \tag{2.5}$$

Note, that it is unnecessary to use superscript indices to provide a distinction between covariant and contravariant quantities since only covariant bases are used in this thesis.

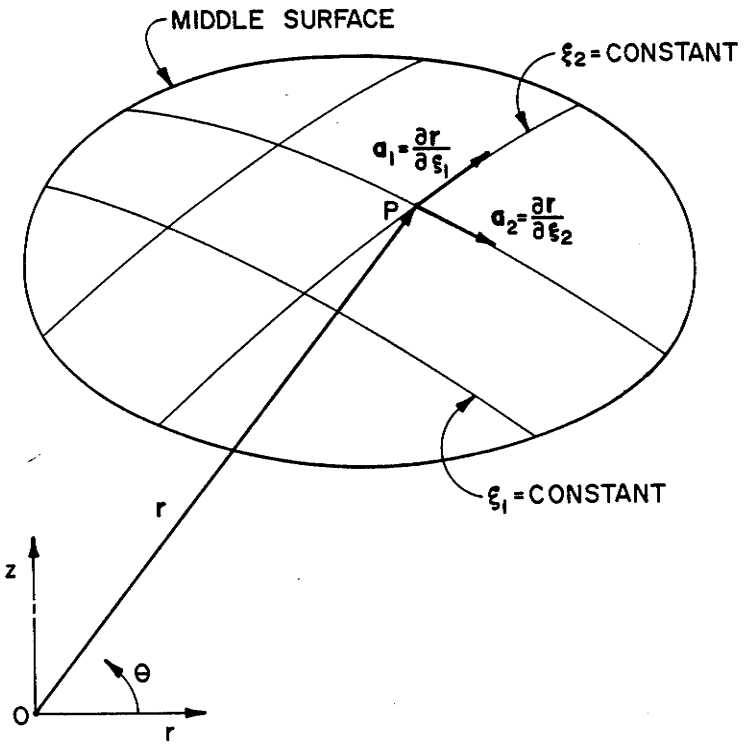

Figure 2.1 Gaussian Coordinate System

Consideration of the squared magnitude of the distance ds between adjacent points $\mathbf{r}$ and $\mathbf{r} + d\mathbf{r}$ on the surface gives rise to the so-called first fundamental form of the surface

$$\begin{aligned}(ds)^2 = d\mathbf{r} \cdot d\mathbf{r} &= a_{ij}\, d\xi_i\, d\xi_j \\ &= \mathbf{a}_1 \cdot \mathbf{a}_1 (d\xi_1)^2 + 2\mathbf{a}_1 \cdot \mathbf{a}_2\, d\xi_1\, d\xi_2 + \mathbf{a}_2 \cdot \mathbf{a}_2 (d\xi_2)^2 \\ &= E(d\xi_1)^2 + 2F\, d\xi_1\, d\xi_2 + G(d\xi_2)^2 \end{aligned} \tag{2.6}$$

where

$$\begin{aligned} a_{11} &= E = \mathbf{a}_1 \cdot \mathbf{a}_1 , \\ a_{12} &= F = \mathbf{a}_1 \cdot \mathbf{a}_2 , \\ a_{22} &= G = \mathbf{a}_2 \cdot \mathbf{a}_2 . \end{aligned} \tag{2.7}$$

The quantities E and G provide local measures of length squared along the Gauss coordinates. The quantity $F = \sqrt{EG}\cos\phi$ gives the angle ϕ between the local coordinates. A quantity H^2 is defined by

$$H^2 = EG - F^2 = \det [a_{ij}] \tag{2.8}$$

and provides a local measure of surface area.

The unit normal to the surface at P is given by

$$\mathbf{n} = \frac{\mathbf{a}_1 \times \mathbf{a}_2}{|\mathbf{a}_1 \times \mathbf{a}_2|} = \frac{\mathbf{a}_1 \times \mathbf{a}_2}{H} \tag{2.9}$$

We define the second fundamental form of a surface as the negative of the inner product of the differentials $d\mathbf{r}$ and $d\mathbf{n}$, and in general have

$$-d\mathbf{n} \cdot d\mathbf{r} = L(d\xi_1)^2 + Md\xi_1\, d\xi_2 + N(d\xi_2)^2 \tag{2.10}$$

where the so-called fundamental magnitudes of the second order L, M and N can, using the orthogonality of $\mathbf{n}$ to $\partial \mathbf{r}/\partial \xi_1$ and $\partial \mathbf{r}/\partial \xi_2$, be shown to be

$$\begin{aligned} L &= \mathbf{n} \cdot \frac{\partial^2 \mathbf{r}}{\partial \xi_1^2} \\ M &= \mathbf{n} \cdot \frac{\partial^2 \mathbf{r}}{\partial \xi_1 \partial \xi_2} \\ N &= \mathbf{n} \cdot \frac{\partial^2 \mathbf{r}}{\partial \xi_2^2} \end{aligned} \tag{2.11}$$

These quantities are projections of the local second derivatives of the surface and are useful in determining the local curvature of the surface. Using Meuniers Theorem and the geometry of curves, it is possible to show that the local curvature C of the surface in the direction ds is given by

$$\begin{aligned} C &= \mathbf{n} \cdot \frac{d^2 \mathbf{r}}{ds^2} = L\left(\frac{d\xi_1}{ds}\right)^2 + 2M \frac{d\xi_1}{ds}\frac{d\xi_2}{ds} + N\left(\frac{d\xi_2}{ds}\right)^2 \\ &= \frac{L(d\xi_1)^2 + 2M\, d\xi_1\, d\xi_2 + N(d\xi_2)^2}{E(d\xi_1)^2 + 2F\, d\xi_1\, d\xi_2 + G(d\xi_2)^2} \\ &= \frac{L\left(\frac{d\xi_1}{d\xi_2}\right)^2 + 2M\left(\frac{d\xi_1}{d\xi_2}\right)^2 + N}{E\left(\frac{d\xi_1}{d\xi_2}\right)^2 + 2F\left(\frac{d\xi_1}{d\xi_2}\right)^2 + G} \end{aligned} \tag{2.12}$$

From Equation (2.12) it is clear that the local curvature depends on the direction in which it is measured. It can be shown that the curvature C will take its largest and smallest values along directions normal to each other. If the surface is not locally planar or spherical, that is if it is not umbilic, these so-called principle directions will be uniquely given by the solutions $\left(\frac{d\xi_1}{d\xi_2}\right)$ to

$$(EM - FL)\left(\frac{d\xi_1}{d\xi_2}\right)^2 + (EN - GL)\left(\frac{d\xi_1}{d\xi_2}\right) + (FN - GM) = 0 \tag{2.13}$$

The corresponding curvatures are given by Equation (2.12).

Curves satisfying Equation (2.13) at all points are known as lines of curvature and are everywhere mutually orthogonal. If F = M = 0, the Gaussian coordinates are lines of curvature.

For an axisymmetric surface such as shown in Figure 2.2, the 3-space coordinates take the simplified form

$$\begin{aligned} r &= r(\xi_1) \\ z &= z(\xi_1) \\ \theta &= \theta(\xi_2) \end{aligned} \tag{2.14}$$

By setting ξ_1= constant, a series of circles concentric to the z-axis and known as parallels are produced. Setting ξ_2 = constant produces the meridians, which are the curves contained in radial planes intersecting the surface. Any one of the meridians is a so called generator as it would generate the entire surface by its rotation about the z-axis. Together, the parallels and meridians produce a curvilinear Gaussian coordinate system with base vectors

$$\begin{aligned} \mathbf{a}_1 &= \frac{\partial \mathbf{r}}{\partial \xi_1} = \frac{dr}{d\xi_1}\mathbf{e}_r + \frac{dz}{d\xi_1}\mathbf{e}_z \\ \mathbf{a}_2 &= \frac{\partial \mathbf{r}}{\partial \xi_2} = \frac{d\theta}{d\xi_2}\mathbf{e}_\theta \end{aligned} \tag{2.15}$$

which covers the surface.

Since $\mathbf{e}_r$, $\mathbf{e}_z$ and $\mathbf{e}_\theta$ form an orthogonal coordinate system at P, the first fundamental magnitudes are

$$\begin{aligned} E &= \left(\frac{dr}{d\xi_1}\right)^2 + \left(\frac{dz}{d\xi_1}\right)^2 \\ F &= 0 \\ G &= \left(\frac{d\theta}{d\xi_2}\right)^2 \end{aligned} \tag{2.16}$$

and the surface area measure is

$$H^2 = EG - F^2 = \left(\frac{d\theta}{d\xi_2}\right)^2 \left[\left(\frac{dr}{d\xi_1}\right)^2 + \left(\frac{dz}{d\xi_1}\right)^2\right] . \tag{2.17}$$

The unit surface normal is

$$\mathbf{n} = \frac{\mathbf{a}_1 \times \mathbf{a}_2}{H} = \frac{\frac{dr}{d\xi_1}\frac{d\theta}{d\xi_2}\mathbf{e}_z - \frac{dz}{d\xi_1}\frac{d\theta}{d\xi_2}\mathbf{e}_r}{H}$$

$$= \frac{\frac{dr}{d\xi_1}\mathbf{e}_z - \frac{dz}{d\xi_1}\mathbf{e}_r}{\left(\frac{dr}{d\xi_1}^2 + \frac{dz}{d\xi_1}\right)^{1/2}} . \tag{2.18}$$

and the fundamental magnitudes of second order L, M and N as calculated from Equation (2.11) are

$$L = -\frac{1}{H}\frac{dz}{d\xi_1}\frac{d\theta}{d\xi_2}\frac{d^2r}{d\xi_1^2}$$

$$M = 0, \text{ and} \tag{2.19}$$

$$N = \frac{1}{H}\frac{dz}{d\xi_1}\left(\frac{d\theta}{d\xi_2}\right)^2 .$$

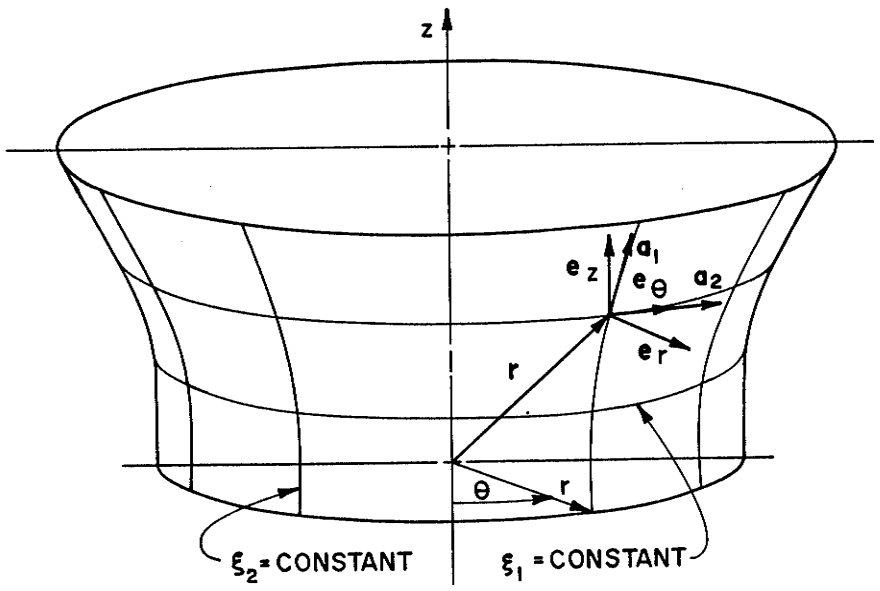

Figure 2.2 Coordinates on an Axisymmetric Surface

Since the coordinate curves are lines of curvature ($F = M = 0$), the extreme curvatures K_1 , K_2 occur along the orthogonal coordinate meridian curves ξ_2= constant and parallel curves ξ_1= constant. They have respective radii

$$R_1 = \frac{1}{K_1} = \frac{E}{L}$$

$$R_2 = \frac{1}{K_2} = \frac{G}{N} \tag{2.20}$$

which in this case are,

$$R_1 = - \frac{\left[\left(\frac{dr}{d\xi_1}\right)^2 + \left(\frac{dz}{d\xi_1}\right)^2\right]^{3/2}}{\frac{dz}{d\xi_1}\frac{d^2r}{d\xi_1^2}}$$

and

$$R_2 = \frac{\frac{d\theta}{d\xi_2}\left[\left(\frac{dr}{d\xi_1}\right)^2 + \left(\frac{dz}{d\xi_1}\right)^2\right]^{1/2}}{\frac{dz}{d\xi_1}} \tag{2.21}$$

If $dz/d\,\xi_1 \neq 0$, we have

$$R_1 = - \frac{\left[\left(\frac{dr}{dz}\right)^2 + 1\right]^{3/2}}{\frac{d^2r}{dz^2}}$$

and

$$R_2 = R\left[\left(\frac{dr}{dz}\right)^2 + 1\right]^{1/2} \tag{2.22}$$

where R is the radial distance from the axis of symmetry

The above radii can be written in terms of easily identified geometric quantities. Consider Figure 2.3 which shows a radial section through the surface. Since

$$\frac{dr}{dz} = - \cot\phi \tag{2.23}$$

where ϕ is the angle between the z-axis and the surface normal, we have

$$R_1 = \frac{\csc^3\phi}{\frac{d^2r}{dz^2}} = \frac{1}{\frac{d^2r}{dz^2}\sin^3\phi} \qquad (2.24)$$

and

$$R_2 = R\csc\phi$$

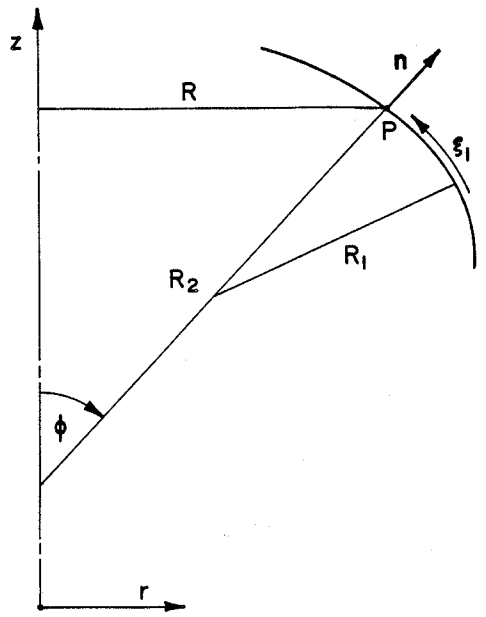

Figure 2.3 Axisymmetric Surface Geometry

Because of its derivation, it is known that the radius of curvature R_1 is the radius of curvature of the meridian. This meaning can also be derived from Equation (2.24(a)) recognizing that two factors of $\sin\phi$ occur from foreshortening of the arc length ds to dz and one factor occurs from foreshortening of distances normal to the surface. The radius R_2 is more easily interpreted.It is the intersection of the z-axis and an extension of the surface normal. Interpretation

of R_1 and R_2 as the meridian radius of curvature and intersection of a normal with the z-axis, respectively, will be used exclusively from this point. These are the meaning of Equation (2.22), and are valid even as $\frac{dz}{d\xi_1} \to 0$.

The theory of surfaces shows that the surface length measures dL_1 and dL_2 along the meridian and parallel directions, respectively, are

$$dL_1 = \sqrt{E}\, d\xi_1 = \left[\left(\frac{dr}{d\xi_1}\right)^2 + \left(\frac{dz}{d\xi_1}\right)^2\right]^{1/2} d\xi_1 = dS$$

$$dL_2 = \sqrt{G}\, d\xi_2 = \frac{d\theta}{d\xi_2}\, d\xi_2 = R\, d\theta \,. \tag{2.25}$$

Let the surface be deformed axisymmetrically to some new state. Its radii of curvature r_1 , r_2 will be determined respectively by the radius of curvature of the deformed meridian and the intersection of a normal to the deformed surface with the z-axis. The new surface measures $d\ell_1$ and $d\ell_2$ are

$$d\ell_1 = \sqrt{e}\, d\xi_1 = ds$$

$$d\ell_2 = \sqrt{g}\, d\xi_2 = r d\theta \tag{2.26}$$

The surface extensions λ_1 and λ_2 in the meridian and parallel directions are

$$\lambda_1 = \frac{ds}{dS}$$

and

$$\lambda_2 = \frac{r\, d\theta}{R\, d\theta} = \frac{r}{R} \tag{2.27}$$

The fundamental magnitude F is identically zero in all axisymmetric states indicating that the meridians and parallels remain orthogonal and that the middle surface does not undergo shear deformation. Similarly, M is identically zero, indicating that the middle surface does not twist or warp. Hence, the surface is completely described at any point by its curvatures K_1 , K_2 and k_1 , k_2 before and after deformation and by its extension ratios λ_1 and λ_2 .

2.2 STRAIN FIELD REPRESENTATION

Having established the geometry of an axisymmetric middle surface in terms of its meridian, we wish to determine the strain field through the thickness of the shell. This can be done using a relaxed form of the Love - Kirchoff hypothesis. In particular, we will assume that fibers normal to the middle surface before deformation remain straight and normal to it in the deformed state. As shown in Section 1.1, this assumption supresses shear strain between successive layers through the thickness of the shell and consequently makes the strain state dependent on the local middle surface configuration only. The strict form of the Love - Kirchoff hypothesis, which we will not use, further assumes the normal fibers to be inextensible and consequently is valid only when strains are small. In the development which follows, we wish to accommodate large strains and hence must consider the effects of fiber extension.

Since strains may be large, care must be taken to distinguish the undeformed and deformed states. Upper case letters are used to describe the undeformed state, and lower case letters are used to describe corresponding quantities in the deformed state. Since we are concerned with thin shells, the radii of curvature will be assumed to be at least 10 times the shell thickness. This further assumption ensures that the relaxed Kirchoff-Love hypothesis is accurate, and simplifies the derivation of the strain field.

When strains are not small compared to unity, definition of a consistent strain measure is not a trivial problem. We will consider a Lagrangian formulation for the strain-displacement relations. The reader is referred to Malvern [45, Chapter 4] or Truesdell [81] for the details of the formulation.

Consider a simply connected body deformed from a reference state χ in which strains are taken to be zero to a new state x as shown in Figure 2.4. The

position vector $\mathbf{x}$ of a generic point in the new or current position can be expressed in terms of its position vector $\mathbf{X}$ in the reference configuration by the automorphism

$$\mathbf{x} = \mathbf{x}(\mathbf{X}) \tag{2.28}$$

which can be written in component form

$$x_i = x_i(X_1, X_2, X_3). \tag{2.29}$$

It is possible to define a deformation gradient tensor $\mathbf{F}$ which operates on an arbitrary infinitesimal vector $d\mathbf{X}$ in the reference configuration to produce its corresponding vector $d\mathbf{x}$ in the current configuration

$$d\mathbf{x} = \mathbf{F} \cdot d\mathbf{X}. \tag{2.30}$$

It can be shown that the components F_{ij} of $\mathbf{F}$ are given by

$$F_{ij} = \frac{\partial x_i}{\partial X_j} \tag{2.31}$$

whence equation (2.30) is equivalent to

$$dx_i = \frac{\partial x_i}{\partial X_j}\, dX_j. \tag{2.32}$$

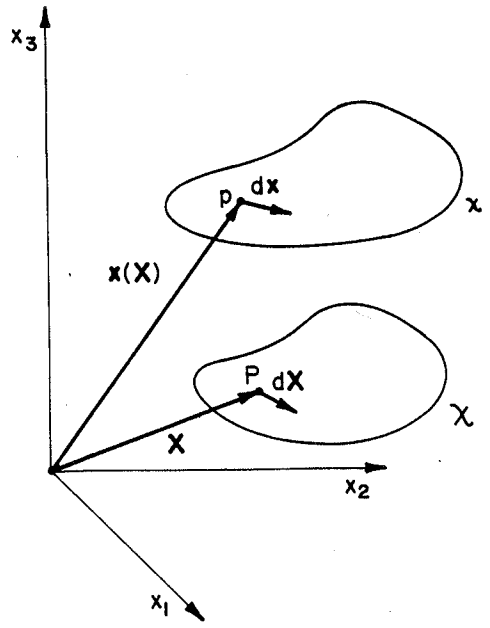

Figure 2.4 Body Deformation

By convention, the strain tensor $\mathbf{E}$ is defined so as to give the change in the squared length $(dS)^2$ of the vector $d\mathbf{X}$

$$(ds)^2 - (dS)^2 = 2d\mathbf{X} \cdot \mathbf{E} \cdot d\mathbf{X} \tag{2.33}$$

The strain tensor $\mathbf{E}$ can be expressed in terms of the deformation gradient $\mathbf{F}$ by

$$\mathbf{E} = \frac{1}{2}[\mathbf{F}^T \cdot \mathbf{F} - \mathbf{1}] = \frac{1}{2}[\mathbf{C} - \mathbf{1}] \tag{2.34}$$

since the product $\mathbf{F}^T \cdot \mathbf{F}$ is equal to the right Cauchy-Green deformation tensor $\mathbf{C}$. Furthermore, if the deformation tensor $\mathbf{F}$ is decomposed through polar decomposition into stretch $\mathbf{U}$ and rotation $\mathbf{R}$ by

$$\mathbf{F} = \mathbf{R} \cdot \mathbf{U} \tag{2.35}$$

then strain must be produced only by the stretch tensor $\mathbf{U}$. The foregoing definitions of deformation and strain satisfy this requirement in that the so-called right stretch tensor $\mathbf{U}$ is given by

$$\mathbf{U} = \mathbf{C}^{\frac{1}{2}} = [\mathbf{F}^T \cdot \mathbf{F}]^{\frac{1}{2}} \tag{2.36}$$

and the strain tensor

$$\mathbf{E} = \frac{1}{2}[\mathbf{F}^T \mathbf{F} - \mathbf{1}] = \frac{1}{2}[\mathbf{C} - \mathbf{1}] = \frac{1}{2}[\mathbf{U}^2 - \mathbf{1}] \tag{2.37}$$

depends only on the stretch tensor of any arbitrary deformation $\mathbf{F}$. For a deformation described by displacement $\mathbf{u(X)}$ in a Cartesian coordinate system,

$$\mathbf{x} = \mathbf{X} + \mathbf{u}(\mathbf{X}) \tag{2.38}$$

or $$x_i = X_i + u_i(X_1, X_2, X_3)$$

typical strains according to the above definition are

$$E_{11} = \frac{\partial u_1}{\partial X_1} + \frac{1}{2}\left[\left(\frac{\partial u_1}{\partial X_1}\right)^2 + \left(\frac{\partial u_2}{\partial X_1}\right)^2 + \left(\frac{\partial u_3}{\partial X_1}\right)^2\right] \tag{2.39}$$

and

$$E_{12} = \frac{1}{2}\left[\frac{\partial u_1}{\partial X_2} + \frac{\partial u_2}{\partial X_1}\right] + \frac{1}{2}\left[\frac{\partial u_1}{\partial X_1}\frac{\partial u_1}{\partial X_2} + \frac{\partial u_2}{\partial X_1}\frac{\partial u_2}{\partial X_2} + \frac{\partial u_3}{\partial X_1}\frac{\partial u_3}{\partial X_2}\right]$$

Note that these definitions are exact and are not just second order approximations. The above definitions simplify to the common small strain definitions

$$E_{11} = \frac{\partial u_1}{\partial X_1}$$

and

$$E_{12} = \frac{1}{2}\left[\frac{\partial u_1}{\partial X_2} + \frac{\partial u_2}{\partial X_1}\right] \tag{2.40}$$

when deformation gradients $\partial u_i / \partial X_j$ are small compared with unity.

It will frequently be useful to have a measure of the stretch $ds/dS = \lambda_{\hat{\mathbf{N}}}$ in a particular direction indicated by unit vector $\hat{\mathbf{N}}$. The square of the stretch is given by

$$\lambda_{\hat{\mathbf{N}}}^2 = \mathbf{N} \cdot \mathbf{C} \cdot \mathbf{N} \tag{2.41}$$

For uniaxial extension in the direction of the X_1 axis, the stretch λ_1 in the X_1 direction is given by

$$\lambda_1^2 = C_{11} = 1 + 2E_{11}$$

$$= 1 + 2\frac{\partial u_1}{\partial X_1} + \left(\frac{\partial u_1}{\partial X_1}\right)^2 \tag{2.42}$$

Hence,

$$\lambda_1 = 1 + \frac{\partial u_1}{\partial X_1} = 1 + \varepsilon_1 \tag{2.43}$$

which agrees with the common definition of stretch. Note also that the strain measure E is quadratic in ε_1 since

$$E_{11} = \varepsilon_1 + \frac{1}{2}\varepsilon_1^2 \tag{2.44}$$

When simultaneous extensions λ_i occur in the directions of their corresponding coordinate directions, we have

$$\lambda_i = 1 + \varepsilon_i \tag{2.45}$$

and

$$E_{ii} = \varepsilon_i + \frac{1}{2}\varepsilon_i^2 \tag{2.46}$$

Consider the small element of shell shown in Figure 2.5(a). Its middle surface is defined in the undeformed state as the collection of all points midway through the thickness of the shell and is permanently fixed to the material through which

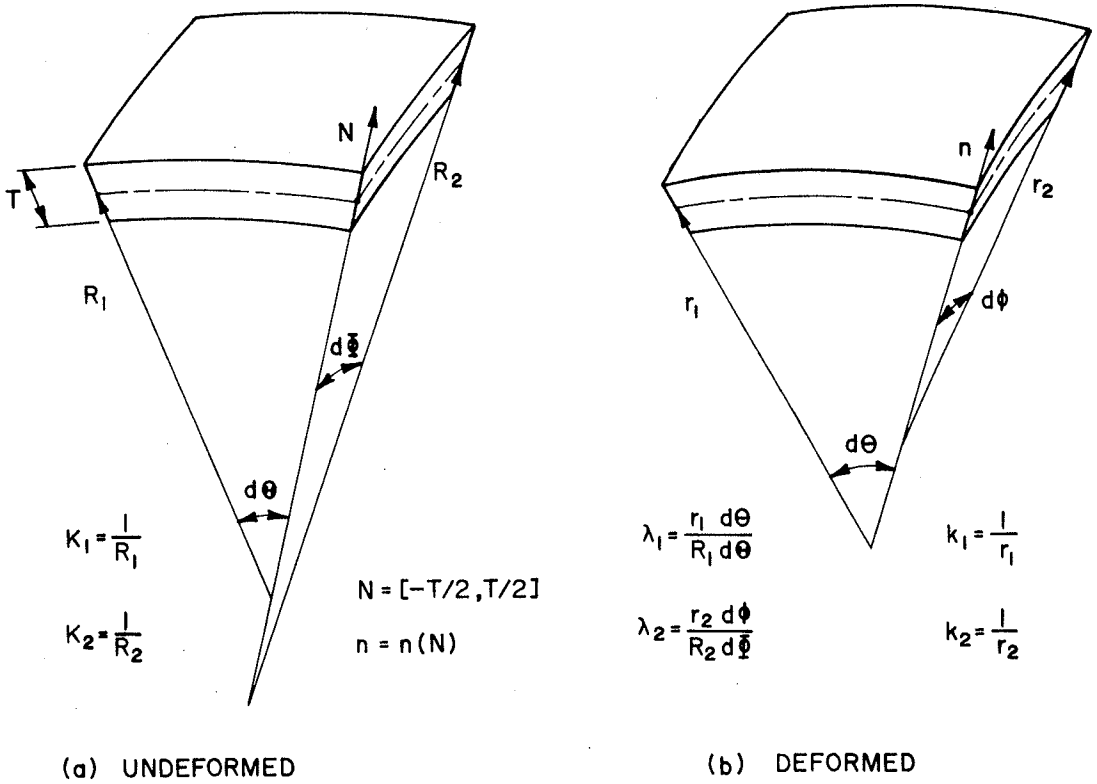

Figure 2.5 Element of a Shell

it passes. Hence, its behaviour under deformation can be visualized by imagining the material through which it passes to have been dyed a different color than the rest of the shell. Like the imaginary dyed layer, the middle surface will not under deformation necessarily remain midway between the free surfaces of the shell, but may shift slightly across the shell in response primarily to bending.

Before deformation, the shell will have two principal radii of curvature R_1 and R_2 as measured from the middle surface, and their corresponding inverses - the curvatures K_1 and K_2 . In a deformed state, the corresponding radii and principal curvatures are r_1 , r_2 , and k_1 , k_2 , respectively. The middle surface extensions are λ_1 and λ_2.

Define coordinates N and n normal to the middle surface of the undeformed and deformed shell respectively and zero at the middle surface . Call the respective elemental middle surface areas dA and da. Thin layers or sheets of the undeformed surface parallel to its middle surface and starting there can be thought of as laminated successively onto the deformed middle surface. Since the material is incompressible, the volume of these sheets (e.g.$(1 + K N)(1 + K N)dA\ dN$) remains constant between the two states and we have

$$(1 + K_1 N)(1 + K_2 N)\, dA\ dN = (1 + k_1 n)(1 + k_2 n)\, da\ dn \qquad (2.47)$$

where dN, dn are the thicknesses of the sheets in the undeformed and deformed states;

dA, da are the middle surface areas, and terms of the form

$(1 + K_i N)$ are the corrections for variation of the length of the sheet sides through the shell thickness.

Since

$$\frac{da}{dA} = \lambda_1 \lambda_2 \qquad (2.48)$$

we have

$$[1 + (K_1 + K_2)N + K_1K_2N^2]dN = \lambda_1\lambda_2[1 + (k_1k_2)n + k_1k_2n^2]dn \qquad (2.49)$$

Integration of this equation through the shell thickness yields the relationship

$$N + (K_1 + K_2)\frac{N^2}{2} + K_1K_2\frac{N^3}{3} = \lambda_1\lambda_2[n + (k_1 + k_2)\frac{n^2}{2} + k_1k_2\frac{n^3}{3}] \qquad (2.50)$$

between the transverse coordinates N and n of a sheet before and after deformation. This cubic is not easily solved to yield n(N). Since all radii of curvature are assumed to be at least 10 times the thickness, the product $KN \leq 1/10 \cdot 1/2 = 0.05$. It is therefore reasonable to eliminate terms having (KN) to the second power relative to those having (KN) to the first in differential Equation (2.47). This simplification reduces Equation (2.50) to a quadratic

$$N + (K_1 + K_2)\frac{N^2}{2} = \lambda_1\lambda_2[n + (k_1 + k_2)\frac{n^2}{2}] \qquad (2.51)$$

which can be solved explicitly to yield

$$n(N) = \frac{-1}{k_1 + k_2} + \sqrt{\frac{1}{(k_1+k_2)^2} + \frac{2(N + (K_1 + K_2)\frac{N^2}{2})}{\lambda_1\lambda_2(k_1 + k_2)}} \qquad (2.52)$$

The Taylor series expansion of this relationship is

$$n(N) = \left(\frac{N}{\lambda_1\lambda_2}\right) + \frac{1}{2}\left(\frac{N}{\lambda_1\lambda_2}\right)^2[\lambda_1\lambda_2(K_1 + K_2) - (k_1 + k_2)]$$
$$- \frac{1}{2}\left(\frac{N}{\lambda_1\lambda_2}\right)^3(k_1 + k_2)[\lambda_1\lambda_2(K_1 + K_2) - (k_1 + k_2)] + \ldots. \qquad (2.53)$$

Shifting of the middle surface was mentioned earlier. This shift can be demonstrated by calculating the location δm of the middle of the deformed surface

$$\delta m = \frac{n(-\frac{T}{2}) + n(\frac{T}{2})}{2} \qquad (2.54)$$

$$= \frac{T^2}{4\lambda_1^2 \lambda_2^2}[\lambda_1 \lambda_2(K_1 + K_2) - (k_1 + k_2)] + \ldots.$$

It can be shown that the quantity $\lambda_1\lambda_2(K_1 + K_2) - (k_1 + k_2)$ is a primary measure of bending. Hence, from Equation (2.54) we see that the middle surface shift is primarily due to bending and that it is attenuated by extension of the middle surface.

The deformed shell thickness t is given by

$$t = n(\frac{T}{2}) - n(-\frac{T}{2})$$

$$t = \frac{T}{\lambda_1\lambda_2} - \frac{T^3}{\lambda^3 \lambda^3}(k_1 + k_2)[\lambda_1\lambda_2(K_1 + K_2) - (k_1 + k_2)] + \ldots.. \qquad (2.55)$$

and is primarily dependent on middle surface strains. In the absence of bending, $T = \lambda_1\lambda_2 t$. In the presence of bending, the shell thickness will change as a third order effect because of asymmetrical sheet strains.

It was shown in Section 2.1 that the middle surface undergoes no shear or twisting. Consequently, sheets through the thickness will not undergo shear or rotation in their own planes. Further, the directions of principal stretch and of principal curvature are fixed in the meridian and parallel directions. The principal stretches λ_I and λ_{II} in the sheets are therefore also in the meridian directions [29, pp.231,232] and are given respectively by

$$\lambda_I = \frac{\lambda_1(1 + k_1 n)}{(1 + K_1 N)}$$

and

$$\lambda_{II} = \frac{\lambda_2(1 + k_2 n)}{(1 + K_2 N)} \qquad (2.56)$$

The variable n can be eliminated using Equation (2.52) or (2.53) and in both cases the Taylor series

$$\lambda_I = \lambda_1 + \left(\frac{k_1}{\lambda_2} - K_1\lambda_1\right)N + \left\{\frac{k_1}{2\lambda_1\,\lambda_2^2}\,[\lambda_1\lambda_2(K_1+K_2) - (k_1+k_2)] - K_1\left(\frac{k_1}{\lambda_2} - K_1\lambda_1\right)\right\}N^2 + \ldots.$$

$$\lambda_{II} = \lambda_2 + \left(\frac{k_2}{\lambda_1} - K_2\lambda_2\right)N + \left\{\frac{k_2}{2\lambda_1^2\,\lambda_2}\,[\lambda_1\lambda_2(K_1+K_2) - (k_1+k_2)] - K_2\left(\frac{k_2}{\lambda_1} - K_2\lambda_2\right)\right\}N^2 + \ldots. \qquad (2.57)$$

result. These equations explicitly give the principal stretches of any sheet initially located a distance N from the middle surface, in terms of the initial and final curvatures and principal stretches of the middle surface.

2.3 CONSTITUTIVE EQUATIONS

Having established the strain-displacement relationships in the previous section, attention is now turned to determination of the stress-strain relationships or constitutive equations. Real materials exhibit a wide array of physical responses to applied loads. These responses include such effects as anisotropy, where the response of the material is not the same in all directions, viscoelastic effects where stress depends on the instantaneous rate of deformation, memory effects where the instantaneous stress is dependent on the history of the deformation, and various nonlinear effects. General constitutive equations accommodating these phenomena are very difficult to work with. It is usual to choose the simplest constitutive equation which models the essential behavior of the real material.

We are interested in materials which are incompressible and isotropic. The third strain invariant I_3 of such incompressible materials satisfies

$$I_3 = \lambda_1^2 \lambda_2^2 \lambda_3^2 \equiv 1. \tag{2.58}$$

The assumption of isotropy allows considerable simplification of the strain energy function, as shown later in this chapter. It also ensures [29, pp. 231,232] that the directions of principal stress and principal strain coincide. Since the ensuing deformation analysis is carefully designed to permit large deformations and large strains, it is desirable to accommodate the nonlinear material response which is typical at large strains. To determine reasonable forms of the constitutive equations we appeal to modern continuum mechanics.

We are concerned with so-called simple elastic materials in which the local stress depends only on the local instantaneous strain. It does not depend on the strain loading path, nor on the strain rate. For a general nonlinear elastic material, each of the nine second Piola-Kirchoff stress components T_{ij} is dependent on all nine of the strain components ε_{rs} . i.e.

$$T_{ij} = f_{ij}(\varepsilon_{rs}). \tag{2.59}$$

When it is possible to construct an elastic potential function $w(\varepsilon_{rs})$ or $w(\mathbf{E})$ giving the strain energy per unit undeformed volume, the material is said to be hyperelastic or Green elastic. Stress is related to the elastic potential function by

$$T_{ij} = \frac{\partial w(\mathbf{E})}{\partial E_{ij}}. \tag{2.60}$$

From this we note that the functions f_{ij} in Equation (2.59) are neither arbitrary nor independent of each other. It may be useful to model certain materials by functions f_{ij} which do not satisfy Equation (2.60). Such materials do not have an elastic potential function and are said to be Cauchy elastic or simply "elastic".

Since we wish to use an energy minimization technique to find the displacement of loaded shells, we restrict our attention to hyperelastic materials. We may therefore write

$$w = w(\mathbf{E}) = w'(\mathbf{C}) \tag{2.61}$$

since

$$\mathbf{C} = 2\mathbf{E} + \mathbf{I} \tag{2.62}$$

Since we assume that the material is isotropic, the strain energy w does not depend on the orientation of the strain field and hence

$$w = w'(\mathbf{C}) = w'(\mathbf{Q}\mathbf{C}\mathbf{Q}^T) \tag{2.63}$$

for all $\mathbf{Q}$ where $\mathbf{Q}$ is orthogonal and by definition satisfies

$$\mathbf{Q}^T\mathbf{Q} = \mathbf{Q}\mathbf{Q}^T = \mathbf{I} \rightarrow \mathbf{Q}^T = \mathbf{Q}^{-1} \tag{2.64}$$

where $\mathbf{I}$ is the identity tensor. It can be shown mathematically [29, pp. 230-231] that the scalar function w' satisfying Equation (2.63) is isotropic, and that the elastic potential w' can therefore be written in terms of the three invariants of $\mathbf{C}$

$$\begin{aligned} I_1 &= \lambda_1^2 + \lambda_2^2 + \lambda_3^2 \\ I_2 &= \lambda_1^2\,\lambda_2^2 + \lambda_2^2\,\lambda_3^2 + \lambda_3^2\,\lambda_1^2 \\ I_3 &= \lambda_1^2\,\lambda_2^2\,\lambda_3^2 \end{aligned} \tag{2.65}$$

where $\lambda_i = 1 + \varepsilon_i$ are the principal stretches, and are always strictly positive. That is

$$w'(\mathbf{C}) = w''(I_1, I_2, I_3)\ . \tag{2.66}$$

See also Green and Zerna [28, Section 2.3]. The invariants I_i are the coefficients of the characteristic equation

$$\lambda^6 - I_1 \lambda^4 + I_2 \lambda^2 - I_3 = 0 \tag{2.67}$$

associated with

$$|\mathbf{C} - \lambda \mathbf{I}| = 0 \tag{2.68}$$

It is formally possible, therefore, to calculate λ_i^2 and consequently λ_i for any given invariants I_i which are physically admissible. Hence, we can write the energy function as

$$w = w'(\mathbf{C}) \equiv w''(I_1, I_2, I_3) \equiv w'''(\lambda_1, \lambda_2, \lambda_3) \tag{2.69}$$

A great deal of work has been done to establish theoretical limitations on representations of w', w" and w'". The reader is referred to [45, Section 6.8] for a survey of various approaches to the representation of three-dimensional isotropic functions.

Certain restraints on the general energy form of the constitutive equations have been established from a mathematical basis. We must now find a specific form which is general enough to represent a range of nonlinear materials, but which is simple enough to be manipulated mathematically. To this end, we consider some of the extensive experimental research which has been done. See for example Alexander [1].

It is possible to argue for a particular form of the strain energy function from a molecular basis. Rubbers and other polymers are the most important materials which exhibit large elastic strains. They are composed of very long chain molecules. The change in entropy associated with their deformation, and

hence their strain energy, is easily calculated, as shown in Treloar [80, Chapter 4], and takes the form

$$w = \frac{1}{2} G(I_1 - 3) \tag{2.70}$$

where G is the material shear modulus. This strain energy function has been shown experimentally to be especially effective in describing swollen rubbers where the molecular chains are separated sufficiently as not to interfere with each other during extension.

Treloar [80] argues from a mathematical perspective, that the strain energy function for an incompressible isotropic elastic material can be given in the form

$$w = \sum_{\substack{i=o \\ j=o}}^{\infty} C_{ij}(I_1 - 3)^i (I_2 - 3)^j \tag{2.71}$$

where C_{ij} are constants. The simplified, first order form of this relationship

$$w = A + C_1(I_1 - 3) + C_2(I_2 - 3) \tag{2.72}$$

by analogy with the first terms of a Taylor series, will clearly describe any sufficiently smooth energy surface over a small enough domain. Hence, its ability to describe experimental results cannot be taken as verification that its form has any necessary connection with the physical behavior of polymers. The most commonly used strain energy form is the so-called Mooney-Rivlin form [50]

$$w = C_1(I_1 - 3) + C_2(I_2 - 3) . \tag{2.73}$$

It is also reasonable to propose a representation of strain energy in terms of a function which is symmetric in the three principal stretches. Valanis and Landel [82] have suggested that the strain energy can be represented by

$$w = w(\lambda_1) + w(\lambda_2) + w(\lambda_3) \tag{2.74}$$

They have demonstrated that simple functions for w such as

$$w(\lambda) = 2\mu \ell n(\lambda) \tag{2.75}$$

are accurate over ranges as large as $\lambda = [0.35, 2.5]$. The Mooney-Rivlin function can be written in this form by making use of the fact that $I_3 \equiv 1$.

Ogden [57] proposed the form

$$w = \sum_n \frac{\mu_n}{\alpha_n} (\lambda_1^{\alpha_n} + \lambda_2^{\alpha_n} + \lambda_3^{\alpha_n} - 3) \tag{2.76}$$

for the strain energy function. This formulation can, in certain cases, represent stretches up to $\lambda_i = 7$ using only three terms ($n = 3$). Ogden's proposed form is consistent with the Valanis-Landel hypothesis, and includes the Mooney-Rivlin form as a special case, again using $I_3 \equiv 1$.

The Mooney-Rivlin strain energy function is used for the ensuing analysis. Though its form is simple, it is a good representation of any strain energy function, at least over a limited strain range, and it is easy to manipulate mathematically. It is further consistent with the Valanis-Landel hypothesis and has a stronger physical motivation than the other forms mentioned above.

To show how the Mooney-Rivlin coefficients can be chosen, we consider a linear material under principal strains ε_i. Its strain energy w_L is given [83, p.47] by

$$w_L = G\left\{\varepsilon_1^2 + \varepsilon_2^2 + \varepsilon_3^2 + \frac{\nu}{(1-2\nu)} (\varepsilon_1 + \varepsilon_2 + \varepsilon_3)^2\right\} \tag{2.77}$$

where G is the material shear modulus. The Mooney-Rivlin strain energy

w_M is given in terms of the strain invariants.

$$w_M = C_1(I_1 - 3) + C_2(I_2 - 3) \tag{2.78}$$

In order to equate the energy representations given in Equations (2.77) and (2.78) so that C_1 and C_2 can be found, they must both be written in terms of the same variables. If we assume incompressibility ($I_3 \equiv 1$) and if we let $\lambda_i = \varepsilon_i + 1$, then the respective material strain energies can both be written in terms of ε_1 and ε_2 as

$$\begin{aligned} w_L = G \Big\{ & 2(\varepsilon_1^2 + \varepsilon_2^2 + \varepsilon_1\varepsilon_2) - 2\varepsilon_1^3 - 4\varepsilon_1^2\,\varepsilon_2 + 2\varepsilon_1\,\varepsilon_2^2 - 4\varepsilon_2^3 \\ & + 3\varepsilon_1^4 + 6\varepsilon_1^3\,\varepsilon_2 + 7\varepsilon_1^2\,\varepsilon_2^2 + 6\varepsilon_1\,\varepsilon_2^3 + 3\varepsilon_2^4 + \ldots \Big\} \end{aligned} \tag{2.79}$$

and

$$\begin{aligned} w_M = C_1 \Big\{ & 4(\varepsilon_1^2 + \varepsilon_2^2 + \varepsilon_1\varepsilon_2) - 4\varepsilon_1^3 - 6\varepsilon_1^2\,\varepsilon_2 - 6\varepsilon_1\,\varepsilon_2^2 - 4\varepsilon_2^3 \\ & + 5\varepsilon_1^4 + 8\varepsilon_1^3\,\varepsilon_2 + 9\varepsilon_1^2\,\varepsilon_2^2 + 8\varepsilon_1\,\varepsilon_2^3 + 5\varepsilon_2^4 + \ldots \Big\} \\ & + C_2 \Big\{ 4(\varepsilon_1^2 + \varepsilon_2^2 + \varepsilon_1\varepsilon_2) - 4\varepsilon_1^3 + 2\varepsilon_1\varepsilon_2 + 2\varepsilon_1\,\varepsilon_2^2 - 4\varepsilon_2^3 \\ & + 5\varepsilon_1^4 + \varepsilon_1^2\,\varepsilon_2^2 + 5\varepsilon_2^4 + \ldots \Big\} \end{aligned} \tag{2.80}$$

By setting

$$C_1 = \frac{5G}{8}$$

and

$$C_2 = \frac{-G}{8} \tag{2.81}$$

the coefficients of second and third order terms in equations (2.79) and (2.80) are made identical and coefficients on fourth order terms are within 80 percent of each other. The difference between Equations (2.79) and (2.80) is of the order of $5\varepsilon^4$. If these series are equated on the basis that the sum of the strains is zero, rather than $I_3 \equiv 1$, identical coefficients on terms up to fourth order are achieved by setting

$$C_1 = \frac{1}{2} G$$

and

$$C_2 = 0 \ . \tag{2.82}$$

The coefficients C_1 and C_2 can be chosen in a similar fashion to model a nonlinear material.

Principal forces per unit unstrained area f_i are easily calculated from the strain energy function. The relationship

$$f_i = \frac{\partial w}{\partial \lambda_i} \tag{2.83}$$

can be derived from variational principles or from Equation (2.60). To calculate the stress σ_i per unit deformed area for f_1, for example, we must multiply by $1/(\lambda_2\lambda_3)$ or for an incompressible material, by λ_1, to correct for the change in cross-sectional area. Hence,

$$\sigma_i = \lambda_i \frac{\partial w}{\partial \lambda_i} \tag{2.84}$$

For the Mooney-Rivlin strain energy function

$$w = C_1\left(\lambda_1^2 + \lambda_2^2 + \frac{1}{\lambda_1^2 \lambda_2^2} - 3\right) + C_2\left(\lambda_1^{-2} + \lambda_2^{-2} + \lambda_1^2 \lambda_2^2 - 3\right) \tag{2.85}$$

we have

$$\sigma_1 = 2C_1(\lambda_1^2 - \frac{1}{\lambda_1^2 \lambda_2^2}) - 2C_2(\lambda_1^{-2} - \lambda_1^2 \lambda_2^2) \ ,$$

$$\sigma_2 = 2C_1(\lambda_2^2 - \frac{1}{\lambda_1^2 \lambda_2^2}) - 2C_2(\lambda_2^{-2} - \lambda_1^2 \lambda_2^2) \ ,$$

$$\sigma_3 = 0 \tag{2.86}$$

Since the material is assumed incompressible, no work is done by a hydrostatic pressure, and the strain energy is unaffected. Consequently, stresses found from the strain energy function do not include the hydrostatic component. In thin shell analysis, σ_3 is assumed to be zero. Since this is the value produced above, no correction for hydrostatic stress is required.

2.4 ENERGY CONSIDERATIONS

It is frequently possible to formulate problems in terms of an objective quantity. Solution of the problem then involves finding the maximum or minimum value(s) of the objective quantity. In the case of solid mechanics, the objective quantity, which is frequently used, is total system energy. Local minima of this quantity represent equilibriium solutions. In the case of a static problem only the potential energy components need be considered. When the solution takes the form of a function f, the objective quantity F is a function of the function f and is called a functional of f, i.e.

$$F = F(f) \tag{2.87}$$

When the solution consists of finding a finite number n of quantities X_i, called generalized coordinates, the objective quantity g is a function of X_i, i.e.

$$g = g(X_i) \tag{2.88}$$

Since we are primarily interested in systems which are represented using generalized coordinates, functionals will not be discussed further, although much of the ensuing discussion is also applicable to functionals.

We define the objective function, total potential energy $\bar{U}$, as the sum of the strain energy and the work done by body forces and external forces. Solution of the problem consists of finding its minimum. Other functions such as complementary energy [15,39] will work, but total potential energy is usually preferred since it is the quantity naturally minimized by mechanical systems, it is convenient for numerical analysis [96], and certain other useful properties are known about it. In particular, the following properties hold:

1. Principle of Least Work

A stationary value of the total potential energy

$$\frac{\partial \bar{U}}{\partial X_i} = 0 \tag{2.89}$$

is necessary and sufficient for equilibrium of the system [76,p. 87; 83, p.84].

2. Stability Criterion

A strict relative minimum of the total potential energy

$$\left| \frac{\partial^2 \bar{U}}{\partial X_i \, \partial X_j} \right| > 0 \qquad (2.90)$$

is necessary and sufficient for the stability of an equilibrium state [76, p. 87].

3. Principle of Virtual Work

For every virtual deformation δX_i of an elastic solid, the sum of the work done by the external forces F_i is equal to the variation δW of the strain energy of the solid [83, p. 54].

$$\Sigma F_i \, \delta X_i = \delta \bar{W} \qquad (2.91)$$

The principle of least work provides a basis for identifying all possible equilibrium configurations, or solutions, to a particular problem. It would identify as equilibrium states all of the stationary points A through F , shown in Figure 2.6. The figure illustrates an energy surface which is a function of one coordinate X_i only. In general, equlibrium requires simultaneous stationarity with respect to all generalized coordinates X_i. If we think of the energy surface as a track on which the balls shown at the stationary points ride, it is clear that the ball at C and E would not, except under ideal conditions, remain still. These points illustrate unstable equilibria.

Criterion (2.90) provides a measure of the stability of an equilibrium solution. Solutions such as B, D and F which are strict local minima are stable, can occur physically, and are known as points of stable equilibrium. If a small perturbation is applied to these solutions, they will return to their equilibrium states. Solution

B is called metastable as a moderate perturbation will cause the ball to find a new resting point, which in this case would likely be D . The solutions A are indeterminate and are only likely to occur in an incompletely defined problem, where for example, rigid body motion can occur. For a point to be a stable equilibrium point it must, in general, be a local minimum with respect to all generalized coordinates. Figure 2.6 illustrates the possibility of multiple solutions and shows that for a smooth energy curve, at least one unstable equilibrium state exists between multiple stable solutions. This result is easily extended to an n degree of freedom system in which case the energy surface is an n + 1 dimensional hypersurface.

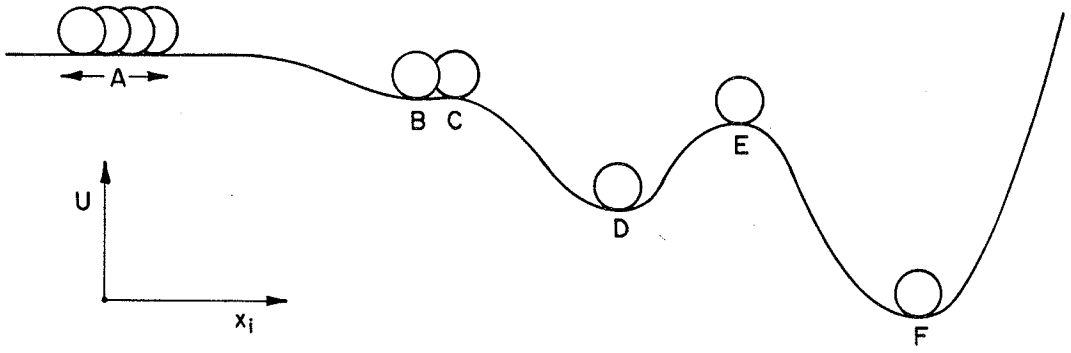

Figure 2.6 Equilibrium States

The principle of virtual work provides a means to determine reaction forces and stress resultants.

Solution of a problem formulated in terms of total potential energy $\bar{U}$ requires location of the local absolute minimua of $\bar{U}$. Numerical techniques to accomplish this are discussed in Chapter 3. We now consider suitable forms for the local shell

strain energy in terms of the middle surface geometry. The strain energy function

$$w = C_1(I_1 - 3) + C_2(I_2 - 3) \tag{2.92}$$

is known in terms of the local strain. Since the strain state through the thickness of the shell is also known from Equations (2.57), the shell energy per unit area of undeformed middle surface W can be calculated. It is

$$W = \int_{-T/2}^{T/2} (1 + K_1N)(1 + K_2N)w(N)\,dN \tag{2.93}$$

where N is the transverse coordinate in terms of the undeformed shell,

$w(N)$ is the volumetric strain energy at N,

$(1 + K_1N)(1 + K_2N)dN$ is the differential volume of the sheet at N, and

T is the shell thickness.

The evaluation of the energy integral is considerably complicated by the $(1 + K_1N)(1 + K_2N)$ terms. Under the assumptions of thin shell theory, $|K_i| \leq 1/10$ T. Hence, since $N = [-T/2, T/2]$, $|K_i N| \leq 0.05$. The greatest magnitudes of the terms in

$$(1 + K_1N)(1 + K_2N) = 1 + (K_1 + K_2)N + K_1K_2N^2 \tag{2.94}$$

are $1 + 0.10 + 0.0025$.

For the applications of interest here, the last term can be neglected. Assume that function $w(N)$ can be written in terms of a Taylor series. Then the total energy W is given by

$$W = \int_{-T/2}^{T/2} (1 + KN)\, w(N)\, dN$$

$$= \int_{-T/2}^{T/2} (1 + KN)(a + bN + cN^2 + dN^3 + eN^4 + fN^5 + gN^6 + \ldots)\, dN$$

$$= aT + (c + Kb)\frac{T^3}{12} + (e + Kd)\frac{T^5}{80} + \ldots \qquad (2.95)$$

$$= aT + \frac{cT^3}{12} + \frac{eT^5}{80} + \ldots$$

$$+ KT\left(\frac{bT^3}{12} + \frac{dT^5}{80} + \ldots\right)$$

$$\simeq aT + \frac{cT^3}{12} + \frac{eT^5}{80} + \ldots \qquad (2.96)$$

Since $|KT| \leq 0.1$, the terms associated with K are small compared with the other terms of the series and can be neglected. We can then approximate W by

$$W = \int_{-T/2}^{T/2} w(N)\, dN \qquad (2.97)$$

The effect of these simplifications turns out to be equivalent to neglecting the changing sheet area through the shell thickness. Since the sheet area increases on one side of the middle surface at nearly the same rate as it decreases on the other, the effect of this simplification is less severe than might be expected.

The principal sheet strains λ_I and λ_{II} can be approximated using the first two terms of Equations (2.57) as

$$\lambda_I = \lambda_1 + A_1 N \qquad (2.98)$$

and

$$\lambda_{II} = \lambda_2 + A_2 N \qquad (2.99)$$

where

$$A_1 = \left(\frac{k_1}{\lambda_2} - K_1\lambda_1\right)$$

$$A_2 = \left(\frac{k_2}{\lambda_1} - K_2\lambda_2\right) \qquad (2.100)$$

This allows linear variation of stretch across the thickness. The strain energy calculated by substituting Equations (2.98) and (2.99) into Equations (2.65), (2.92) and (2.97) in turn, and retaining terms up to fourth order in N is

$$W = \int_{-T/2}^{T/2} \{C_1[\lambda_I^2 + \lambda_{II}^2 + \frac{1}{\lambda_I^2\,\lambda_{II}^2} - 3] + C_1[\lambda_I^{-2} + \lambda_{II}^{-2} + \lambda_I^2\,\lambda_{II}^2 - 3]\}\,dN \qquad (2.101)$$

$$= \int_{-T/2}^{T/2} \{C_1[(\lambda_1^2 + 2\lambda_1 A_1 N + A_1^2 N^2 + \lambda_2^2 + 2\lambda_2 A_2 N + A_2^2 N^2)$$

$$+ \frac{1}{\lambda_1^2\,\lambda_2^2}\left(1 - 2\frac{A_1}{\lambda_1}N + 3\left(\frac{A_1}{\lambda_1}\right)^2 N^2 - 4\left(\frac{A_1}{\lambda_1}\right)^3 N^3 + 5\left(\frac{A_1}{\lambda_1}\right)^4 N^4\right)$$

$$\cdot \left(1 - 2\frac{A_2}{\lambda_2}N + 3\left(\frac{A_2}{\lambda_2}\right)^2 N^2 - 4\left(\frac{A_1}{\lambda_1}\right)^3 N^3 + 5\left(\frac{A_1}{\lambda_1}\right)^4 N^4\right)]$$

$$+ C_2\left[\frac{1}{(\lambda_1 + A_1 N)^2} + \frac{1}{(\lambda_2 + A_2 N)^2}\right.$$

$$+ \lambda_1^2\lambda_2^2 + (2\lambda_1\lambda_2^2 A_1 + 2\lambda_1^2\lambda_2 A_2)N$$

$$+ (\lambda_1^2 A_2^2 + 4\lambda_1\lambda_2 A_1 A_2 + \lambda_2^2 A_1^2)N^2$$

$$\left. + (2\lambda_1 A_1 A_2^2 + 2\lambda_2 A_1^2 A_2)N^3 + (A_1 A_2)^2 N^4\right]\}dN \qquad (2.102)$$

$$= C_1 \left[\left(\lambda_1^2 + \lambda_2^2 + \frac{1}{\lambda_1^2 \lambda_2^2} - 3\right) t \right.$$

$$\left. + \left(A_1^2 + A_2^2 + \frac{3A_1^2}{\lambda_1^4 \lambda_2^2} + \frac{4A_1 A_2}{\lambda_1^3 \lambda_2^3} + \frac{3A_2^2}{\lambda_1^2 \lambda_2^4} \right) \frac{t^3}{12} \right]$$

$$+ C_2 \left[\left(\frac{1}{\left(\lambda_1^2 - \frac{A_1^2 t^2}{4}\right)} + \frac{1}{\left(\lambda_2^2 - \frac{A_2^2 t^2}{4}\right)} + \lambda_1^2 \lambda_2^2 - 3 \right) t \right.$$

$$\left. + \left(\lambda_2^2 A_1^2 + 4\lambda_1 \lambda_2 A_1 A_2 + \lambda_1^2 A_2^2\right) \frac{t^3}{12} \right] \qquad (2.103)$$

Care has been exercised to ensure that all expansions and simplifications are valid for all physically admissible λ_I and λ_{II}. It is possible to express the integral

$$\int_{-T/2}^{T/2} \frac{1}{\lambda_I^2 \lambda_{II}^2} \, dN \qquad (2.104)$$

in closed form. However, the integral takes two completely different forms, depending on whether or not $\lambda_I = \lambda_{II}$. Since $\lambda_I \neq \lambda_{II}$ in general, except at the axis of symmetry where $\lambda_I = \lambda_{II}$ for any axisymmetric deformation, the series form of the integral is used.

A similar approach is used by Libai and Simmonds to derive constitutive equations [41] for analysis [42] of cylindrical shells. Indeed, these papers provided some impetus for this research.

Equation (2.103) in conjunction with Equations (2.100) gives W the total strain energy integrated through the thickness of the shell in terms of the geometry of the undeformed and deformed middle surface. Alternatively, the quantity W can be determined using exact equations (2.50) for the transverse position, (2.56)

for inplane strain, (2.65) for invariants and (2.73) for strain energy; and integrating (numerically) across the shell thickness. The approximation (2.103) compares very well with results obtained from this exact procedure. Percentage errors e between the two approaches are:

1) For $|K_i T| \leq 0.1$
$|k_i T| \leq 0.1$
$\lambda_1 , \lambda_2 \geq 1.0$
$e \leq 2\%$

2) For $|K_i T| \leq 0.1$
$|(K_i - k_i) T| \leq 0.1$
$\lambda_1 \lambda_2 \geq 1.0$
$e \leq 3\%$

3) For $|K_i T| \leq 0.1$
$|(K_i - k_i) T| \leq 0.1$
$\lambda_1 \lambda_2 \geq 0.8$
$e \leq 5\%$

Strictly for purposes of comparison, we note that

4) For $|K_i T| \leq 0.2$
$|(K_i - k_i) T| \leq 0.1$
$\lambda_1 \lambda_2 \geq 0.8$
$e \leq 8\%$

indicating that the energy representation is reasonable even considerably outside the bounds of thin shell theory (e.g., $k_i T$ may be 0.3).

The slope and curvature of the energy surface are required by the energy minimization scheme. Since the difference between the exact and approximate

values increases monotonically and smoothly with k_i , it is reasonable to take surface properties, such as slope and curvature of the approximate hypersurface (2.103) to be good representations of the corresponding properties of the exact energy hypersurface.

Solution of the shell problem by energy minimization requires that the strain energy be integrated over the entire shell. Integration through the shell thickness has been performed analytically. It is not, in general, practical to integrate the strain energy over the middle surface analytically. Fortunately, this integration can be performed easily and quickly by numerical means. A suitable procedure is discussed in Chapter 3.

2.5 FIELD EQUATIONS

The constitutive equations and equilibrium equations, together with certain geometric relationships are jointly known as the field equations. They completely describe the deformation of a body under applied loads, and provide the starting point for classical solution techniques. The energy minimization approach used herein does not explicitly use the equilibrium equations, as the minimum energy solution satisfies them automatically. The constitutive equations are not used to relate stress and strain in the usual way either, but are used only in strain energy form. Nonetheless, these equations are discussed here since they provide the starting point for most analytical solutions, including those with which the numerical solutions calculated here are compared.

Consider the element of a deformed axisymmetric shell, shown in Figure 2.7. Since the loads and deformations are assumed axisymmetric, all shear resultants except Q_1 are zero, and all twisting resultants are zero. The element will be in equilibrium in the meridian direction when

$$- N_1 r \cos\frac{d\phi}{2} - Q_1 r \sin\frac{d\phi}{2} - N_1 \cos\phi \, ds$$

$$- (Q_1 + dQ_1)(r + dr)\sin\frac{d\phi}{2} + (N_1 + dN_1)(r + dr)\cos\frac{d\phi}{2} = 0$$

or
$$\frac{d(N_1 r)}{ds} - Q_1 r \frac{d\phi}{ds} - N_2 \cos\phi = 0 \, . \tag{2.105}$$

Since the meridian curvature k_1 is

$$k_1 = \frac{d\phi}{ds} \tag{2.106}$$

we have

$$\frac{d(N_1 r)}{ds} - Q_1 r k_2 - N_2 \cos\phi = 0 \tag{2.107}$$

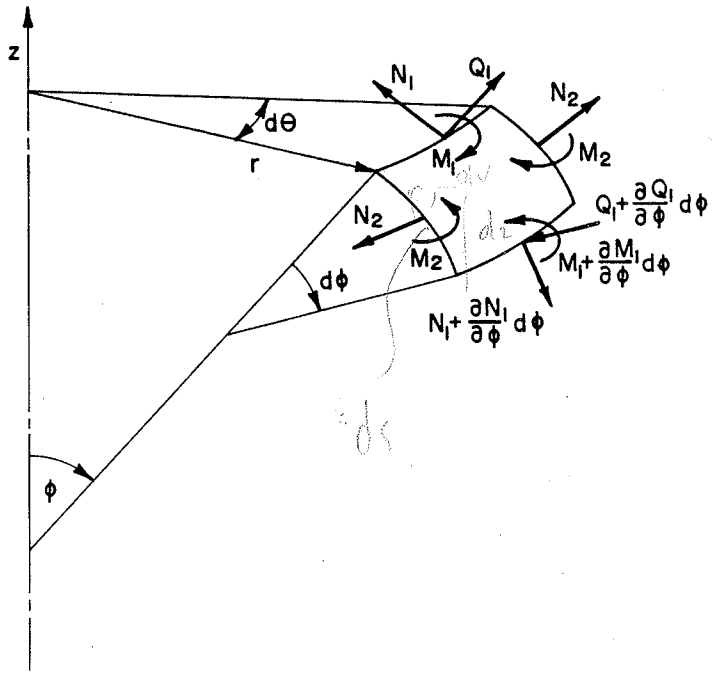

Figure 2.7 Resultants Acting on an Element of Middle Surface

For equilibrium with respect to the direction normal to the meridian, and with respect to rotation about a parallel, we have respectively

$$\frac{d(Q_1 r)}{ds} + N_1 r k_2 + N_2 \sin\phi - qr = 0 \tag{2.108}$$

and

$$\frac{d(M_1 r)}{ds} - M_2 \cos\phi - Q_1 r = 0 \tag{2.109}$$

where q is the outward directed pressure force acting on the element. Note that these equations are in terms of the Eulerian or deformed coordinates.

The stress resultants N_1, N_2, M_1 and M_2 depend on the strain field, as determined from the middle surface geometry, and the constitutive equations which are embodied in the strain energy function W. When deflections are small and fibers normal to the middle surface remain unchanged in length and normal to the middle surface after deformation, normal and bending stress resultants are given by

$$N_i = \int_{-T/2}^{T/2} T_{ii}(N)\, dN \tag{2.110}$$

$$N_i = \int_{-T/2}^{T/2} \frac{\partial w}{\partial \lambda_i}\, dN = \frac{\partial}{\partial \lambda_i} \int_{-T/2}^{T/2} w\, dN = \frac{\partial W}{\partial \lambda_i} \tag{2.111}$$

$$M_i = \int_{-T/2}^{T/2} N T_{ii}(N)\, dN \tag{2.112}$$

and

$$M_i = \int_{-T/2}^{T/2} \frac{\partial w}{\partial k_i}\, dN = \frac{\partial}{\partial k_i} \int_{-T/2}^{T/2} w\, dN = \frac{\partial W}{\partial k_i} \tag{2.113}$$

where N_i is the normal stress resultant,

N is the transverse Lagrangian coordinate,

M_i is the bending stress resultant,

$T_{ii}(N)$ is the normal stress in the i-direction in a sheet of material at transverse position N,

T is the undeformed shell thickness.

w is the strain energy per unit of undeformed volume, and

W is the strain energy per unit of undeformed middle surface.

When the normal fibers are permitted to change in length, the expressions (2.110) and (2.112) given above for N_i and M_i are only approximately correct. These expressions do not account for such effects as the change in the moment arm in the bending resultant expression. The expressions (2.111) and (2.113), however, are exact [45, Section 5.5] and show that the stress resultants are given by the partial derivatives of the local shell energy W with respect to the middle surface strains and final curvatures. The constitutive equations can then be written as

$$\begin{aligned} N_1 &= N_1(K_1,K_2,k_1,k_2,\lambda_1,\lambda_2) \ , \\ N_2 &= N_2(K_1,K_2,k_1,k_2,\lambda_1,\lambda_2) \ , \\ M_1 &= M_1(K_1,K_2,k_1,k_2,\lambda_1,\lambda_2) \ , \\ M_2 &= M_2(K_1,K_2,k_1,k_2,\lambda_1,\lambda_2) \ . \end{aligned} \tag{2.114}$$

Six geometric relationships are required to complete the classical problem formulation. From Figure 2.7 we have

$$\frac{dr}{ds} = \cos\phi \tag{2.115}$$

and

$$\frac{dz}{ds} = \sin\phi \tag{2.116}$$

From Section 2.1 we know the deformed middle surfaces strains and curvatures to be

$$\lambda_1 = \frac{ds}{dS} \quad , \tag{2.117}$$

$$\lambda_2 = \frac{r}{R} \quad , \tag{2.118}$$

$$k_1 = \frac{d\phi}{ds} \quad . \tag{2.119}$$

$$k_2 = \frac{\sin\phi}{r} \quad , \tag{2.120}$$

Together, the three equilibrium equations, (2.107 to 2.109) four constitutive equations, (2.114) and six geometric equations, (2.115 to 2.120) constitute a total of thirteen field equations. They collectively determine the thirteen unknowns N_1, N_2, M_1, M_2, Q_1, λ_1, λ_2, k_1, k_2, s, r, z and ϕ.

CHAPTER 3

NUMERICAL ANALYSIS

3.1 INTRODUCTION

We are interested in the class of thin shells for which the loads and deformations are axisymmetric. Although these shells are completely described by a single meridian of their middle surface, it is rarely possible to find their deformation by strictly analytical methods. Solution of most practical problems, and virtually all nonlinear problems requires the use of numerical techniques.

Most numerical approaches determine the displacement of the meridian from its rest configuration, or from some previous configuration. Its actual position, if required, is calculated as the vector sum of its rest, or previous position, plus its displacement. Since we are concerned with gross changes in shape, it is expedient to deal directly with the meridian position (rather than using displacement). A numerical representation of the meridian must therefore include the rest meridian configuration, as well as all deformed meridian configurations.

This section outlines certain general requirements which a numerical representation of the meridian must have, and shows that a piecewise representation is preferred, since the energy minimization technique used here requires that derivatives of the total shell energy with respect to meridian position be calculated. Section 3.2 presents a particular piecewise representation or discrete element, and shows that it satisfies the general requirements set forth in Section 3.1. The energy of an element is calculated using Equation (2.103), which gives the local strain energy of the shell per unit of undeformed middle surface, and Gaussian quadrature to integrate this quantity over the area of the element. The

total potential energy of the shell is the sum of these elemental strain energies and the work done by external forces. The final section presents an iterative numerical descent scheme which uses the gradient and Hessian of the total potential energy with respect to the meridian position, together with line search, to find the meridian positions(s) of lowest energy. These positions correspond to the static equilibrium configurations of the shell under the particular given load.

The first and most important step in analysis is to find a suitable numerically tractable representation of the meridian. See Irons[36, Section 8.5] for disconcerting examples of representations which are surprisingly ineffective.

Suppose we represent the meridian parametrically, as shown in Figure 3.1 in terms of functions

$$r = f(S)$$
$$z = g(S) \qquad (3.1)$$

where r,z are the radial and axial positions of points of the deformed meridian,

S is a parameterization of the undeformed meridian, and

f(S),g(S) are functions giving the radial and axial positions of points parameterized by S.

Unlike other common representations, this one describes highly convoluted configurations without difficulty. Since the functions f(S) and g(S) cannot in general be found analytically, we must represent them numerically;

$$f(S) = F(c_j, S) \quad j = 1 \text{ to } m$$
$$g(S) = G(c_k, S) \quad k = m + 1 \text{ to } n \qquad (3.2)$$

where $F(c_j, S)$, $G(c_k, S)$ are numerical representations of f and g, and

c_i are a finite number n of constants.

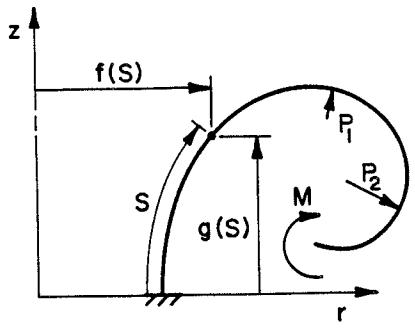

Figure 3.1 Functional Representation of Meridian

These functions are often defined as a linear combination of a set of basis functions $\phi_i(S)$; i.e.

$$f(S) = F(c_i, S) = c_i \phi_i(S)$$

$$g(S) = G(c_k, S) = c_k \phi_k(S) \qquad (3.3)$$

Hencky [30] and Way [87], for example, use power series representations to analyze the nonlinear behaviour of a circular plate. Representations in terms of orthogonal functions, such as Fourier Series, though they are more complicated than power series, are often preferred. However, the particular advantages of orthogonal functions are usually precluded in nonlinear problems.

A drawback of solutions in the form of Equation (3.3) is that adjustment of any one constant c_i will, in general, alter the entire meridian. This drawback is particularly serious here, since as shown in Section 3.3, the constants c_i are found by minimization of the total potential energy $\bar{U}(c_i)$ using its partial derivatives $\frac{\partial \bar{U}}{\partial c_i}$ and $\frac{\partial^2 \bar{U}}{\partial c_i \partial c_j}$. When the quantities c_i affect the entire meridian, numerical calculation of these derivatives requires integration of their effect along the entire meridian. If the quantities c_i only affect the displacement over

some small length of the meridian, however, the calculation of the required derivatives is considerably simplified.

Let the constants c_i be chosen such that triplets of quantities c_i represent the radial, axial and angular positions of distinct points or nodes n_j along the meridian, as shown in Figure 3.2. Further, assume that the shape of the meridian between any two nodes n_j and n_{j+1} is uniquely determined by the six quantities c_i describing the positions of n_j and n_{j+1}. This type of representation gives rise to so-called discrete element methods. A popular form of discrete element analysis which is used extensively to study shells [32,33,56,59 et cetera] is the finite element method (F.E.M.). The F.E.M. embodies certain specific formulation and solution procedures to calculate displacements. See references [8,36,54 and 90]. The method presented here is motivated directly by energy considerations and although certain steps in the method can be shown to be similar to the F.E.M., the motivation is different. Also, position rather than displacement is solved for.

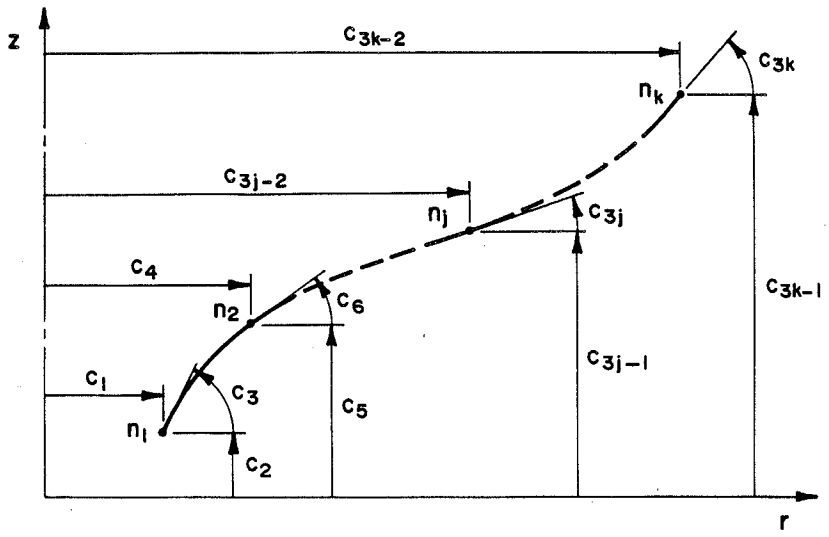

Figure 3.2 Numerical Representation of Meridian

Finite elements used to represent a structure must possess certain properties [54, Chapter 8] if their success is to be guaranteed. (Finite element formulations which do not possess all of these properties are sometimes successful. See [54,36]). These properties are associated with rigid body motion, element conformity, and element completeness. In general, an element must be able to undergo rigid body motion without inducing strain within itself if it is to be satisfactory. This requirement is clear from the well known fact that any displacement field can be broken into two components. One component produces strain, and the other, known as the rigid body component does not. If the rigid body component of displacement, which is often a significant portion of the displacement, is not accurately represented, either the total displacement field or its strain producing components will be in error. In either case, the numerical solution will be in error. Sufficiently good rigid body displacements are provided by standard polynomial displacement fields when element rotations are small. When displacements, and particularly rotations are large, as is the case here, special formulations are required to ensure that rigid body motion of the element does not induce internal strain and consequently internal stress.

The set of all physically possible solution meridians forms an infinite dimensional set V_∞. Numerical solutions, however, can at most span an n-dimensional set V_n since they must be represented by a finite quantity n of numbers. The difference between the exact solution in V_∞ and the solution found in V_n is the amount by which the numerical solution is in error. Unfortunately, no reliable technique has yet been found to estimate maximum bounds on this error for nonlinear problems. Indeed, even the error analysis of linear problems [8, Chapter 2] is far from complete.

While it is very difficult to estimate the magnitude of the error associated

with any particular discrete element representation, as compared with the exact solution, we would hope that this error would decrease as more elements are used and as the size of the finite elements decreases. That is, we desire the discrete element representation to converge to the exact solution as the set V_n becomes a larger subset of V_∞. Conditions under which convergence can be assured are only available for the linear F.E.M. Proof of convergence generally requires a great deal of work, is not necessarily even possible using the mathematical methods currently available, and is therefore beyond the scope of this thesis.

Fortunately, the limited but very useful convergence criteria which have been established for linear analysis can be applied here. Arguments to show this can be made in either the analytical domain or in the numerical domain. In the analytical domain, one can appeal to the common mathematical practice of linearizing nonlinear problems. Conclusions drawn from the solution to the linearized problem are argued to apply at least approximately to that region of the nonlinear problem which is close to the linearized solution. In the numerical domain one can argue that since the energy minimization technique used here can be thought of as a step-wise linearization of the generalized finite element problem, (as shown in Section 3.3), it is possible to take advantage of the convergence theorems which have been established for linear finite element analysis.

An assemblage of elements is said to be conforming if the position of the meridian and its derivatives up to order p - 1 (slope, curvature, et cetera) as measured along the meridian are continuous across boundaries between elements, when the highest order derivative appearing in the potential energy function $\bar{U}(X_i)$ is p . An alternate and practically equivalent definition [8, Section 2.1] of a

conforming representation is that the set V_n all of its members be a subset of the set $V\infty$ of all physically possible solutions; i.e.

$$V_n \subset V\infty \tag{3.4}$$

The conformity criterion is physically reasonable. It is particularly clear from the form of this criterion given in Equation (3.4), for example, that conic segments are not satisfactory for representation of a shell. Sudden changes of slope in the meridian direction do not occur physically, even under (non-dense) point loads. Furthermore, the derivative form of the criterion is violated by this representation as the local curvature (second derivative of position), which is used in the functional, is not correct when the slope (first derivative) is not continuous across element boundaries. If a membrane is being modelled, however, the functional does not contain bending energy associated with shell curvature, and a representation by conic segments is quite satisfactory. Furthermore, the criterion of Equation (3.4) is satisfied, as membranes can deform physically to shapes represented by conic segments.

A linearly independent basis $\phi_i(\mathbf{X})$ is said to be complete if any arbitrary function $f(\mathbf{X})$ can be approximated to any desired degree of accuracy by a linear combination of a sufficient number m of bases; i.e.

$$\left\| \sum_{i=1}^{m} c_i\phi_i(\mathbf{X}) - f(\mathbf{X}) \right\| \leq \varepsilon, \ \forall \mathbf{X}, \ m > M \tag{3.5}$$

where $\| \cdot \|$ is a suitable norm,

$\mathbf{X} = (X_1, X_2, X_3, \ldots X_n)$,

c_i are constants,

ε is an arbitrarily small non-negative number, and

M, m are integers.

Since the class of arbitrary functions $f(\mathbf{X})$ spans an infinite-dimensional space, an infinite number of bases $\phi_i(\mathbf{X})$ will in general be required as $\varepsilon \to 0$. Any numerical representation will have a finite number of bases (one associated with each nodal degree of freedom), and consequently will not be complete in the mathematical sense unless the element size is made arbitrarily small. The finite element representation is said to be complete for purposes of convergence if the meridian position (slope and curvature) and those of its meridian derivatives which appear in the functional, tend to their exact values over an element as the element size tends to zero. This criterion is also physically reasonable, as the solution method works in the domain of the total potential energy functional. For the solution to converge to the exact solution, the potential energy functional and all quantities used in its calculation must also converge to their exact values. A complete polynomial ($R = a_0 + a_1 x + a_2 x^2 + \ldots + a_p x^p$), of order p, for example, is complete [54, Section 8.3] in this sense if p is the highest order derivative appearing in the functional.

It has been shown by Oliviera [58] for complete polynomials and the Ritz method, and by Oden [56] for more general interpolation functions that completeness and conformity, as defined above, are sufficient conditions for convergence of a linear finite element representation. It has been further shown by Oden [56, Theorem 10.6], that a sequence of finite element representations will generate a sequence of solutions which not only converge, but which converge monotonically to the exact solution if:

1) The element representation satisfies the completeness and conformity conditions given above,
2) Successive representations are regular in that every node and interelement boundary of one model is a node and interelement boundary

respectively of the next refined model,

3) Successive representations are uniform in that the maximum distance between any two points on any one element decreases, and

4) Any condition which can be represented at one level of refinement can be represented at the next.

A practical test for convergence has been proposed by Irons [34,35] and proved mathematically by Strang [74]. See Irons [36, Chapters 9 and 25] for a discussion of the test and its implications. This so-called patch test requires that a patch of elements containing at least one node which is completely surrounded by elements, be loaded by specification of either edge loads or displacements which produce a state of uniform strain. The resulting stresses, strains, displacements and reactions must all be correct to 5 or 6 digits, in order for the element to pass this test. More complex strain states can also be used.

It is worth noting that any discrete element model will, in general, be stiffer than the structure it is modelling. The discrete element model is more severely restrained than the body it is representing, since the model is limited to those deformations accommodated by its shape functions. For linear problems, deflections predicted by a discrete element analysis will be slightly smaller than their true values. However, for nonlinear problems where the load-deflection relationship is not monotonic, such as for a point loaded spherical cap, predicted deflections, even at the point of load application, are sometimes too large.

3.2 ELEMENT FORMULATION

The success of the numerical analysis of a shell is intimately related to the representation which is used. In the previous section, the general requirements of a local representation or element as embodied in conformioty, completeness and rigid body properties are presented. Here, we derive a specific element and

show that it meets these requirements. The derivation of an element, or family of elements, can often be achieved using strictly mathematical arguments. However, the author, like many, finds it more instructive to devise an element which embodies the essential behavior of the structure being modelled, and then to check that it has the necessary mathematical properties.

The class of shell problems of interest here requires a discrete element which will represent the axisymmetric membrane and bending behavior of thin shells. It must accommodate large displacements, rotations and strains; and it should allow efficient computation of the total shell energy. The element shown in Figure 3.3 is designed to fulfill these criteria.

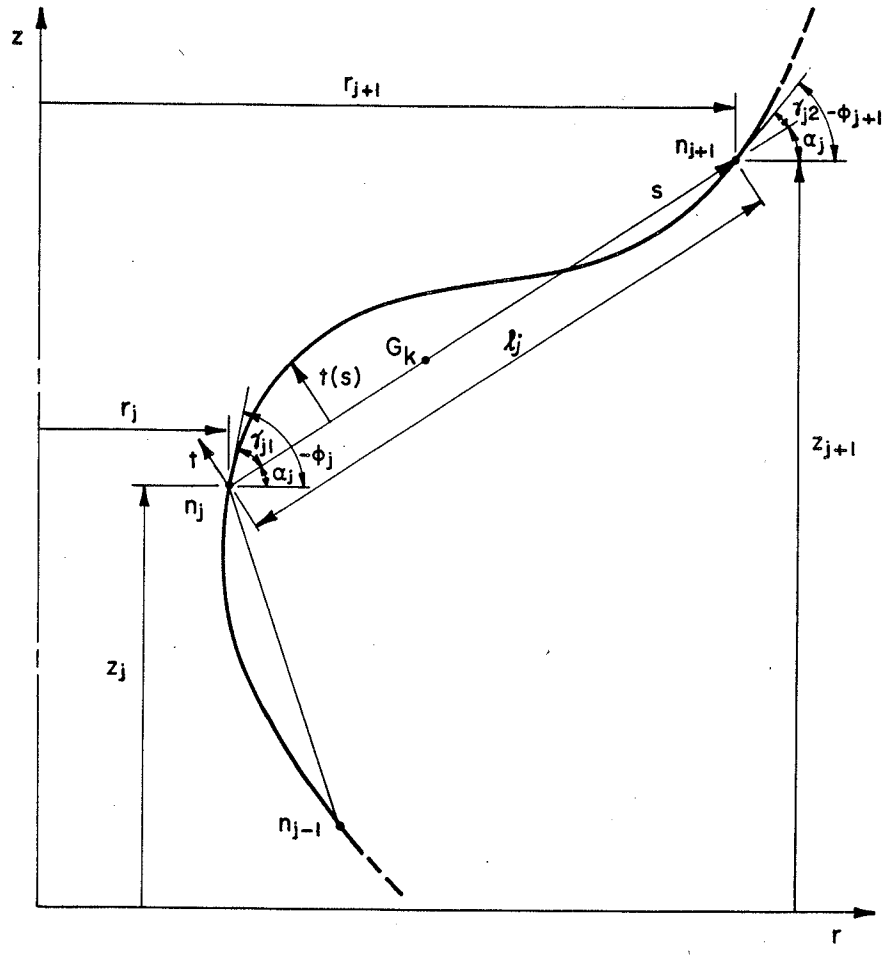

Figure 3.3 Element Formulation

This element is formed by first constructing a directed line segment from the j^{th} node n_j of the meridian to the next successive node n_{j+1}. This line segment, s , together with its normal t , provide a local rectangular cartesian coordinate system for the element. The local coordinate system s-t is chosen over the global coordinate system r-z as the former is free to rotate: a feature which is particularly desirable for analysis of problems such as the elastica where large rotations occur. The parameter s is defined as a natural coordinate; and varies from 0 at n_j to 1 at n_{j+1}. The meridian must next be described uniquely in terms of coordinates s and t by the six nodal quantities r_j , z_j , ϕ_j , r_{j+1} , z_{j+1} and ϕ_{j+1} . This can be accomplished by considering the components in the s and t directions separately since the displacement in the t direction over an element is assumed to be small, compared with its length.

Assume the strain in the s direction to be uniform. This assumption in the standard finite element formulation would imply use of shape functions (s) and (1-s) for the position in the s direction. Alternatively, this strain could be defined to vary linearly from node to node. Linear variation is perhaps a more appropriate assumption for problems such as snapthrough of a hemispherical cap which involves considerably variable meridian strains and which could therefore be modelled by significantly fewer slightly more complex elements. The net result would be an equally good representation of the meridian in terms of fewer variables. The problem of varying meridian strains was anticipated in connection with the hemisphere problem discussed in Chapter 5. However, linear variation of meridian strain was deemed unnecessary complication in view of the resulting mathematical complications, and the fact that nearly uniform meridian extensions were anticipated in all the other problems - namely the plate and cylinder - considered here.

Let transverse position t take the shape of a cubic

$$t(s) = as + bs^2 + cs^3 \qquad (3.6)$$

The coefficients a, b and c are uniquely and easily determined from the node angles γ_{ji}. The transverse meridian position t(s), slope m(s) and curvature c(s) of the j^{th} element with respect to the s-t coordinate system in terms of γ_{ji} are

$$t(s) = \gamma_{j1}\ell_j s(1-2s + s^2) + \gamma_{j2}\ell_j s(- s + s^2) \tag{3.7}$$

$$m(s) = \frac{1}{\ell_j}\frac{dt}{ds} = \gamma_{j1} (i -4s + 3s^2) + \gamma_{j2}(-2s + 3s^2) \tag{3.8}$$

and

$$c(s) = \frac{1}{\ell_j{}^2}\frac{d^2t}{ds^2} = \frac{\gamma_{j1}}{\ell_j} (-4 + 6s) + \frac{\gamma_{j2}}{\ell_j}(-2 + 6s) \tag{3.9}$$

Other forms could have been assumed for t(s), but the incomplete cubic given in Equation (3.6) is both simple and effective. Note from Equation (3.7) that the two transverse shape functions which would be associated with a standard finite element analysis are $\ell s(1-2s + s^2)$ and $\ell s(-s + s^2)$. The choice of uniform strain in the s direction and cubic transverse position provides a piecewise cubic model of the meridian.

Evaluation of local strain energy per unit of undeformed middle surface using Equations (2.100) and (2.103) requires that the quantities K_1, K_2, k_1, k_2, λ_1 and λ_2 be known.

$$A_1 = \left(\frac{k_1}{\lambda_2} - K_1\lambda_1\right)$$

$$A_2 = \left(\frac{k_2}{\lambda_1} - K_2\lambda_2\right) \tag{2.100}$$

$$W = C_1 \left[(\lambda_1^2 + \lambda_2^2 + \frac{1}{\lambda_1^2\,\lambda_2^2} - 3)t + \left(A_1^2 + A_2^2 + \frac{3A_1^2}{\lambda_1^4\,\lambda_2^2} + \frac{4A_1\,A_2}{\lambda_1^3\,\lambda_2^3} + \frac{3A_2^2}{\lambda_1^2\,\lambda_2^4}\right)\frac{t^3}{12}\right.$$

$$+ C_2 \left[\left(\frac{1}{(\lambda_1^2 - \frac{A_1^2 t^2}{4})} + \frac{1}{(\lambda_2^2 - \frac{A_2^2 t^2}{4})} + \lambda_1^2\,\lambda_2^2 - 3\right)t\right.$$

$$\left.\left. + (\lambda_2^2\,A_1^2 + 4\lambda_1\,\lambda_2 A_1 A_2 + \lambda_1^2\,A_2^2)\,\frac{t^3}{12}\right]\right] \qquad (2.103)$$

The intermediate quantities L, R, Φ, K_1 and Z in the undeformed state and corresponding quantities ℓ, r, ϕ, k_1 and z in the deformed state are found using Equations (3.7) to (3.9) and Figure 3.3 to be

$$L, \ell = \sqrt{(r_{j+1} - r_j)^2 + (z_{j+1} - z_j)^2}\ , \qquad (3.10)$$

$$R(S),\ r(s) = r_j(1-s) + r_{j+1}(s) - t(s)\sin\alpha_j\ , \qquad (3.11)$$

$$\Phi(S)\ ,\ \phi(s) = \alpha_j + \tan^{-1}(m(s))\ , \qquad (3.12)$$

$$K_1(S)\ ,\ k_1(s) = c(s)\ , \qquad (3.13)$$

and

$$Z(S),\ z(s) = z_j\,(1-s) + z_{j+1}(s) + t(s)\cos\alpha_j\ . \qquad (3.14)$$

Evaluation of Equations (3.10) to (3.14) in the undeformed and deformed configurations gives upper and lower case quantities, respectively. The local

curvatures and stretches are then found using geometric Equations (2.117) to (2.120) to be

$$\lambda_1 = \frac{ds}{dS} \simeq \frac{\ell}{L} \quad , \tag{3.15}$$

$$\lambda_2 = \frac{r}{R} \simeq \frac{r(s)}{R(S)} \quad , \tag{3.16}$$

$$K_1, k_1 = \frac{d\phi}{ds} \simeq c(s) \quad , \tag{3.17}$$

and

$$K_2, k_2 = \frac{\sin\phi}{r} \simeq \frac{\sin\phi(s)}{r(s)} \quad . \tag{3.18}$$

Evaluation of the strain energy $\bar{W}_j$ associated with the j^{th} element is accomplished by Gaussian quadrature using n Gauss points G_k and is given by

$$\bar{W}_j = \sum_{k=1}^{n} 2\pi R(G_k)\ f_k W(G_k) \tag{3.19}$$

where f_k are the standard Gauss weighting factors for n-points, and $R(G_k)$ is the radial position of the point G_k before deformation. For two Gauss points, as used exclusively here for calculations,

$$\bar{W}_j = \frac{1}{2} W(0.2113) + \frac{1}{2} W(0.7887) \tag{3.20}$$

Elements are pieced together end to end with the position and rotation of adjacent ends matched. Boundary conditions which take the form of restraints are imposed on appropriate nodal degrees of freedom. The total strain energy

is simply the sum of the elemental strain energies;i.e.

$$\overline{W} = \sum_{j=1}^{k} \overline{W}_j \tag{3.21}$$

Applied loads are introduced at the nodes. In the case of distributed normal and tangential loads q_t and q_s respectively, equivalent nodal loads are easily calculated [36, Chapter 5] using shape function matrix **N** by the familiar equation [90, Equation 2.15]

$$\mathbf{f} = \int_0^1 \mathbf{N}^T \mathbf{q} \, ds \tag{3.22}$$

or in detail

$$\begin{Bmatrix} f_{s_j} \\ f_{t_j} \\ f_{m_j} \\ f_{s_{j+1}} \\ f_{t_{j+1}} \\ f_{m_{j+1}} \end{Bmatrix} = \ell \int_0^1 \begin{Bmatrix} 1 - 3s^2 + 2s^3 & 0 \\ 0 & 1 - s \\ \ell s(1 - 2s + s^2) & 0 \\ 3s^2 - 2s^3 & 0 \\ 0 & s \\ s(-s + s^2) & 0 \end{Bmatrix} 2\pi t(s) \begin{Bmatrix} q_s \\ q_t \end{Bmatrix} ds \tag{3.23}$$

The meaning of the terms is clear form Figure 3.4. The terms in shape function matrix **N** are approximations only and ignore coupling effects. Equation (3.23) however, has proved quite satisfactory for the research presented herein - possibly because it is used in conjunction with an iterative solution technique.

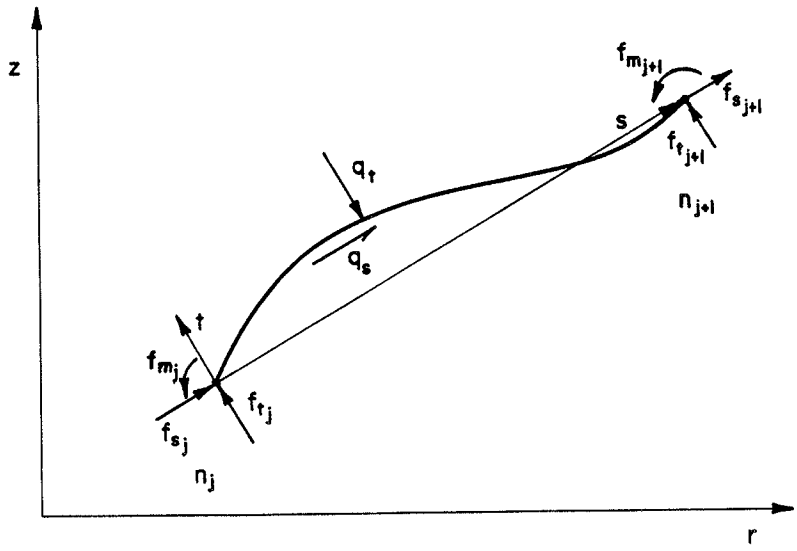

Figure 3.4 Equivalent Nodal Loads

The element proposed above must now be shown to satisfy the physical requirements discussed in Section 3.1. Recall that these requirements are associated with rigid body motion, element conformity, and element completeness. Consideration of Equations (3.10) to (3.14) in connection with Equations (3.15) to (3.18) shows that rigid body motion - which physically can only occur in the axial or z-direction - does not change the middle surface parameters k_1, k_2, λ_1 and λ_2, and consequently does not affect the stress and strain in the element. When the initial shell diameter is large compared with its other dimensions, radial strains become negligible and curvatures K_2 and k_2 become zero. This occurs, for example, in the relatively short cylinders discussed in Chapter 6. The shell problem is reduced to a two-dimensional rod or elastica problem. Rigid body motion in the radial direction and rotation about a parallel are then possible. Again, consideration of the element formulation shows that stress and strain are not affected by these rigid body motions, when radial strain is neglected and curvatures K_2 and k_2 are taken as zero. Considerable care was exercised in the design of the element to ensure that unlimited rigid body motion of the three kinds noted above induced

no strains in the element. Most element formulations are strain free only for infinitesimal rigid body motions.

To ensure convergence of the numerical solution, position and it derivatives (slope and curvature) up to order p - 1 as measured along the meridian must be continuous across element boundaries when the highest order derivative occurring in the functional is p . From Equations (3.17) it is clear that the highest order derivatives required for calculation of the shell energy $\bar{W}$ are the meridian curvatures

$$K_1 = \frac{d\Phi}{dS} \tag{3.24}$$

and

$$k_1 = \frac{d\phi}{ds} \tag{3.25}$$

Hence both position and slope, (its first derivative) must be continuous across each node. This criterion is satisfied since, as noted earlier in this section, the model makes the displacement and slope of adjacent elements the same at each node. Alternatively, by Equation (3.4) one can show that all numerical representations are (at least theoretically) physically possible.

Finally, it is necessary to show that the element formulation is complete. This can be done by showing that each of the quantities K_1, K_2, k_1, k_2, λ_1 and λ_2 approach their exact values over the element as the element size tends to zero. Since these quantities depend only on $R, \Phi, K_1, r, \phi, k_1$ and λ_1 it is sufficient to show that this latter set approach their correct values. That R, Φ, r, ϕ and λ_1 approach their correct limiting values as the element size tends to zero is clear from examination of Figure 3.3. Any doubt about meridial curvatures K_1 and k_1 approaching their correct values over the element can be alleviated by considering a short element of length ℓ whose curvature is k. Then by setting

$$\gamma_1 = -\gamma_2 = \frac{-k\ell}{2}$$

$k_1 = k$ and the element boundary conditions are satisfied. From Equation (3.9),

$$c(s) = -\frac{k\ell}{2\ell}(6s-4) + \frac{k\ell}{2\ell}(6s-2)$$

$$c(s) = k$$

as required. It can be shown by similar considerations, that all seven quantities above except λ can in fact vary linearly over a small element. Convergence is therefore expected [54, pp. 170-171] to be better than for an element which has only the minimum requirements for completeness.

As a practical verification of solution convergence, a patch of four elements representing a plate under plane strain was made. The element passed the patch test without difficulty, even for large strains and displacements ($\lambda_1 = \lambda_2 = 2$).

3.3 POTENTIAL ENERGY MINIMIZATION

As shown in the previous sections of this work, the total potential energy $\bar{U}$ of a shell, consisting of the sum of its strain energy $\bar{W}$ and the work done on it by external loads, can be calculated in terms of generalized coordinates **X**. It has further been shown that it is convenient to define the generalized coordinates **X** of an axisymmetric shell as triplets of numbers describing the radial, axial and angular positions of discrete points, or nodes along the shell meridian. In conjunction with methods discussed in the previous section to uniquely define the shell contour between nodes, the shell is completely determined by the values of the coordinates **X**. From considerations discussed in Section 2.4 it is known that the shell will be in static equilibrium in that configuration which locally has the least total potential energy. By careful formulation of the analysis, it has been possible to give a good representation of the axisymmetric configurations

of the shell in terms of coordinates $\mathbf{X}$, and to accurately represent the total potential energy $\bar{U}(\mathbf{X})$ of the shell using these coordinates. The balance of this chapter considers various numerically tractable schemes to find coordinates $\mathbf{X}^*$ which at least locally minimize $\bar{U}(\mathbf{X})$, and thereby represent deformed configurations of the shell which are in equilibriium under the applied load.

A host of numerical schemes [56,62,73] exist for minimization of a nonlinear scalar function

$$\bar{U} = \bar{U}(X_i) = \bar{U}(\mathbf{X}) \ . \tag{3.26}$$

of n independent variables X_i or $\mathbf{X}$. These schemes can be classified as sequential or nonsequential. Sequential techniques start from an initial test point and through a sequence of iterations find successively better estimates of $\mathbf{X}^*$. Most sequential techniques take the form of a descent method in that $\bar{U}(\mathbf{X})$ is reduced with each successive step. These can in turn be further classified as gradient, or search methods. Search methods generate sets of test points at each iteration and by discarding less suitable points generate sets of points, which are collectively successively closer to $\mathbf{X}^*$. Search techniques are well suited to analysis of problems where the hypersurface $\bar{U}$ or its lowest order derivatives are not well behaved, or easily calculated, and to diophantine problems. Sequential descent methods tend to converge to $\mathbf{X}^*$ more quickly than other methods, and hence are generally preferred when the hypersurface $\bar{U}(\mathbf{X})$ is everywhere continuous and at least once differentiable. Higher order methods converge more quickly but require regularity of higher order derivatives, as well. Sequential descent methods are generally preferred for analysis of solid mechanics problems, since the energy hypersurface $\bar{U}(\mathbf{X})$ is well behaved and all of its derivatives are regular.

The value of $\bar{U}(\mathbf{X} + \mathbf{D})$ at a point displaced $\mathbf{D}$ or in component form D_j from $\mathbf{X}$ is given by the Taylor series

$$\bar{U}\ (\mathbf{X}+\mathbf{D}) = \bar{U}(\mathbf{X}) + \frac{\partial U}{\partial X}\bigg|_{\mathbf{X}} D_i + \frac{1}{2} D_j \frac{\partial^2 U}{\partial X_j\ \partial X_k}\bigg|_{\mathbf{X}} D_k + \ldots \tag{3.27}$$

or $$\bar{U}(\mathbf{X}+\mathbf{D}) = \bar{U}(\mathbf{X}) + \mathbf{g}^T\mathbf{D} + \frac{1}{2}\ \mathbf{D}^T\mathbf{H}\ \mathbf{D} + \ldots \tag{3.28}$$

where $g_i = \frac{\partial \bar{U}}{\partial X_i}$ are the components of g, the gradient of $\bar{U}$ and describe its local slope, and

$H_{jk} = \frac{\partial^2 \bar{U}}{\partial X_j\, \partial X_k}$ is the Hessian of U and describes its local curvature and warp.

Note that **X** should be thought of as a column vector. The above equation can be used to find the value of **D** which minimizes $\bar{U}$ by setting

$$\mathbf{0} = \frac{\partial \bar{U}(\mathbf{X}+\mathbf{D})}{\partial \mathbf{D}} = \frac{\partial \bar{U}\ (\mathbf{X})}{\partial \mathbf{D}} + \mathbf{g}^T + \mathbf{D}^T\mathbf{H} + \ldots \tag{3.29}$$

or $$\mathbf{0} = \mathbf{0} + \mathbf{g} + \mathbf{D}^T\mathbf{H} + \ldots. \tag{3.30}$$

since **H** is symmetric. Equation (3.30) is easily solved for **D**, on the (physically reasonable) assumption that lower order terms of the Taylor series predominate, allowing only the first two terms of the equation to be retained. Then

$$\mathbf{H}\,\mathbf{D} = -\,\mathbf{g}$$

or

$$\mathbf{D} = -\,\mathbf{H}^{-1}\mathbf{g} \tag{3.31}$$

Figure 3.5 shows the projection of an energy surface $\bar{U}(X_i)$ where $i = 1,2$ onto the $X_1 - X_2$ plane. Contours of constant energy are shown. The r^{th}

displacement vector $\mathbf{D}^r$ calculated at $\mathbf{X}^r$ using Equation (3.30) is shown. The point

$$\mathbf{X}^{r+1} = \mathbf{X}^r + \mathbf{D}^r \tag{3.32}$$

physically corresponds to the minimum or vertex of that paraboloid P shown in the figure, which has the same slope and curvature as the surface $\bar{U}$ at $\mathbf{X}^r$. This observation applies similarly to n-hypersurfaces $\bar{U}$ and corresponding n-paraboloids. It is also clear from the figure, that it may be advantageous to move a greater or lesser distance than $|\mathbf{D}^r|$ in the direction indicated by $\mathbf{D}^r$. Hence we have

$$\mathbf{X}^{r+1} = \mathbf{X}^r + \alpha \mathbf{D}^r \tag{3.33}$$

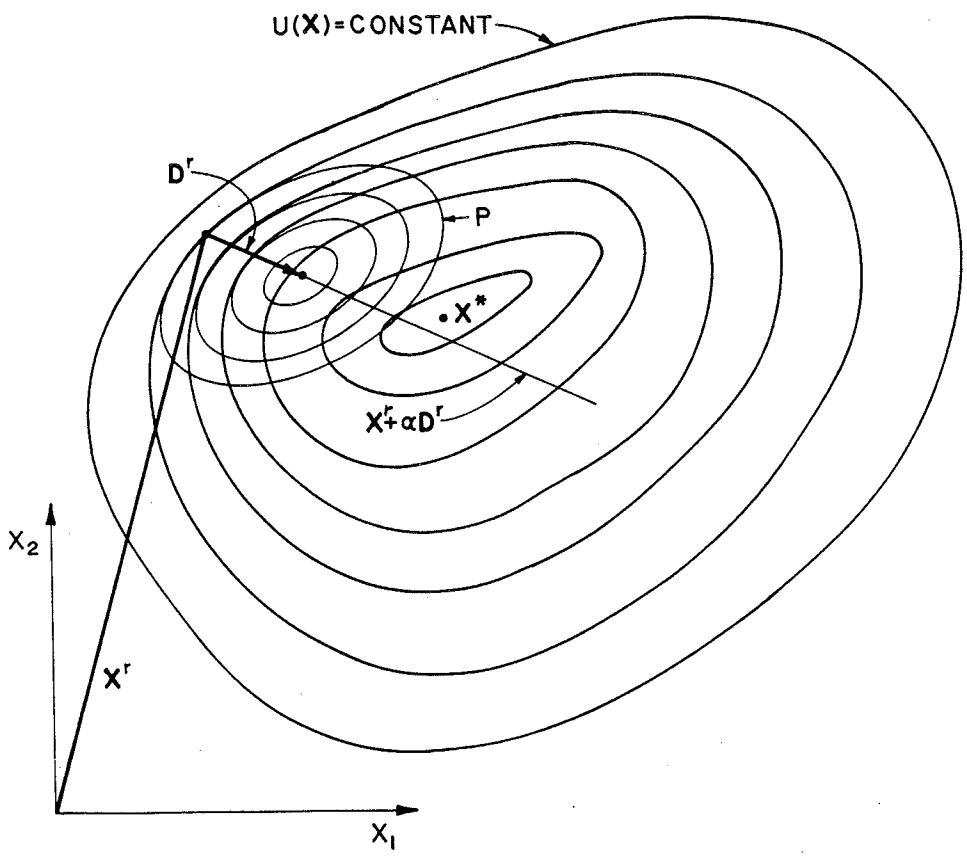

Figure 3.5 Projection of Energy Surface

where α is chosen by numerical sampling along the direction of $\mathbf{D}^r$ or so-called line search for each iteration to minimize $\bar{U}(\mathbf{X}^{r+1})$. This procedure is numerically efficient as evaluation of $\bar{U}(\mathbf{X}^r + \alpha\mathbf{D}^r)$ is much less costly in computer time than evaluation of $\mathbf{g}$ and $\mathbf{H}$.

Consider Equation (3.31) at $\mathbf{X} = \mathbf{X}^r$. The gradient $\mathbf{g}$ associated with the slope of the energy surface $\bar{U}$ at $\mathbf{X}^r$ has units of "force" and represents the imbalanced forces at each of the nodes. The second order tensor $\mathbf{H}$ has units of "force/length" and gives the (tangential) stiffness of the structure when it is in the configuration represented by $\mathbf{X}^r$. The incremental step $\mathbf{D}^r$ can be thought of as the displacement produced by imbalanced forces $\mathbf{g}$ acting on a structure of unchanging stiffness $\mathbf{H}$. In the language of the finite element method, we have

$$\mathbf{f} = \mathbf{K}\,\mathbf{x}$$

or

$$\mathbf{x} = \mathbf{K}^{-1}\,\mathbf{f} \tag{3.34}$$

cf.

$$\mathbf{D}^r = -\mathbf{H}^{-1}\,\mathbf{g} \tag{3.31}$$

where $\mathbf{X}$ is the incremental displacement,

$\mathbf{f}$ is the imbalanced force applied to the structure, and

$\mathbf{K}$ is its stiffness.

For a linear problem, the stiffness $\mathbf{H}$ (or $\mathbf{K}$) is constant and the change in position $\mathbf{D}^r$(or displacement $\mathbf{x}$) is found immediately from Equation (3.31) or Equation (3.34) by methods of linear algebra. For a linearized problem, the energy surface is a paraboloid and the equations solved by a linear finite element analysis and the equations solved by the method presented here are identical. Hence, as claimed earlier in this chapter, mathematical arguments regarding such things as

convergence derived for linearized finite element analysis are applicable here. When strains or displacements are large, the structure stiffness changes with $\mathbf{X}$, i.e. $\mathbf{H} = \mathbf{H}(\mathbf{X})$, and Equations (3.31) and (3.34) can no longer be solved directly.

The potential of actual or equivalent nodal loads $\mathbf{f}$ is

$$\bar{S} = -\mathbf{f}^T \mathbf{X} \tag{3.36}$$

where $\mathbf{f}$ is the load matrix given by Equation (3.22), and

$\mathbf{X}$ is the generalized displacement vector taken as $\mathbf{0}$ when the body is in its rest or unloaded state.

The total system energy $\bar{U}$ is the sum of the strain energy $\bar{W}$ in the shell and $\bar{S}$ the work done by external forces.

$$\bar{U} = \bar{W} + \bar{S} \tag{3.37}$$

Application of external loads $\mathbf{f}$ can be thought of as addition of a sloped hyperplane to the energy surface $\bar{W}$ or roughly, as tilting it. By increasing the nodal loads incrementally, a load-deflection relationship is produced. Not only is an incremental procedure more efficient than applying the loads needed to plot a nonlinear load-deflection curve in random order, but in the case of shells with multiple equilibrium states, it provides control over which equilibrium state is found.

A similar procedure, known as incremental loading, is often followed in nonlinear finite element analysis. Loads are applied in not necessarily equal increments $\mathbf{f}^r$ over the load range of interest. Incremental displacements $\mathbf{X}^r$ associated with the incremental load are calculated using an up-dated stiffness matrix $\mathbf{K}^r$ and the equation

$$\delta\mathbf{x}^r = (\mathbf{K}^r)^{-1} \delta\mathbf{f}^r \tag{3.38}$$

Errors are cumulative [57, p.288; 59, p.199] with each step of this process, since $\delta \mathbf{f}$ is the incremental load only, and does not include imbalanced forces caused by errors produced in previous iterations by such factors as possible variation of $\mathbf{K}$ within each previous step.

Since the total error increases with step size, hundreds of steps [33,p.179] may be required to keep errors within acceptable bounds. As an alternative, correcting procedures using a basic or modified Newton-Raphson method [56,pp.288-289] may be incorporated in the scheme. In constrast, the method presented here is self correcting and typically requires 10 to 20 iterations to solve for the meridian configuration associated with a large load, and may require as few as two or three iterations per step when moderate incremental loads are used.

For a discussion of other numerical techniques commonly used in structural mechanics, see Oden [56] (Newton-Raphson methods) and Rektorys [67] (variational methods, including the Ritz and Galerkin methods).

CHAPTER 4

UNIFORMLY LOADED CIRCULAR PLATE

4.1 INTRODUCTION

The following three chapters consider specific axisymmetric shell problems for which solutions exist over at least a limited load range. This chapter deals with the simplest axisymmetric shell - the circular plate. In particular, the behavior of clamped and simply supported plates with radial edge restraints are considered under uniform transverse loads.

The second section of this chapter presents the derivation of the so-called von Karman equations, paying special attention to the implications of the assumptions used. These two coupled fourth order differential equations are based on a simplified, but still nonlinear form of the strain-displacement relationships. Unlike the so-called linear equations which result from use of a linear strain-displacement relationship, and which are valid only for deflections small compared with the plate thickness, the von Karman equations accurately describe the plate until deflections are of the order of the plate thickness. The linear equations and the equations governing a membrane are shown to be special cases of the von Karman equations. Since this derivation illustrates the essential features of large deflection analyses, similar derivations will not be done for the shells discussed in subsequent chapters. The third section considers a number of analytical solutions - many of which begin with the von Karman equations, or their equivalent. These solutions include the linear solution of Lagrange; the nonlinear plate solutions of Nadai [51], Timoshenko [77], Way [87], Berger [7], and Goldberg [25]; and the membrane solution of Hencky [30].

The final section will compare in some detail, the analytical solutions of

Lagrange, Way, Berger, Hencky, and the author's numerical solutions. Stresses and deflections produced over a load range of 5 magnitudes will be considered as will stress and deflection profiles at selected loads.

Consider a circular plate of radius a and thickness h such as that shown in Figure 4.1, subjected to a transverse load q(r). Assume the material behavior

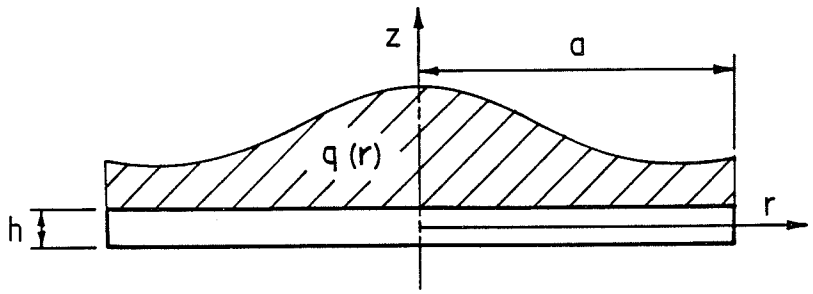

Figure 4.1 Transversely Loaded Plate

to be adequately described by two quantities E , Young's modulus and ν, Poisson's ratio. It would be equally reasonable to choose any number of material parameters, such as C_1 and C_2 associated with a Mooney-Rivlin constitutive equation, but E and ν are more useful for the comparisons which follow. If the load q(r) is uniform, then the plate is completely specified by its boundary conditions and five quantities: a, h, E, ν and q. From principles of dimensional similitude [75], it is known that h and E can be chosen arbitrarily as units of length and pressure, respectively, and that the plate is sufficiently specified by only three independent dimensionless quantities, or parameters. While many different mathematically equivalent triplets of parameters can be chosen, the geometric parameter a/h, material parameter ν, and load parameter qa^4/Dh suggested by the Lagrange solutions and a general knowledge of the problem are

perhaps the most useful. The dimensionless deflection w/h can then be written in terms of these parameters using a general function ; i.e.

$$\phi\left(\frac{a}{h}\ ,\ \nu\ ,\ \frac{qa}{Dh}\ ,\ \frac{w}{h}\right) = 0$$

Dimensionless stresses and radial deflections, of a form which are shown in Equations (4.52) are uniquely determined by the three parameters, a/h, ν and qa^4/Dh. Analysis and presentation of results is simplified considerably by reduction of the problem to dependence on these three quantities. Dimensional values of deflection and stress, should they be required, are easily obtained from their dimensionless counterparts.

4.2 GOVERNING EQUATIONS

We wish to consider the deformation of uniformly loaded plates with clamped and simply supported boundary conditions. In both cases, the edge is also restrained radially. Radial restrain does not affect the linear solutions, but has a significant effect [79, p402] on the nonlinear solutions. For the simply supported plate, the axial and radial deflections w and u respectively, at its outer edge $r = a$ are zero

$$w\Big|_{r=a} = u\Big|_{r=a} = 0$$

as is its radial moment M_r.

$$M_r\Big|_{r=a} = 0$$

For the clamped plate axial and radial deflections w and u are again zero

$$w\Big|_{r=a} = u\Big|_{r=a}$$

but in this case the edge rotation is set to zero by making

$$\left.\frac{dw}{dr}\right|_{r=a} = 0 \ .$$

For the sake of completeness, the linear Lagrange equation for the infinitesimal deflection of a transversely loaded plate is presented. Solutions of this equation for uniformly loaded clamped and simply supported plates are included. The so-called von Karman equations governing the nonlinear axisymmetric deflection of circular plates are then derived. They are then compared with the linear equations to identify and provide an understanding of the additional terms in the nonlinear equations. The von Karman equations for non-axisymmetric deformations are also given in polar and rectangular cartesian coordinate forms.

When a plate is subjected to transverse loading q(r) and its deflections are small compared with the plate thickness, its transverse deflection w(r) is given by the Lagrange equation

$$\nabla^4 w \equiv \left(\frac{d^2}{dr^2} + \frac{1}{r}\frac{d}{dr}\right)\left(\frac{d^2w}{dr^2} + \frac{1}{r}\frac{dw}{dr}\right) = \frac{q}{D} \qquad (4.1)$$

where D is the flexural rigidity of the plate given by

$$D = \frac{Eh^3}{12(1-\nu^2)} \qquad (4.2)$$

where E is Young's modulus and

ν is Poisson's ratio for the plate material.

The derivation of this equation is shown in most strength of materials texts and is a special case of the nonlinear equations derived subsequently in this section. No membrane strains or displacements are predicted as a result of transverse loading.

The transverse deflection w, and bending stresses σ^b for a uniformly loaded clamped plate are:

$$w = \frac{qa^4}{64D}\left(\frac{r^4}{a^4} - 2\frac{r^2}{a^2} + 1\right) \tag{4.3}$$

$$\sigma_r^b = \frac{-3qa^2z}{4h^3}\left[(3+\nu)\frac{r^2}{a^2} - 1 - \nu\right] \tag{4.4}$$

and

$$\sigma_\theta^b = \frac{-3qa^2z}{4h^3}\left[(1+3\nu)\frac{r^2}{a^2} - 1 - \nu\right] \tag{4.5}$$

where $z = [-h/2, h/2]$ is the transverse position of a generic point from the deformed middle surface.

For a uniformly loaded simply supported plate, solution of Equation (4.1) gives

$$w = \frac{qa^4}{64D}\left[\frac{r^4}{a^4} - 2\frac{(3+\nu)}{(1+\nu)}\frac{r^2}{a^2} + \frac{(5+\nu)}{(1+\nu)}\right] \tag{4.6}$$

$$\sigma_r^b = \frac{3qa^2z}{4h^3}(3+\nu)\left(1 - \frac{r^2}{a^2}\right) \tag{4.7}$$

and

$$\sigma_\theta^b = \frac{3qa^2z}{4h^3}\left[3 + \nu - (1+3\nu)\frac{r^2}{a^2}\right] \tag{4.8}$$

The linear solutions result from using the most elementary strain-displacement relations and are valid only when strains are very small, and when deflections are small compared with the plate thickness. Here we use a second order strain-displacement relation. The resulting equations are valid for small strains and for deflections as large as the plate thickness. Timoshenko [79, p. 48] shows that the range over which a solution is valid is governed by the ratio of maximum deflection to plate thickness. This criterion is more stringent than the maximum slope criterion which governs beams, and which might be expected to apply here as well.

Consider the class of axisymmetric plates for which the following assumptions

are valid:

1. The plate is thin, $h << a$.
2. The Kirchoff hypothesis holds; i.e., fibers normal to the undeformed middle surface remain normal to it after deformation and do not change length.
3. The transverse deflection w is small compared with the outer radius a and does not exceed the order of the plate thickness.
4. The slope is everywhere small.
5. Radial strains are infinitesimal.
6. Hooke's Law holds.

These assumptions are the same as those made in the linear analysis, except that the linear analysis does not allow the radial strains implicitly permitted by assumption (5) here, and the transverse deflection (3) is assumed small compared with the plate thickness. Consider the axisymmetric deformation of an axisymmetric plate of uniform thickness h. Let its transverse and radial deflections be given by $w(r)$ and $u(r)$, respectively. The radial strain ε_r of the middle surface as shown in Figure 4.2 is

$$\varepsilon_r = \sqrt{\left(1 + \frac{du}{dr}\right)^2 + \left(\frac{dw}{dr}\right)^2} - 1 \tag{4.9}$$

$$= \frac{du}{dr} + \frac{1}{2}\left(\frac{dw}{dr}\right)^2 - \frac{1}{2}\frac{du}{dr}\left(\frac{dw}{dr}\right)^2 + \cdots \tag{4.9a}$$

$$\approx \frac{du}{dr} + \frac{1}{2}\left(\frac{dw}{dr}\right)^2 \tag{4.10}$$

since by assumptions (5) and (4), respectively du/dr is assumed infinitesimal and dw/dr is assumed to be small. See Donnell [17] for an alternate derivation. The

only difference between the derivation of the Lagrange or linear equations and the von Karman or nonlinear derivation is that ε_r is taken simply as du/dr in the linear derivation, resulting in significantly simplified mathematics throughout and simplified linear final equations.

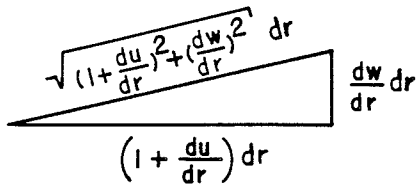

Figure 4.2 Radial Strain

Note that the equation

$$\varepsilon_r = \frac{du}{dr} + \frac{1}{2}\left(\frac{du}{dr}\right)^2 + \frac{1}{2}\left(\frac{dw}{dr}\right)^2 \qquad (4.10a)$$

commonly published [79,65] for Equation (4.9a) is incorrect. The error is likely due to evaluation of Equation (4.9) using a Maclaurin series for $\sqrt{1+x}$ and not including the second order term $-(du/dr)^2/2$ which occurs in the third term of the Maclaurin series. The erroneous series agrees with the Green strain tensor given in Equation (2.39), but which as noted in Section 2.2 is not a measure of stretch and is therefore not suitable for use here. Since the erroneous Equation (4.10a) is invariably simplified to Equation (4.10) on the grounds that $\left(\frac{du}{dr}\right)^2$ is much smaller than $\left(\frac{dw}{dr}\right)^2$, the error does not affect the final results.

The transverse strain ε_θ is simply

$$\varepsilon_\theta = \frac{u+r}{r} - 1 = \frac{u}{r} \qquad (4.11)$$

The strain a distance z above the middle surface is using the Kirchoff hypothesis (2):

$$\varepsilon_r = \frac{du}{dr} - z\frac{d^2w}{dr^2} + \frac{1}{2}\left(\frac{dw}{dr}\right)^2 \qquad (4.12)$$

and

$$\varepsilon_\theta = \frac{u}{r} - \frac{z}{r}\frac{dw}{dr} \quad . \tag{4.13}$$

Let Kirchoff stresses S be denoted as shown in Figure 4.3. Normal stresses are denoted by one subscript and shear stresses by two. By assumption (1) the plate is thin and hence transverse stress S_z and can be taken as zero. Further, deformation produced by shear stress is neglected. The transverse strain ε_z produced by non-zero normal stresses S_r and S_θ is small and is neglected. Its inclusion in the analysis would, in a strict sense, be incompatible with fiber inextensibility assumed in (2). With these observations and assumption (6) that Hooke's Law applies, stress and strain can be related by

$$S_r = \frac{E}{1-\nu^2}\left[\frac{du}{dr} + \frac{1}{2}\left(\frac{dw}{dr}\right)^2 + \nu\frac{u}{r} - z\left(\frac{d^2w}{dr^2} + \frac{\nu}{r}\frac{dw}{dr}\right)\right] \tag{4.14}$$

and

$$S_\theta = \frac{E}{1-\nu^2}\left[\frac{u}{r} + \nu\frac{du}{dr} + \frac{\nu}{2}\left(\frac{dw}{dr}\right)^2 - z\left(\frac{1}{r}\frac{dw}{dr} + \nu\frac{d^2w}{dr^2}\right)\right] \tag{4.15}$$

Bending resultants M_i and normal resultants N_i are calculated using the assumption of normal fibre inextensibility to be

$$N_r = \int_{-h/2}^{h/2} S_r\, dz = \frac{Eh}{1-\nu^2}\left[\frac{du}{dr} + \frac{1}{2}\left(\frac{dw}{dr}\right)^2 + \nu\frac{u}{r}\right] \tag{4.16}$$

$$N_\theta = \int_{-h/2}^{h/2} S_\theta\, dz = \frac{Eh}{1-\nu^2}\left[\frac{u}{r} + \nu\frac{du}{dr} + \frac{\nu}{2}\left(\frac{dw}{dr}\right)^2\right] \tag{4.17}$$

$$M_r = \int_{-h/2}^{h/2} S_r\, z dz = \frac{-Eh^3}{12(1-\nu^2)}\left[\frac{d^2w}{dr^2} + \frac{\nu}{r}\frac{dw}{dr}\right] \tag{4.18}$$

$$M_\theta = \int_{-h/2}^{h/2} S_\theta\, z dz = \frac{-Eh^3}{12(1-\nu^2)}\left[\frac{1}{r}\frac{dw}{dr} + \nu\frac{d^2w}{dr^2}\right] \tag{4.19}$$

The shear resultant is defined as

$$Q_r = \int_{-h/2}^{h/2} S_{rz}\, dz \tag{4.20}$$

At this point a relationship between stress resultants and displacement in the undeformed or Lagrangian coordinate system has been established using strain-displacement relationships and Hooke's Law. Since dw/dr , du/dr and u/r are small compared with unity, stresses and resultants which are given in terms of the undeformed plate are to a first approximation [23, p. 466], equal to their corresponding quantities in the deformed or Eulerian coordinates. They can therefore be used in the ensuing equations which are derived in the deformed state, from equilibrium considerations. These equilibrium considerations establish additional relationships between stress resultants and displacement.

Consider the volumetric element shown in Figure 4.3. It will be in radial equilibrium when

$$(S_r + \frac{dS_r}{dr}\, dr)\ (r + dr)d\theta\, dz - S_r\, r\, d\theta\, dz + (S_{rz} + \frac{dS_{rz}}{dz}\, dz)r\, d\theta\, dr$$

$$- S_{rz}\, r\, d\theta\, dr - 2S_\theta \frac{d\theta}{2}\, dr\, dz + \bar{R} r\, dr\, d\theta\, dz = 0 \tag{4.21}$$

or

$$\frac{dS_r}{dr} + \frac{S_r - S_\theta}{r} + \frac{ds_{rz}}{dz} + \bar{R} = 0 \tag{4.22}$$

where $\bar{R}$ is the radial volumetric body force. Axial equilibrium requires

$$\frac{dS_r}{dr}\frac{dw}{dr} + \frac{S_r}{r}\frac{dw}{dr} + S_r \frac{d^2w}{dr^2} \frac{dS_{rz}}{dr} + \frac{dS_{rz}}{dz}\frac{dw}{dr} + \frac{dS_{zz}}{dz} + \frac{S_{rz}}{r} + \bar{Z} = 0 \tag{4.23}$$

where $\bar{Z}$ is the axial volumetric body force.

Integration of Equations (4.22) and (4.23) with respect to dz from -h/2 to h/2 followed by substitution of Equations (4.16), (4.17) and (4.20) yields

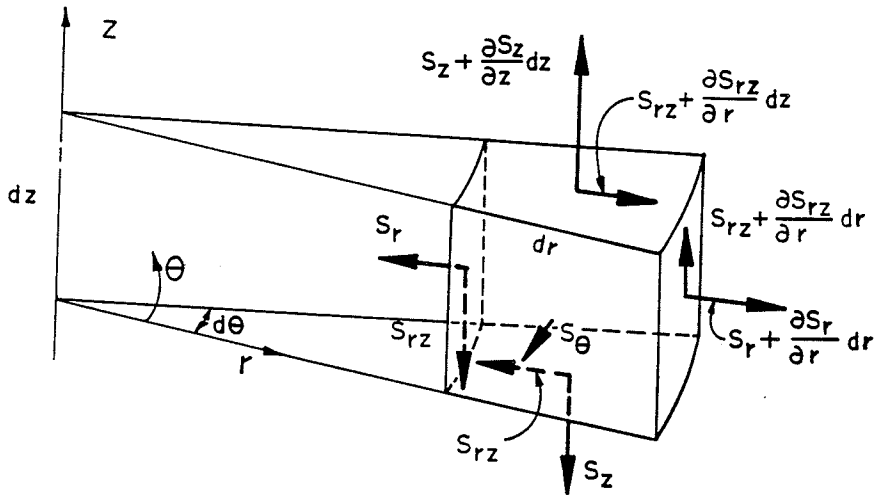

Figure 4.3 Volumetric Element Under Stress

$$\frac{dN_r}{dr} + \frac{N_r - N_\theta}{r} + f_r = 0 \tag{4.24}$$

and

$$\frac{dN_r}{dr}\frac{dw}{dr} + \frac{dQ_r}{dr}\frac{dw}{dr} + \frac{Q_r}{r} + f_z = 0 \tag{4.25}$$

where

$$f_r = \int_{-h/2}^{h/2} \bar{R}\, dz + S_{rz}\Big|_{-h/2}^{h/2} \tag{4.26}$$

and

$$f_z = \int_{-h/2}^{h/2} \bar{Z}\, dz + S_z\Big|_{-h/2}^{h/2} \tag{4.27}$$

are the total radial and axial forces per unit area of middle surface due to body and traction forces. Integration of (4.22) from $-h/2$ to $h/2$ with respect to z dz followed by substitution of Equations (4.19) to (4.21) yields

$$\frac{dM_r}{dr} + \frac{M_r - M_\theta}{r} - Q_r + m_r = 0 \tag{4.28}$$

where

$$m_r = \int_{-h/2}^{h/2} z\,\bar{R}\,dz + \int_{-h/2}^{h/2} z\,\frac{dS_{zr}}{dz}\,dz + Q_r = \int_{-h/2}^{h/2} z\,\bar{R}\,dz + (z\,S_{zr})\Big|_{-h/2}^{h/2} \tag{4.29}$$

is the total applied moment per unit area of middle surface.

In the absence of radial surface tractions and body forces, Equations (4.24), (4.25) and (4.28) reduce to

$$\frac{dN_r}{dr} + \frac{N_r - N_\theta}{r} = 0 \tag{4.30}$$

$$\frac{dN_r}{dr}\frac{dw}{dr} + \frac{N_r}{r}\frac{dw}{dr} + N_r\frac{d^2w}{dr^2} + \frac{dQ_r}{dr} + \frac{Q_r}{r} + q = 0 \tag{4.31}$$

and

$$\frac{dM_r}{dr} + \frac{M_r - M_\theta}{r} - Q_r = 0 \tag{4.32}$$

where the replacement $q = f_z$ has been made in favor of common notation.

Further simplification requires combination of Equations (4.16) to (4.20) governing the geometric and material behavior, with equilibrium Equations (4.29) to (4.32). Elimination of Q from Equation (4.31) using (4.32) and rearranging, we have

$$D\left(-\frac{d^2M_r}{dr^2} - \frac{2}{r}\frac{dM_r}{dr} + \frac{1}{r}\frac{dM_\theta}{dr}\right) = q + \frac{dN_r}{dr}\frac{dw}{dr} + \frac{N_r}{r}\frac{dw}{dr} + N_r\frac{d^2w}{dr^2} \tag{4.33}$$

Substitution of Equations (4.18) and (4.19) in (4.3) to eliminate M_r and M_θ gives

$$D\left(\frac{d^4w}{dr^4} + \frac{2}{r}\frac{d^3w}{dr^3} - \frac{1}{r^2}\frac{d^2w}{dr^2} + \frac{1}{r^3}\frac{dw}{dr}\right) = q + \frac{1}{r}\frac{d}{dr}\left(r\,N_r\frac{dw}{dr}\right) \tag{4.34}$$

Assume the existence of a stress potention function ϕ defined such that

$$N_r = \frac{1}{r} \frac{d\phi}{dr} \tag{4.35}$$

and

$$N_\theta = \frac{d^2\phi}{dr^2} \tag{4.36}$$

Equation (4.34) can then be written as

$$\nabla^4 w = \frac{1}{D} \left[q + \frac{1}{r} \frac{d^2\phi}{dr^2} \frac{dw}{dr} + \frac{1}{r} \frac{d\phi}{dr} \frac{d^2w}{dr^2} \right] \tag{4.37}$$

Consider the quantity

$$\left(\frac{d^2}{dr^2} + \frac{1}{r} \frac{d}{dr} \right) \left(N_r + N_\theta \right)$$

Substitution of (4.35) and (4.36) into this expression yields an equation

$$\left(\frac{d^2}{dr^2} + \frac{1}{r} \frac{d}{dr} \right) \left(N_r + N_\theta \right) = \nabla^4 \phi \tag{4.38}$$

which is similar to the plane stress compatibility equations. Elimination of u from stress resultant Equations (4.16) and (4.17) gives

$$N_r - \nu N_\theta - \frac{d}{dr} \left[r(N_\theta - \nu N_r) \right] = \frac{Eh}{2} \left(\frac{dw}{dr} \right)^2 . \tag{4.39}$$

Differentiation of this equation with respect to r followed by two suitable substitutions of equilibrium Equation (4.30) and comparison with (4.38) yields the equation

$$\nabla^4 \phi = - \frac{Eh}{r} \frac{d^2w}{dr^2} \frac{dw}{dr} \tag{4.40}$$

See Donnell [17] for an alternate derivation.

Together Equations (4.37) and (4.40) are known as the axisymmetric von Karman equations. These fourth order coupled nonlinear equations describe the nonlinear response of a transversely loaded thin plate. They are a special

case of the non-axisymmetric von-Karman equations for the nonlinear deflection of a transversely loaded plate.

$$\nabla^4 w = \frac{1}{D}\left[q + \frac{1}{r}\frac{d^2\phi}{dr^2}\left(\frac{1}{r}\frac{d^2w}{d\theta^2} + \frac{dw}{dr}\right) - \frac{2}{r^2}\left(\frac{d^2w}{dr\,d\theta} - \frac{1}{r}\frac{dw}{d\theta}\right)\left(\frac{d^2\phi}{dr\,d\theta} - \frac{1}{r}\frac{d\phi}{d\theta}\right) + \frac{1}{r}\frac{d^2w}{dr^2}\left(\frac{1}{r}\frac{d^2\phi}{d\theta^2} + \frac{d\phi}{dr}\right)\right] \tag{4.41}$$

and

$$\nabla^4 \phi = Eh\left[\frac{1}{r^2}\left(\frac{d^2w}{dr\,d\theta} - \frac{1}{r}\frac{dw}{d\theta}\right)^2 - \frac{1}{r}\frac{d^2w}{dr^2}\left(\frac{1}{r}\frac{d^2w}{d\theta^2} + \frac{dw}{dr}\right)\right] \tag{4.42}$$

which are more commonly given in rectangular form [84, 23]

$$\nabla^4 w = \frac{1}{D}\left[q + \frac{\partial^2\phi}{\partial y^2}\frac{\partial^2 w}{\partial x^2} - 2\frac{\partial^2\phi}{\partial x\,\partial y}\frac{\partial^2 w}{\partial x\,\partial y} + \frac{\partial^2\phi}{\partial x^2}\frac{\partial^2 w}{\partial y^2}\right] \tag{4.43}$$

and

$$\nabla^4 \phi = Eh\left[\left(\frac{\partial^2 w}{\partial x\,\partial y}\right)^2 - \frac{\partial^2 w}{\partial x^2}\frac{\partial^2 w}{\partial y^2}\right] \tag{4.44}$$

The first and second equations in each of these pairs are known respectively as the equilibrium and compatibility equations.

The meaning of these equations is best explained by comparison with the linear plate equations. When the transverse deflection w and its first derivatives are assumed to be very small, second order terms can be neglected in strain expressions, such as Equation (4.10). The resulting deflection equations for linear materials are the well known linear equations

$$\nabla^4 w = \frac{q}{D} \tag{4.45}$$

and

$$\nabla^4 \phi = 0 \tag{4.46}$$

The first of these equations is a statement of equilibrium in the transverse direction. The $D\nabla^4 w$ term expresses the net transverse force on a small element of the

plate which results from shear along its perimeter and which is induced by bending of the plate into the configuration w. For equilibrium this must balance the applied load q . The second equation is a condition for compatibility of the stress field in a plate which is in a state of plane stress, in terms of its Airy stress function ϕ.

The von Karman equilibrium equation (4.37) contains two terms on its right hand side, which are not present in the linear equations. These terms are associated with geometrically nonlinear effects. The second nonlinear term in Equation (4.37) is by comparison with Equation (4.35) a product of the radial stress resultant N_r which acts in the plane of the plate and the radial curvature $k_2 = d^2w/dr^2$. The axial component N_r dw/dr of N_r will change with radius by an amount N_r dr (dw/dr) or by N_r d^2w/dr^2 . Hence, the second term is the net axial contribution per unit area from the in plate stress resultant N_r. Similarly, the first nonlinear term in Equation (4.37) is the product of the local curvature $k_1 = 1/r$ dw/dr in the hoop direction and the hoop stress resultant N_θ, and represents the net axial force contribution per unit area induced by in-plane stress resultant N_θ. The non-axisymmetric equilibrium Equations (4.41) and (4.43) contain terms equivalent to these, as well as terms containing a factor of two, which describe the transverse force produced by interaction of the shear resultant with the warp, or twist of the surface.

The compatibility Equation (4.40) contains a single nonlinear term which can be interpreted as minus Eh times the product of $k_1 = 1/r$ dw/dr and $k_2 = d^2w/dr^2$. This is a special case of the Gauss curvature, which is the right hand side of the non-axisymmetric compatibility Equations (4.42) and (4.44). The compatibility equation is associated with stretching of the middle surface. It is not surprising then, that its nonlinear component is Gaussian curvature, which is a measure of in-plane stretching induced by the deformed plate not being

applicable to the undeformed plate.

A common alternate approach is mentioned here as several of the analytical solutions which will be considered make use of it. Equilibrium equation (4.34) can be written as

$$Q_r = - D \left(\frac{d^3w}{dr^3} + \frac{1}{r}\frac{d^2w}{dr^2} - \frac{1}{r^2}\frac{dw}{dr}\right) = - N_r \frac{dw}{dr} \qquad (4.47)$$

in which case we have from Equations (4.30) and (4.47) that:

$$\frac{d^2u}{dr^2} = - \frac{1}{r}\frac{du}{dr} + \frac{u}{r^2} - \frac{1-\nu}{2r}\left(\frac{dw}{dr}\right)^2 - \frac{dw}{dr}\frac{d^2w}{dr^2} \qquad (4.48)$$

and

$$\frac{d^3w}{dr^3} = - \frac{1}{r}\frac{d^2w}{dr^2} + \frac{1}{r^2} + \frac{12}{h^2}\frac{dw}{dr}\left[\frac{du}{dr} + \nu\frac{u}{r} + \frac{1}{2}\left(\frac{dw}{dr}\right)^2\right] \qquad (4.49)$$

These equations are mathematically equivalent to the von-Karman equations, even though their form is quite different.

The various analytical solutions to the large axisymmetric deflection of uniformly loaded plates begin with the axisymmetric von Karman equations, or their equivalent. For the case of a uniform load, these equations can be written in the dimensionless form

$$\nabla^4 W = Q + \frac{1}{R}\frac{d\Phi}{dR}\frac{d^2W}{dR^2} + \frac{1}{R}\frac{d^2\Phi}{dR^2}\frac{dW}{dR} \qquad (4.50)$$

and

$$\nabla^4 \Phi = \frac{1}{12(1-\nu^2)}\frac{1}{R}\frac{d^2W}{dR^2}\frac{dW}{dR} \qquad (4.51)$$

where

$$\Phi = \frac{\phi}{D}, \quad Q = \frac{qa^4}{Dh}, \quad R = \frac{r}{a}, \quad W = \frac{w}{h}, \text{ and } U = \frac{au}{h^2} \qquad (4.52)$$

Equations (4.52) provide the appropriate forms for the dimensionless deflections and stresses.

Equations (4.50) to (4.52) show that the von Karman representation of nonlinear plate behavior is dependent only on the loading parameter qa^4/Dh. It is completely independent of a/h and depends on ν only as it enters through the boundary conditions. Independence of the analytical solution from the parameter a/h is due to simplification of radial strain Equations (4.9) to (4.10) and the assumed equivalence of quantities defined in Lagrangian and Eulerian coordinates, such as occurs between stress resultant Equations (4.16) to (4.20), and equilibrium Equations (4.24), (4.25) and (4.28). When a/h is large, Equation (4.10) does not represent the radial strain well. Also, when a/h is large, meridian rotation is significant and quantities defined in different coordinate systems cannot be equated. The extent of these errors is illustrated at the end of Section 4.4.

4.3 ANALYTICAL SOLUTIONS

The infinitesimal transverse deflection $w(r)$ of a plate subjected to a transverse load $q(r)$ was found by Lagrange in 1811 to be

$$\nabla^4 w = \frac{q}{D} \tag{4.53}$$

This linear solution considers first order effects only, and consequently is only applicable if $w_{max} << h$. Membrane stresses and radial deflection are neglected.

Nearly a hundred years later, T. von Karman [84] presented, without proof, the differential Equations (4.43) and (4.44) derived in the previous section governing the nonlinear transverse and in-plane displacements of a thin plate. His equations include certain second order strain effects, the inclusion of which results in a pair of coupled nonlinear governing differential equations. The mathematical coupling of the equations represents a coupling of the radial and transverse displacements. The load-deflection relation, like the equations, is no longer linear. Because of the mathematical difficulties posed by the nonlinear nature of the

differential equations, and the further complication of their being coupled, closed form solutions do not exist even for simple axisymmetric problems. Attempts to solve the von Karman equations, or their equivalent, for uniform loads rely on simplification of the equations, or on finding suitable values for coefficients governing an assumed form of solution.

In 1915 H. Hencky [30] presented a solution for the deflection of a circular membrane. He used the von Karman compatibility equation and derived a new equation

$$\frac{dw}{dr} = \frac{-qr}{2hS_r} \tag{4.54}$$

for axial equilibrium. The von Karman equilibrium equation (4.37) simplifies to Hencky's equation when we neglect the plate bending term ∇^4.

Because of the assumed form of Hencky's solution,

$$S_r = \frac{1}{4}\sqrt[3]{Eq^2\frac{a^2}{h^2}}\left(B_o + B_2(\frac{r}{a})^2 + B_4(\frac{r}{a})^4 + \ldots.\right)$$

$$S_\theta = \frac{1}{4}\sqrt[3]{Eq^2\frac{a^2}{h^2}}\left(B_o + 3B_2(\frac{r}{a})^2 + 5B_4(\frac{r}{a})^4 + \ldots.\right)$$

$$w = a\sqrt[3]{\frac{qa}{Eh}}\left(\sum_{i=0,2,4,\ldots}^{\infty} A_i - (\frac{r}{a})^2[A_o + A_2(\frac{r}{a})^2 + A_4(\frac{r}{a})^4 + \ldots.\right) \tag{4.55}$$

the shape of his membrane stress and transverse deflection profiles are determined by a single constant B_o, which determines all other constants A_i and B_i through the governing differential equations and the magnitude of the profiles vary uniformly with load. Stresses increase by the 2/3 power of load and transverse deflection by its 1/3 power. Consequently, the center and edge membrane stresses take the form

$$\sigma_r^m(0) = d\,(\frac{Eq^2a^2}{h^2})^{1/3} \tag{4.56}$$

$$\sigma_r^m(a) = e\left(\frac{Eq^2a^2}{h^2}\right)^{1/3} \tag{4.57}$$

and the corresponding center deflection is

$$w(0) = f\, h\left(\frac{pa}{Eh}\right)^{1/3} \tag{4.58}$$

Hencky's solution can be rewritten to yield dimensionless stresses and center deflections which for $\nu = 0.5$ are

$$\frac{\sigma_r^m(0)a^2h}{D} = 0.959\, Q^{2/3} \tag{4.59}$$

$$\frac{\sigma_r^m(a)a^2h}{D} = 0.787\, Q^{2/3} \tag{4.60}$$

and

$$\frac{w(0)}{h} = 0.286\, Q^{1/3} \tag{4.61}$$

where load factor Q is given by $Q = \frac{qa^4}{Dh}$ (4.62)

The frequency quoted results of Hencky for $\nu = 0.3$ are in error by about 2% as a result of an arithmetic error in substituting $\nu = 0.3$ into Hencky's Equation (11a). Hencky erroneously calculates B_o to be 1.713 with resulting constants d = 0.423, e = 0.328 and f = 0.662. The author calculates B_o to be 1.724 with d = 0.431, e = 0.333 and f = 0.654 for $\nu = 0.3$. For $\nu = 0.5$, we have B_o = 1.845, d = 0.461, e = 0.378 and f = 0.595. See also Table 4.1 at the end of this section.

The first plate solution incorporating both bending and membrane effects was published by K. Federhofer [19] in 1918. He assumed the membrane stresses to be either constant or parabolic and then solved for the corresponding displacements.

A. Nadai discusses the large deflection of plates in his book "**Die Elastische Platten**" [51], published in 1925. He proposes a solution to the equations

$$\frac{d^3w}{dr^3} + \frac{1}{r}\frac{d^2w}{dr^2} - \frac{1}{r^2}\frac{dw}{dr} = \frac{qr}{2D} + \frac{12}{h^2}\frac{dw}{dr}\left(\frac{du}{dr} + \frac{1}{2}\left(\frac{dw}{dr}\right)^2 + \nu\frac{u}{r}\right) \tag{4.63}$$

and $$\frac{d^2u}{dr^2} + \frac{1}{r}\frac{du}{dr} - \frac{u}{r^2} = -\frac{dw}{dr}\frac{d^2w}{dr^2} - \frac{1-\nu}{2r}\left(\frac{dw}{dr}\right)^2 \tag{4.64}$$

which are equivalent to Equations (4.48) and (4.49) derived earlier. For a uniformly loaded plate with a clamped edge he assumes the form of dw/dr to be

$$\frac{dw}{dr} = c\left[\frac{r}{a} - \left(\frac{r}{a}\right)^n\right] \tag{4.65}$$

Substitution of this form of dw/dr in Equation (4.63) gives a first approximation for u. Substitution of these first approximations for dw/dr and u in Equation (4.64) provides a relationship between c,n and q . The parameters c and n are then chosen to make q as nearly constant as possible. Cubic relations between load parameter and center deflection such as

$$\frac{w_o}{h} + 0.583\left(\frac{w_o}{h}\right)^3 = 0.0156\ \frac{qa^4}{Dh} \tag{4.66}$$

for $\nu = 0.25$ result. For large deflections w_o/h is small compared to $(w_o/h)^3$ and the above cubic relationship may be approximated by

$$w_o = 0.299\left(\frac{qa^4}{Dh}\right)^{1/3} \tag{4.67}$$

Timoshenko [77] suggested an energy approach to find the solution of the uniformly loaded plate with a simply supported radially restrained edge. He assumed that the large transverse displacements were of the same shape as those produced by plate bending, i.e.

$$w = w_o\left(1 - \frac{r^2}{a^2}\right)^2 \tag{4.68}$$

Figure 4.14 demonstrates the high accuracy of this assumption. He then assumed the radial displacement to be of the form

$$u = r(a - r)(C_1 + C_2 r) \tag{4.69}$$

and chose C_1 and C_2 to minimize the total strain energy. The resulting load-displacement relationship for $\nu = 0.3$ is

$$\frac{w_o}{h} = \frac{qa^4}{64Dh} \frac{1}{1 + 0.488\left(\frac{w_o}{h}\right)^2} \tag{4.70}$$

which for large w_o/h can be approximated by

$$\frac{w_o}{h} = 0.318 \left(\frac{qa^4}{Dh}\right)^{1/3} \tag{4.71}$$

An important and very versatile solution to the deflection of circular plates under uniform loads and various boundary conditions was proposed by S. Way [87] in 1934. Way assumed series for a dimensionless radial membrane stress S_r^m and the radial derivative of transverse displacement dw/dr which he calls ϕ, in terms of a radial parameter $u = r/h$ (not to be confused with radial displacement).

$$S_r^m = B_0 + B_2 u^2 + B_4 u^4 + \cdots \tag{4.72}$$

$$\phi = \frac{dw}{dr} = \sqrt{8}\,(C_1 + C_3 u^3 + C_5 u^5 + \cdots) \tag{4.73}$$

His series are very similar to Hencky's. All of Way's basic equations, such as those relating strain and displacement, agree exactly with those used to derive the von Karman equations. Way's Equation (12) is the von Karman equilibrium equation. The only difficulty in Way's solution is to determine the constants B_i and C_j in Equations (4.72) and (4.73) above. Once the values of B_o and C_1 are chosen, all other constants B_i and C_j are uniquely determined by the fundamental equations

$$\frac{d}{du}(uS_r^m) - S_\theta^m = 0 \tag{4.74}$$

$$\frac{1}{12(1-\nu^2)} \frac{d}{du}\left(\frac{1}{u}\frac{d}{du}(u\phi)\right) = q\frac{u}{2} + S_r^m \phi \tag{4.75}$$

and

$$u\frac{d}{du}(s_r^m + s_\theta^m) + \frac{\phi^2}{2} = 0 \tag{4.76}$$

The resulting relationships between the constants B_i and C_j are

$$C_3 = \frac{3}{2}(1-\nu^2)\frac{q}{2\sqrt{8}} + B_o C_1 \tag{4.77}$$

$$B_k = -\frac{4}{k(k+2)} \sum_{m=1,3,5,\ldots}^{k-1} C_m C_{k-m}\ ,\ k = 2,4,6,\ \ldots. \tag{4.78}$$

$$C_k = \frac{12(1-\nu^2)}{k^2-1} \sum_{m=0,2,4,\ldots}^{k-3} B_m C_{k-2-m}\ ,\ k = 5,7,9,\ldots. \tag{4.79}$$

The constants B_o and C_1 are chosen to satisfy the boundary conditions. Their values can be found readily using modern numerical techniques thereby eliminating the graphical method presented by Way. These constants are linearly related to the membrane strain and curvature at the center of the plate. Timoshenko [79, p. 398)] points out that Equations (4.48) and (4.49) can be integrated numerically if the membrane strain and curvature at the center of the plate are assumed. He points out however, that this direct integration approach is not recommended. Way shows in an appendix, that his solution is completely governed by the boundary conditions and the two parameters qa^4/Dh and ν.

Another important solution to the plate problem was presented by H.M. Berger [7] in 1955. Both rectangular and circular plates are analysed. Starting from the same basic relationships as von Karman, he proposed an energy formulation in which the first variation of the second strain invariant is neglected. Neglect of the second strain invariant is based on examination of Way's results and has no apparent physical justification. Berger derives new governing differential equations

$$\frac{du}{dr} + \frac{u}{r} + \frac{1}{2}\left(\frac{dw}{dr}\right)^2 = \frac{\alpha h^2}{12} \tag{4.80}$$

and

$$\left(\frac{d^2u}{dr^2} + \frac{1}{r}\frac{d}{dr}\right)\left(\frac{d^2w}{dr^2} + \frac{1}{r}\frac{dw}{dr} - \alpha^2 w\right) = \frac{q}{D} \tag{4.81}$$

containing a normalized constant of integration α, using this simplification. His equations are still nonlinear, but more importantly, they are decoupled. For a particular value of the constant of integration α, the second equation which is linear in u can be solved for w and then the first which is linear in n can be solved for u. The resulting displacements are not sufficiently accurate to calculate stresses. A more accurate description of the radial displacement u is required for this purpose and is given by

$$\frac{d^2u}{dr^2} + \frac{1}{r}\frac{du}{dr} - \frac{u}{r^2} = -\frac{(1-\nu)}{dr}\left(\frac{dw}{dr}\right)^2 - \frac{1}{2}\frac{d}{dr}\left(\frac{dw}{dr}\right)^2 \tag{4.82}$$

which is derived from energy considerations, including the effect of the second strain invariant. This equation will be recognized as the standard equation of radial equilibrium. By using this approach, the deformations and stresses can be written in closed form in terms of Bessel functions of the first kind. For example:

$$w = A\, I_o\,(\alpha r) + B - \frac{qr^2}{4D\alpha^2} \tag{4.83}$$

The equations contain three arbitrary constants A, B and α which can be chosen to satisfy any reasonable boundary conditions, including slope, force resultants, moments, and/or specified radial deflection. The author has identified two

typographical errors in Berger's paper. The 'g' in Berger's Equation (48) should be a 'q', and the '+' in the demoninator of Berger's Equation (28) should be a '-' - it will then agree with his Equation (29).

Dimensional analysis shows that Berger's solution, like Way's and Hencky's is completely governed by the boundary conditions and parameters Q and ν.

An interesting solution to the plate problem is given by M. Goldberg [25], 1962. He provides an argument for neglecting the Gaussian curvature in the von Karman compatibility Equation (4.40). He is thus able to decouple the system of equations. A closed form solution in terms of Bessel functions, similar to Berger's, is thus obtained.

Table 4.1 shows the limiting values of deflection and stress for large loads as found by various analytical solutions and the authors numerical solution. The various solutions are in generally good agreement and show the effect of Poisson's ratio ν.

4.4 NUMERICAL SOLUTIONS AND DISCUSSION

This section compares various solutions for uniformly loaded circular plates. Both clamped and radially restrained simply supported boundary conditions solutions are considered. The linear solutions, the classical solutions of Way [87] and Berger [7], the membrane solution of Hencky [30], and the numerical solutions developed herein are compared over their respective domains. Center stresses and deflection and edge stresses over a load range of five magnitudes are discussed, as are stress and deflection profiles at selected loads. Extensive comparisons with the plate, for which nonlinear analytical solutions are known serve also to verify the accuracy of the author's numerical techniques and solutions.

The analytical solutions depend on Q and ν as the dimensionless forms of the governing equations given in Section 4.2 showed they should. Computer

Table 4.1 Limiting Values of Deflection and Stress for Large Loads

Solution	ν	$\frac{w}{Q^{1/3}h}$	$\frac{\sigma_r^m(0)\,a\,h}{Q^{2/3}D}$	$\frac{\sigma_r^m(a)\,a\,h}{Q^{2/3}D}$
Nadai [51]	0.25	0.299	-	
Hencky [30]	0.30	0.298	0.938	0.728
Hencky (corrected)	0.30	0.295	0.956	0.739
Timoshenko [77]	0.30	0.318	-	-
Way [87]	0.30	-	-	-
Berger [7]	0.30	0.275	0.796	0.590
Goldberg [25]	0.30	0.318	1.060	0.788
Hencky	0.50	0.286	0.959	0.787
Goldberg	0.50	0.284	-	-
Brodland (simply supp.)	0.50	0.286	0.951	0.787

programs were written to calculate the solutions of Hencky, Way and Berger. The programs for each method were verified by solving the particular problems discussed by their respective authors. They were then modified to solve the specific problems of interest in this chapter.

It can be shown that the finite element solution depends not only on Q and ν, but also on n, the number of elements used, and on the relative plate thickness h/a. The finite element solutions shown are for a plate with $\nu = 0.5$, relative thickness $h/a = 1/400$, and having $n = 8$ elements, unless noted otherwise.

To quantify the effect of the number of elements used, analyses using four element models were done. For both boundary conditions, membrane stresses and transverse deflections are within 3% of the eight element models over the entire loading range $1 \leq Q \leq 100000$. For $Q \leq 300$ the radial deflections of clamped and simply supported plates are within 10% and 1%, respectively, of their corresponding eight element solutions. Four elements are insufficient to properly accommodate the bipolar radial deflection of the clamped plate. The bending stresses predicted by the four element model are 3% high for clamped plates and $Q \leq 10000$ and 15% high for simply supported plates and $Q \leq 300$. Only alternate model values of the eight element model are plotted on the stress and displacement profiles. The effect of the ratio h/a is discussed in some detail at the end of the chapter.

A Mooney-Rivlin strain energy function is used. The constants C_1 and C_2 of the strain energy function can be chosen to match Hooke's Law and either constancy of the sum of strains or constancy of the product of stretches, as pointed out in Chaper 3. As expected, the choice of one criterion over the other affects the results very slightly. The maximum difference in stresses and deflections for $1 > Q > 100000$ was less than $\frac{1}{2}\%$, and hence for practical purposes the two solutions are indistinguishable. Choice of C_1 to C_2 to make the material response

significantly nonlinear affects the deflections and stresses considerably, as would be expected.

Consider first, radially restrained simply supported plate. Figure 4.4 shows its normalized center deflection w_{max}/h as a function of load factor $Q = qa^4/Dh$. Figure (4.5) shows dimensionless membrane stress $\sigma^m a^2 h/D$ and bending stress $^b a^2 h/D$. Since center and edge stresses are governed by

$$\begin{aligned} \sigma_o^m &= \sigma_r^m(0) = \sigma_\theta^m(0) \\ \sigma_o^b &= \sigma_r^b(0) = \sigma_\theta^b(0) \\ \sigma_a^m &= \sigma_r^m(a) = \frac{1}{\nu}\,\sigma_\theta^m(a) \\ \sigma_a^b &= \sigma_\theta^b(a) \quad \text{and} \quad \sigma_r^b(a) \equiv 0 \end{aligned} \tag{4.84}$$

only σ_o^m, σ_o^b, σ_a^m and σ_a^b are plotted. These are the stresses of greatest magnitude. Note that both Figures 4.4 and 4.5 are plotted on log-log axes so a load domain of five magnitudes can be represented accurately.

For small loads $Q < 2$ deflections are small compared with the plate thickness ($w/h < 0.12$) and the bending analysis of Lagrange is applicable. As shown in Figure 4.5 membrane stresses are nearly a magnitude less than bending stresses at $Q = 2$ and become relatively even less significant with decreasing load. Hence, bending is indeed the dominant load carrying mode. Both the Way and Berger solutions simplify analytically to the linear solution for small loads, a result which the figures verify. The author's solutions also agree with the linear solutions.

The load range $2 < Q < 1000$ is a range of transition. The deflections are no longer infinitesimal, and consequently, the plate is beginning to dish. The possibility of load carrying by membrane effects now exists because of the changed geometry. As shown in Figure 4.5, membrane stresses do become more important, compared to bending stresses, until they actually become twice as large as bending

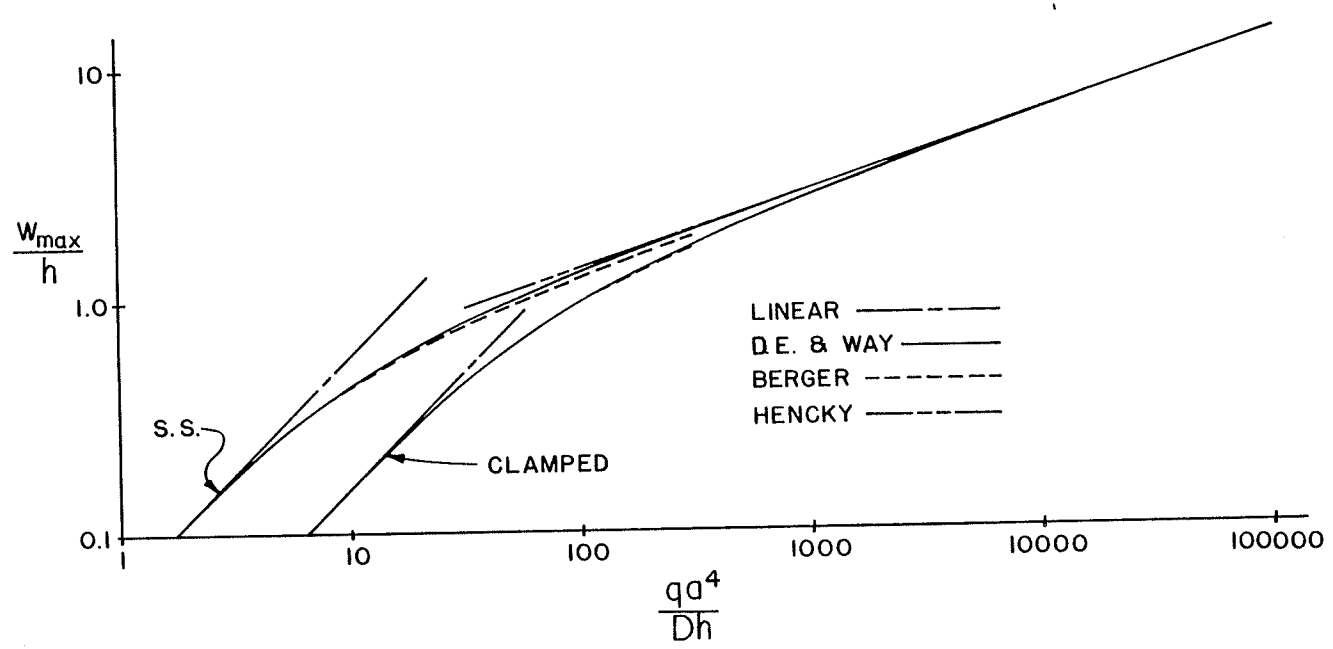

Figure 4.4 Center Deflection versus Load

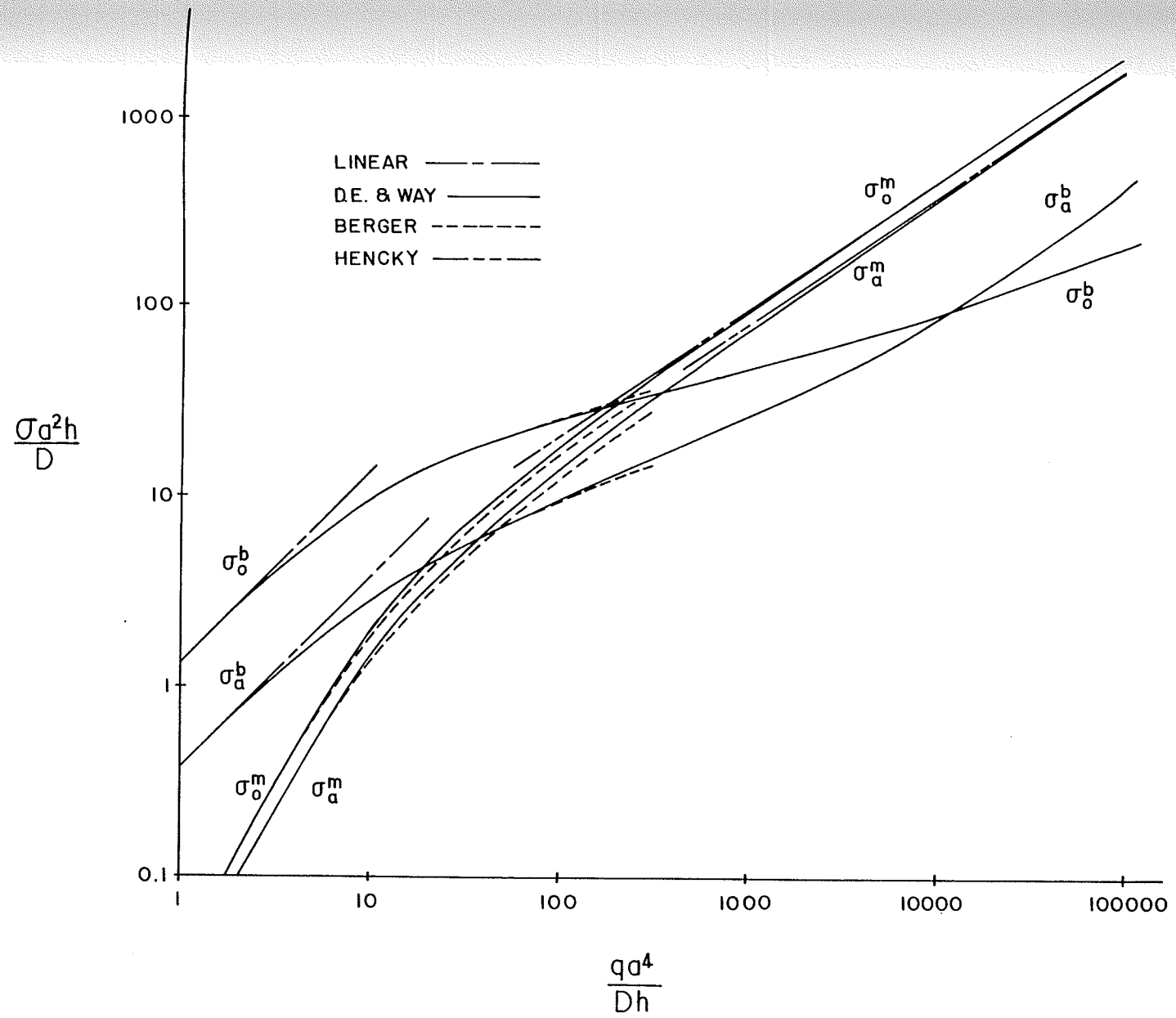

Figure 4.5 Stress versus Load for a Simply Supported Plate

stresses. The membrane mode of support begins to visibly assist the previously predominant bending mode at about $Q = 2$. When the load had increased to about $Q = 20$, sufficient geometric changes have occurred that the load is carried almost equally by bending and membrane modes, and all stresses are of the same magnitude.

The solutions of Way for $Q < 120$ and Berger for $Q < 300$ are also shown. Solutions have been calculated over the domain of application claimed in their respective papers, with $\nu = 0.5$. Way's solution for deflection and stresses agrees with the author's solution within 2% for $Q \leq 120$ except for edge bending stress which is within 4 percent. Berger's solution over this range predicts deflections up to 4 percent less and stresses up to 13% less. Berger's solution maintains the same degree of separation from the finite element solution up to $Q = 300$.

At a load of $Q = 1000$, the bending stresses shown are about half the magnitude of the membrane stresses. Their influence on the plate seems, however, to be slight, and the membrane mode of support predominates. This fact is made clear by comparison of the finite element deflections and stresses with the Hencky solution for a membrane. The Hencky solution predicts the same center deflection to three digits and membrane stresses, which are only 5% higher.

At loads higher than $Q = 1000$, both membrane stresses and center deflection approach the Hencky solution asymptotically. By $Q = 10000$ all three quantities are within 1% of Hencky's solution.

Figures 4.6 to 4.9 show the radial and transverse deflections for $Q = 120$ and $Q = 300$ as determined by the author's analysis, Berger's method, and for $Q = 120$ by Way's method. Figures 4.6 and 4.7 show that for $Q = 120$ the author's solution for radial and transverse displacements agree exactly with Way. Berger's transverse and radial deflections are uniformly 4.5% and 14% less, respectively. For $Q = 300$, Berger's solution is again uniformly less by about 4.4% and 17%.

Figures 4.10 to 4.13 show the stress distributions for $Q = 120$ and $Q = 300$.

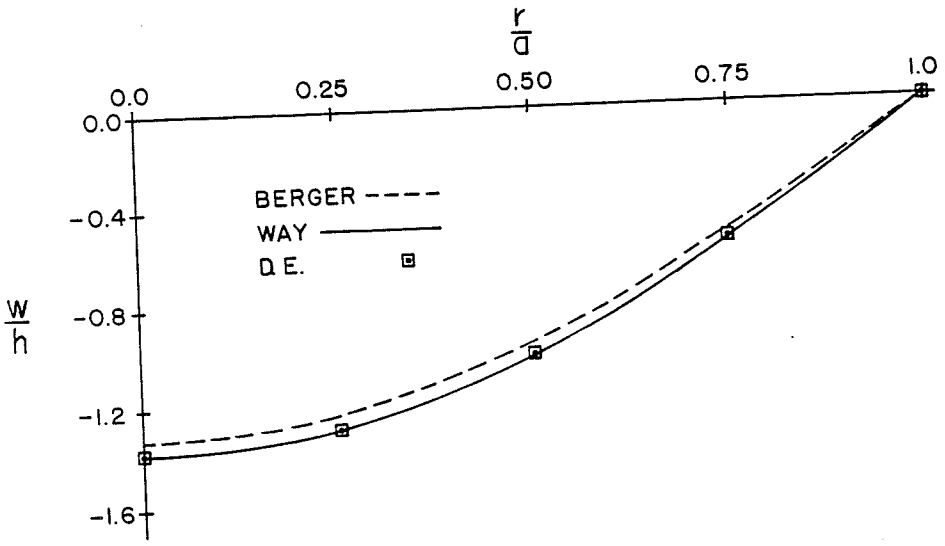

Figure 4.6 Transverse Deflection Profile for Q = 120

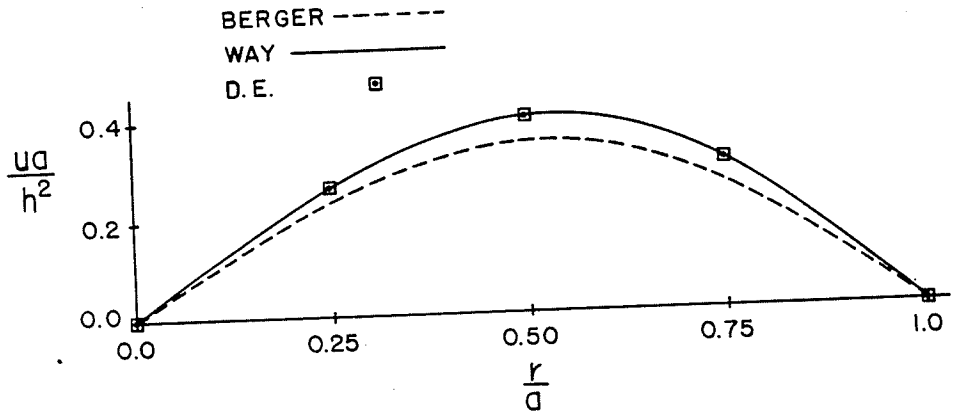

Figure 4.7 Radial Deflection Profile for Q = 120

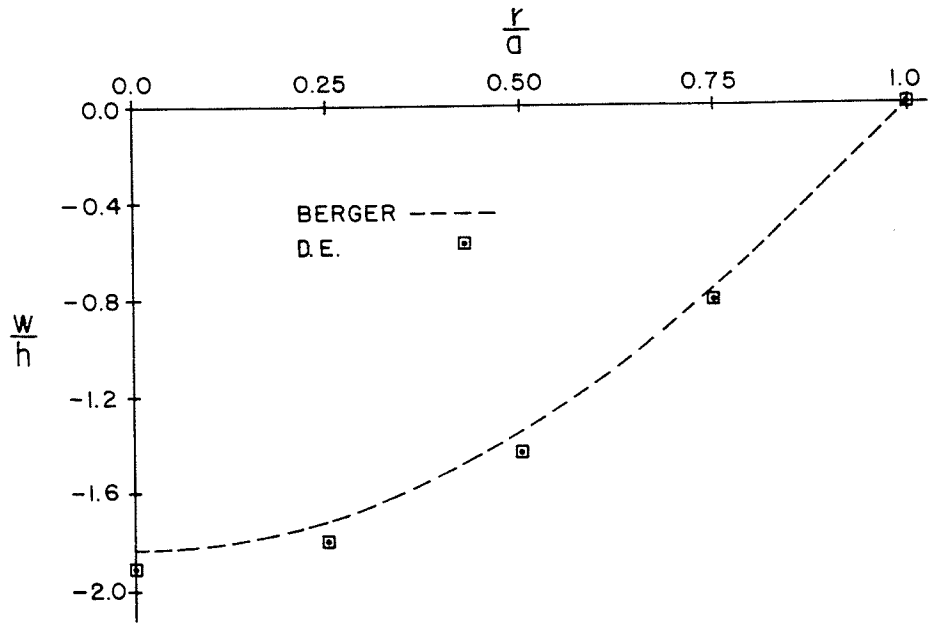

Figure 4.8 Transverse Deflection Profile for Q = 300

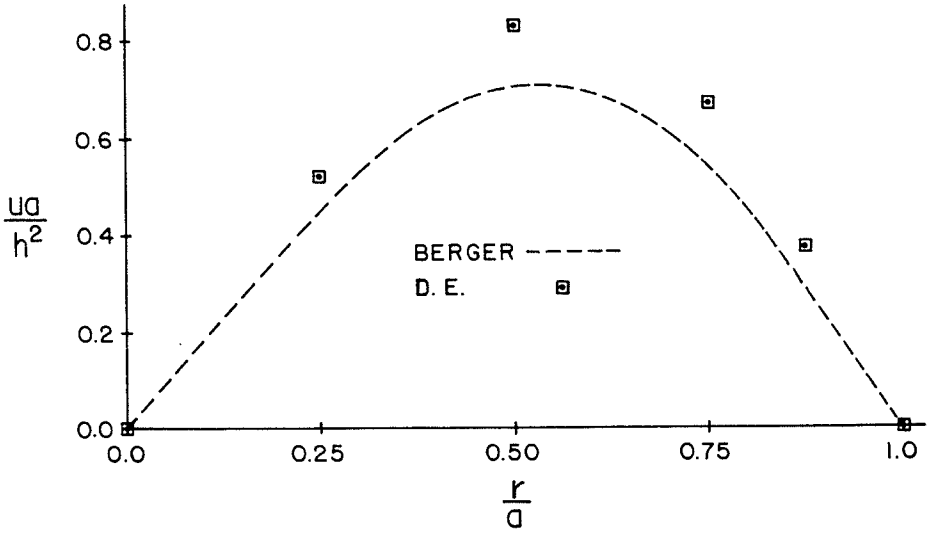

Figure 4.9 Radial Deflection Profile for Q = 300

The author's solution agrees almost exactly with Way's solution for $Q = 120$. Berger's membrane stresses are uniformly lower by about 11%. All three solutions give very similar bending stresses at the center and edge of the plate. Berger's solution gives membrane stresses about 11 percent lower than the others at $r = 0.7a$. For $Q = 300$ similar discrepancies between the author's solution and Berger solution occur.

Figure 4.14 shows the normalized transverse deflection for $Q \leq 0.1$ and $Q = 10000$. It is clear that the shape of the plate changes surprisingly little with load. The normalized membrane profile calculated using Hencky's series, which incidentally is nearly independent of his parameter B_o, is also shown.

The center deflection of a clamped plate is shown in Figure 4.4. Its center and edge stresses are shown in Figure 4.15. The radial and hoop components are related by

$$\begin{aligned} \sigma_o^m &= \sigma_r^m(0) = \sigma_\theta^m(0) \\ \sigma_o^b &= \sigma_r^b(0) = \sigma_\theta^b(0) \\ \sigma_a^m &= \sigma_r^m(a) = \frac{1}{\nu}\sigma_\theta^m(a) \\ \sigma_a^b &= \sigma_r^b(a) = \frac{1}{\nu}\sigma_\theta^b(a) \end{aligned} \tag{4.85}$$

For small loads $Q < 10$ and corresponding small deflections it is clear that the load is carried primarily by bending. Because the edge is clamped the plate is stiffer in bending and a larger load is required to deflect the plate a given amount, compared with a simply supported plate. The linear behavior of both plates is limited by similar deflections of $w/h \simeq 0.15$.

A transition from load carrying by bending to load carrying primarily by membrane effects occurs over $10 < Q < 5000$. The solution of Way agrees extremely

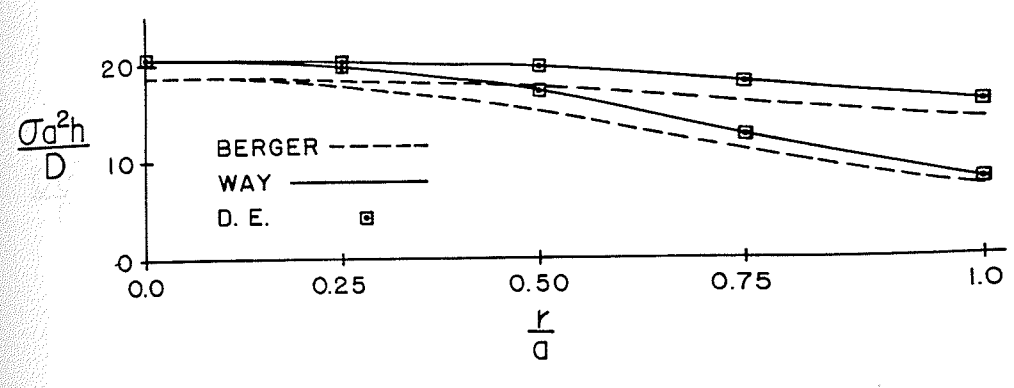

Figure 4.10 Membrane Stress Profiles for Q = 120

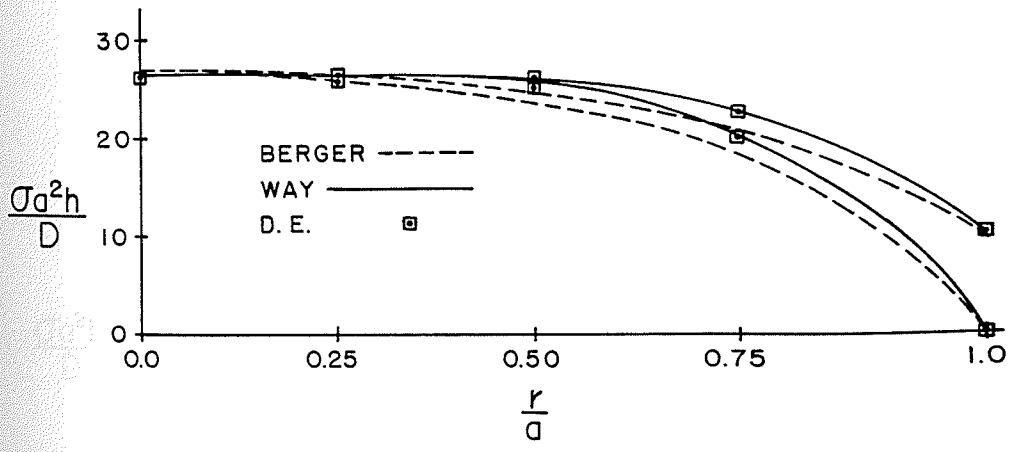

Figure 4.11 Bending Stress Profiles for Q = 120

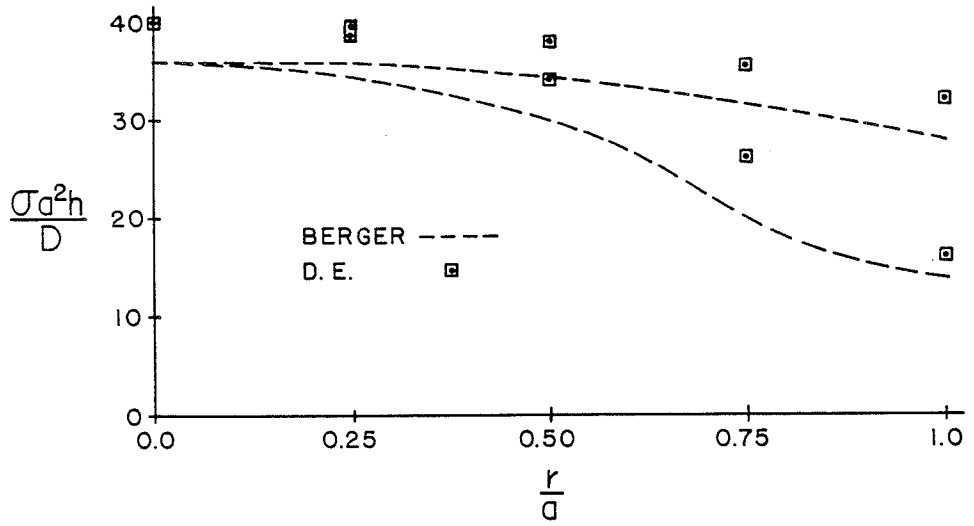

Figure 4.12 Membrane Stress Profiles for Q = 300

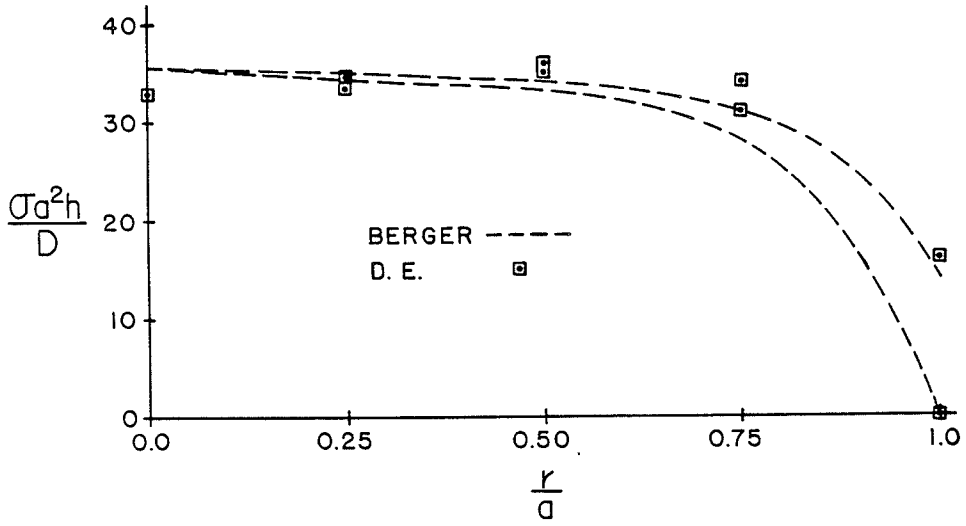

Figure 4.13 Bending Stress Profiles for Q = 300

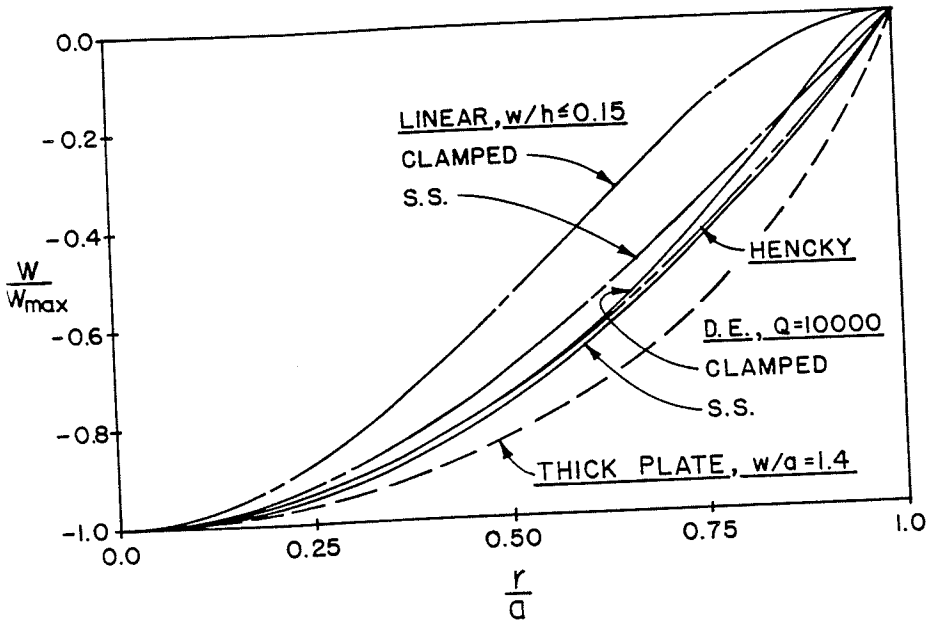

Figure 4.14 Normalized Deflection Profiles

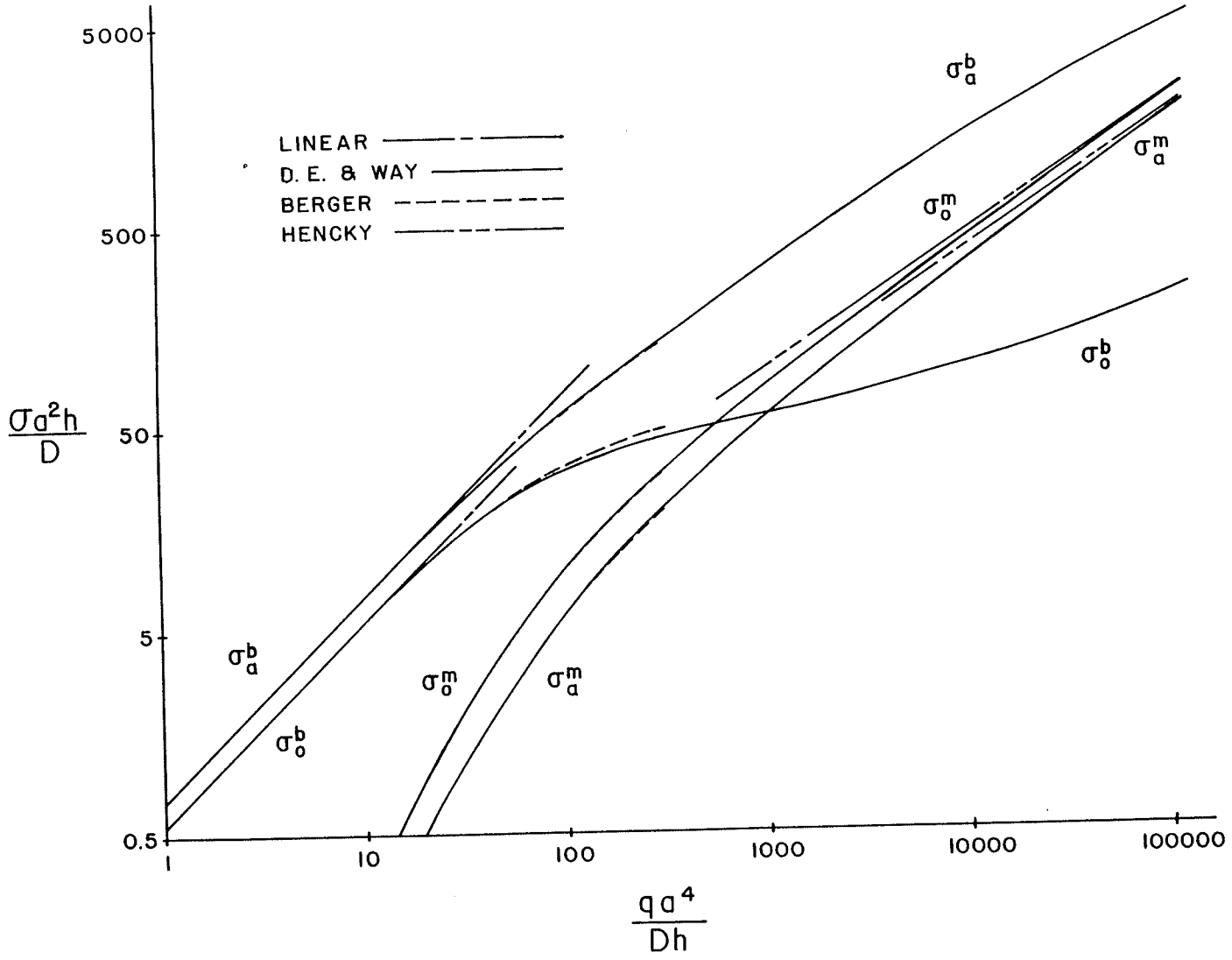

Figure 4.15 Stress versus Load for a Clamped Plate

well with the author's deflections and stresses up to its limiting value of Q = 120. The Berger stresses also agree very well with the author's solution up to Q = 300, except for the center bending stresses which are up to 10% higher.

For loads higher than Q = 50000, the clamped plate deflections and membrane stresses approach those of the simply supported plate and the Hencky membrane solution, as expected.

Figures 4.16 to 4.19 show the radial and transverse deflections for Q = 120 and Q = 300. For Q = 120 the Way, Berger and finite element solutions agree exactly for transverse deflection and within 15% for radial deflection. For Q = 300 the Berger solutions for transverse and radial deflections are about 2.5% and 7.5% lower, respectively.

The membrane and bending stresses for Q = 120 and Q = 300 are shown in Figures 4.20 to 4.23. The author's solution agrees with the Berger solution within 5%.

There is evidence of a boundary layer effect associated with the large restraining moment at the clamped edge interacting with the deformed plate for loads in excess of about Q = 3000. This effect is clearly visible in the radial bending stress profiles for Q = 3000. Figures showing these results are not included here, as considerably more study using a refined mesh at the edge is required to determine the profiles accurately. The occurrence of such boundary layer effects induced by edge moments in shallow shells is well documented. By analogy, it is reasonable [65] to expect this effect to occur in plates which are deformed sufficiently as to qualify as shallow shells in their deformed condition.

Figure 4.14 shows that the nondimensional profile of a clamped plate changes much more with applied load than the simply supported plate does. For very large loads the profiles of clamped and simply supported plates become nearly the same, and approach the shape of a uniformly loaded membrane.

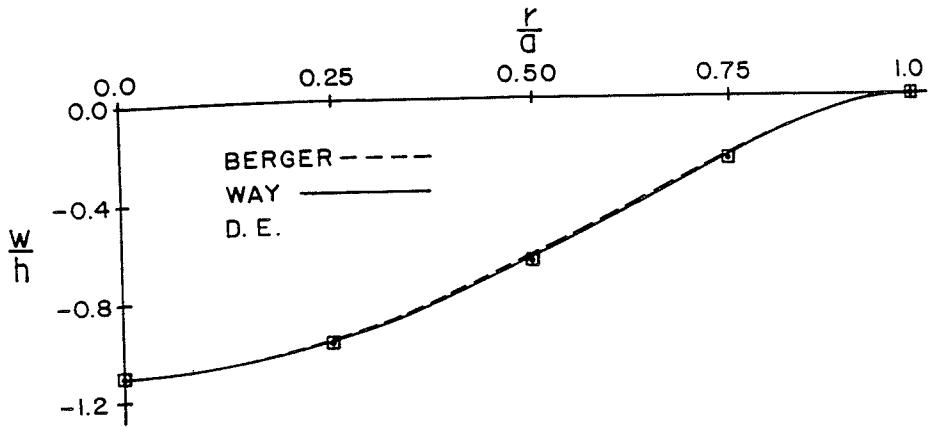

Figure 4.16 Transverse Deflection Profile for Q = 120

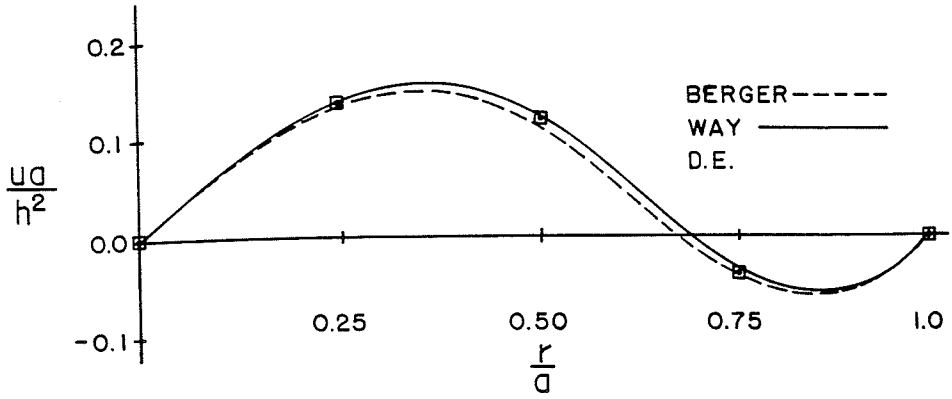

Figure 4.17 Radial Deflection Profile for Q = 120

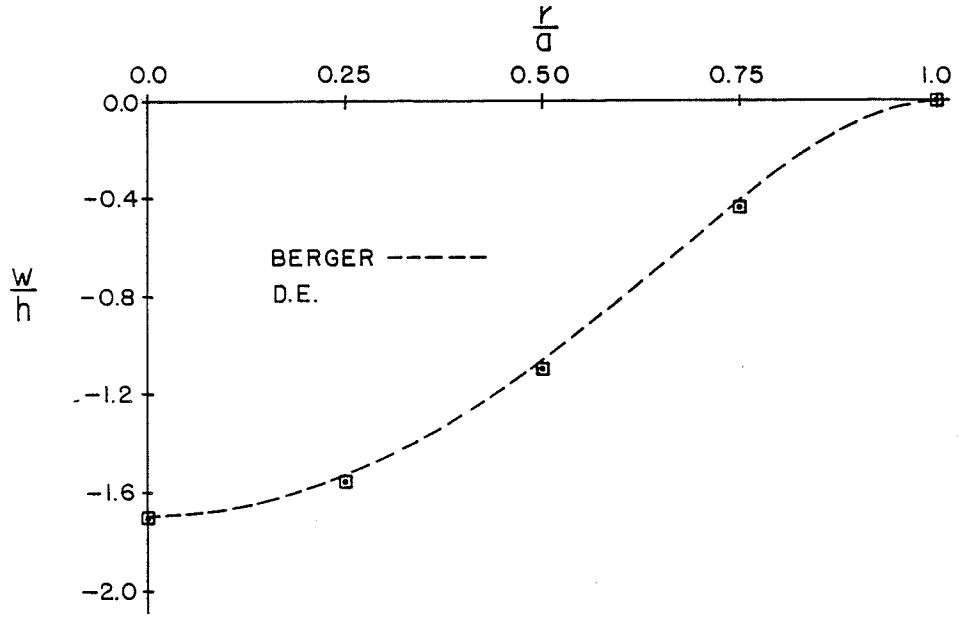

Figure 4.18 Transverse Deflection Profile for Q = 300

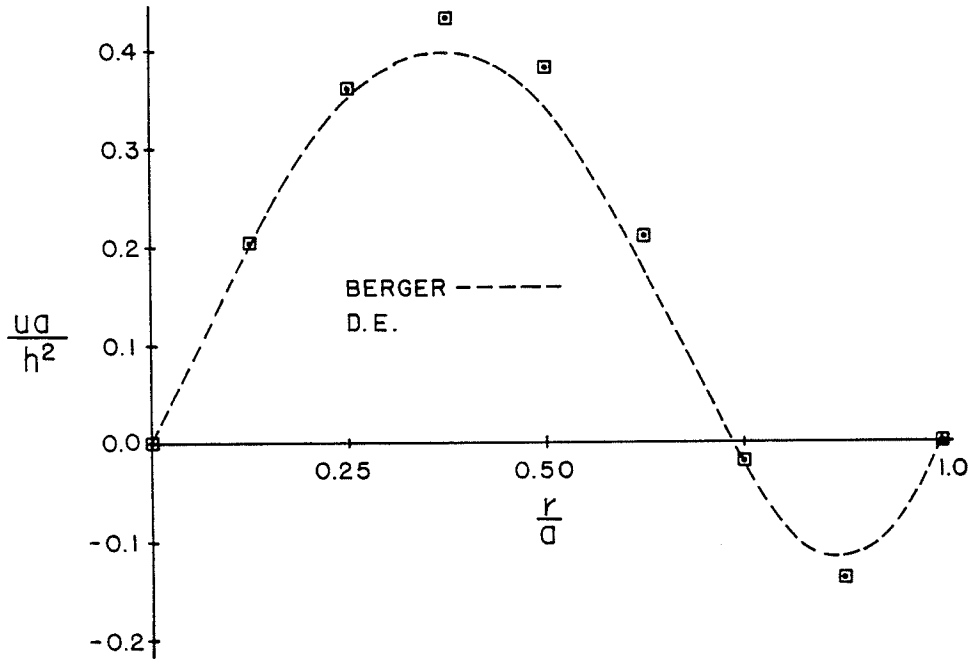

Figure 4.19 Radial Deflection Profile for Q = 300

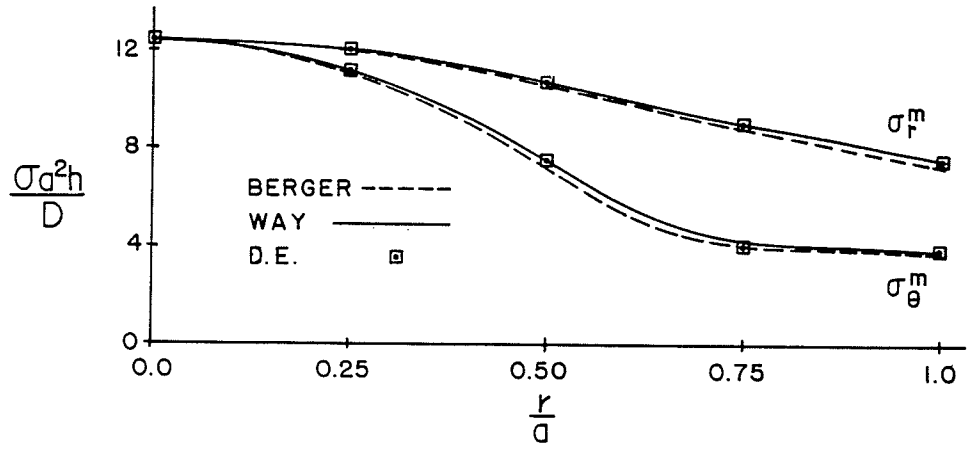

Figure 4.20 Membrane Stress Profiles for Q = 120

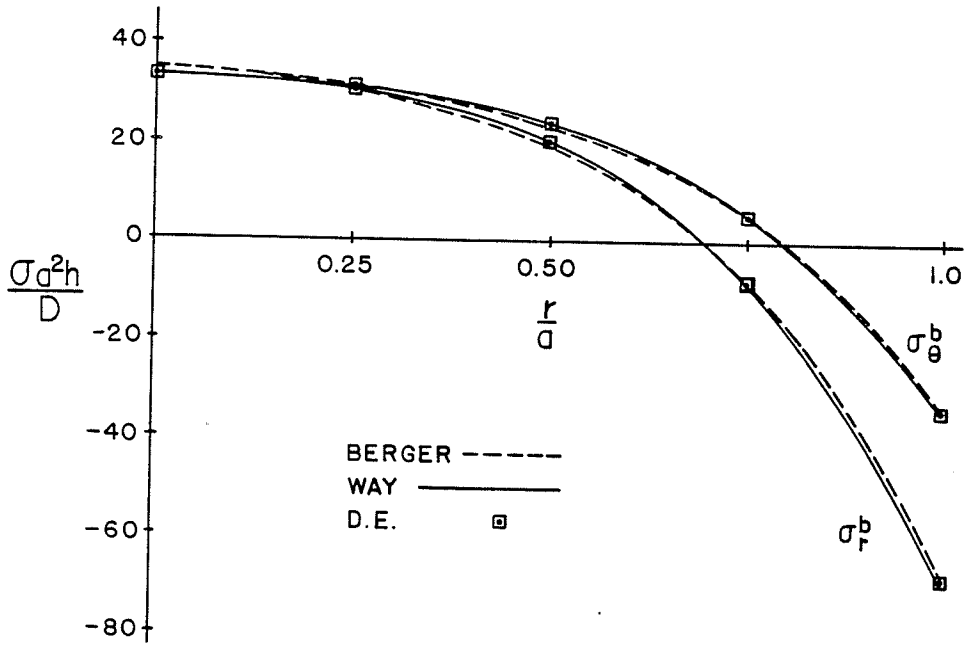

Figure 4.21 Bending Stress Profiles for Q = 120

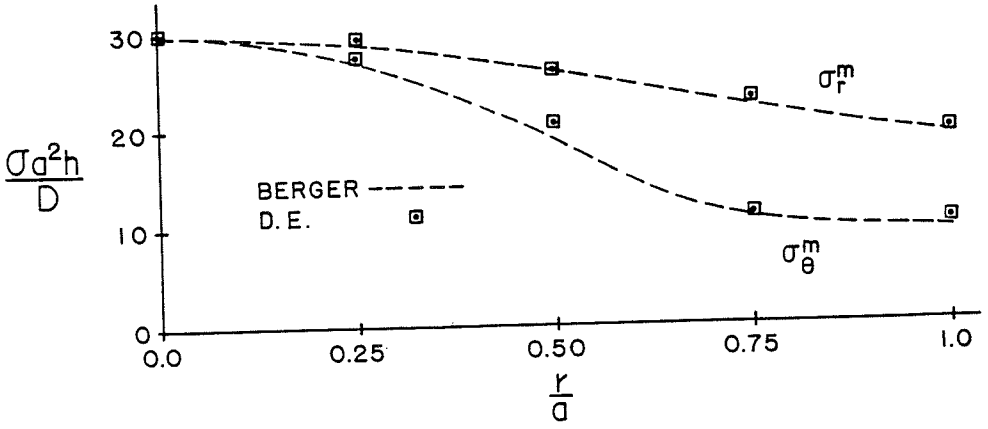

Figure 4.22 Membrane Stress Profiles for Q = 300

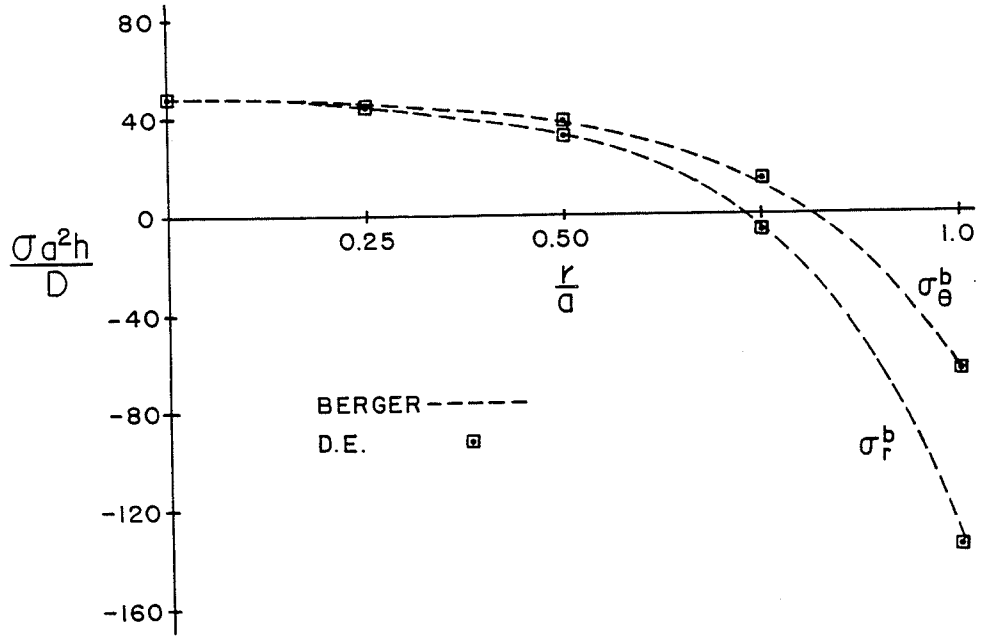

Figure 4.23 Bending Stress Profiles for Q = 300

In conclusion, we see that the 8 element numerical solution agrees very well with the linear and Way solutions over their applicable ranges for both clamped and simply supported plates. The Berger solution for clamped plates is in better agreement with the other solutions than the Berger simply supported plate solution. For large loads $Q \simeq 1000$ the solutions for clamped and simply supported plates approach each other, and together approach the Hencky membrane solution.

The introduction mentioned that the behavior of a uniformly loaded plate may depend on as many as three parameters qa^4/Dh, a/h and ν. It was subsequently noted in Section 4.2 that the analytical solutions depend only on qa^4/Dh , and on ν only as it enters through the boundary conditions. Dependence on a/h is lost by simplification of the radial strain expression and by assumed equivalence of quantities defined in Lagrangian and Eulerian coordinates. Since the author's numerical solution does not rely on these and other simplifications necessary to the derivation of the analytical solutions, it is possible to determine the dependence of the plate behavior on the parameter a/h.

Figure 4.24 shows the effect of a/h on the center deflection of both clamped and simply supported edge restrained plates. Results for a/h = 400 compare very well with the various analytical solutions, as noted earlier in this chapter. For larger values of a/h the ratio w/a of center deflection to plate radius becomes significant, even for moderate values of w/h. For a/h = 40, w/h = 14.2 at Q = 100000 the ratio w/a is approximately 0.35 and the deflection is 10 percent more than predicted by the analytical solution. The discrepancies between the analytical and numerical solutions are more pronounced for h/a = 20; and for h/a = 5 and 10 the numerical solutions diverge from the analytical solutions as soon as the limit of linear theory applicability ($w/h \leq 0.15$) is past.

It is interesting to note that the deflections of simply supported and clamped plates are indistinguishable from each other for $Q \geq 500$. This indicates that the

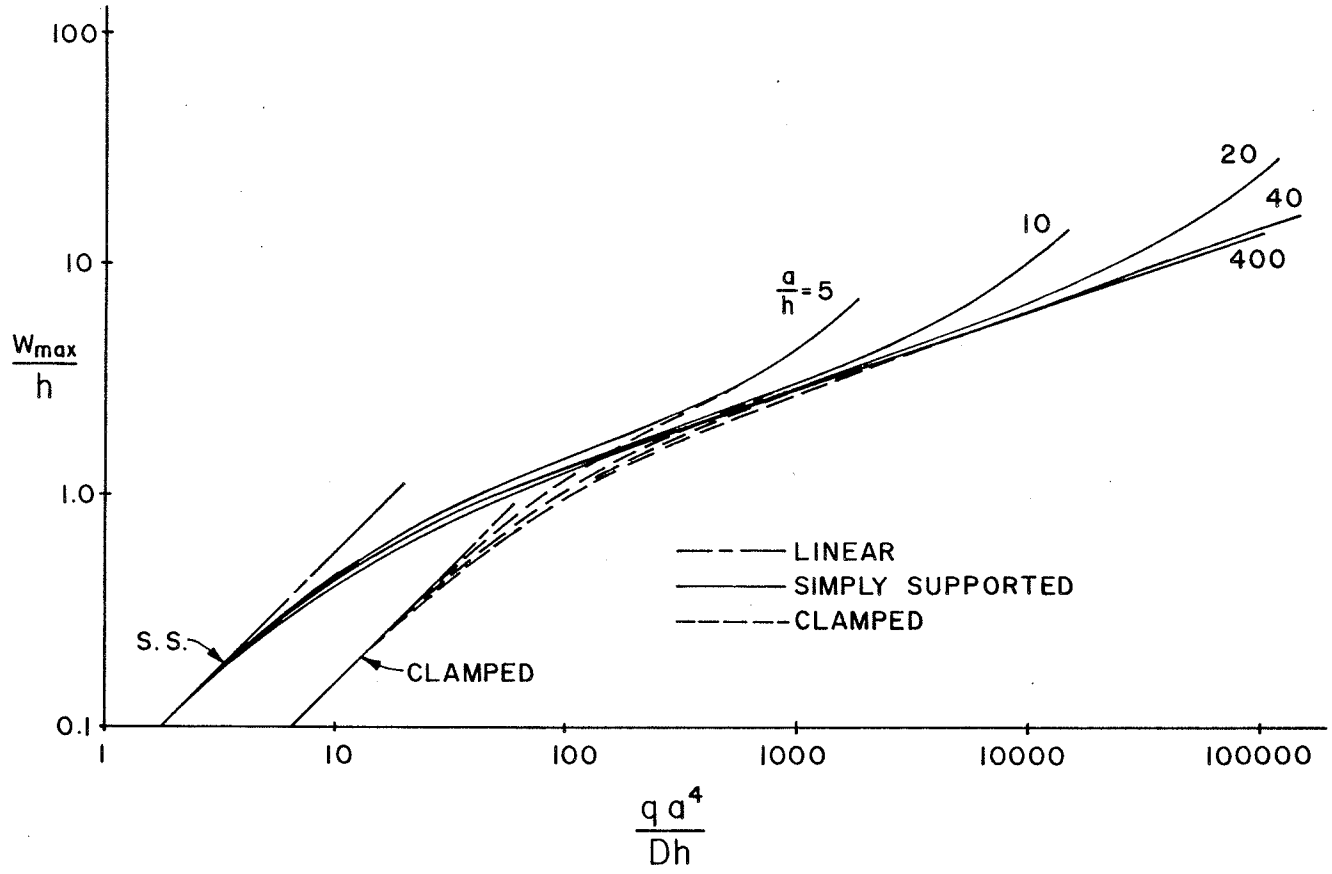

Figure 4.24 Deflection of Moderate and Thick Plates

load is carried almost exclusively by membrane stresses.

The maximum deflections shown for a/h = 5, 10 and 20 have identical meridial shapes. They correspond to center deflections of 1.4 times the plate radius and are nearly double the deflections predicted analytically. A severely deformed thick plate has a meridian shape which is significantly different from a thin plate, as shown in Figure 4.14. Membrane strains are approximately 80% and edge rotations are nearly $\pi/2$. For $du/dr \simeq 0.3$ and $dw/dr \simeq 1.4$, the meridial strain estimated by Equation (4.10) is nearly 40% too large. In addition, approximations associated with assumed equivalence of quantities in Lagrangian and Eulerian coordinates are up to 50% in error, since meridial rotations are large. Errors associated with gross geometric nonlinearities appear to account for nearly 90% of the discrepancy between the analytical and numerical solutions with the remaining 10% discrepancy due to slight material nonlinearities.

CHAPTER 5

POINT LOADED SPHERICAL CAP

5.1 INTRODUCTION

This chapter considers the axisymmetric response of a freely supported spherical cap to a point load. (A freely supported cap is not radially restrained at its edge; a simply supported cap is). Caps of half angle 5°, 22-1/2° and 90°, and varying thickness are considered. By using a displacement formulation in the numerical analysis, the response of the shell to eversion and beyond, including unstable equilibrium configurations is found. The response of the caps to reverse loading, which returns them to their original shape, is also studied. In the case of caps which are deep compared with their thickness, snapthrough is observed in both the eversion and return loading paths. Caps which exhibit snapthrough produce two different sets of meridian contours - one set followed for eversion and the other followed for reverse loading.

A great deal of work has been, and continues to be published on the nonlinear deformation and buckling of the complete sphere and the similarly behaved clamped spherical cap. Most of this work is concerned with pressure loading. See Kaplan [37]. It is unfortunate that relatively little research has been done on freely and simply supported caps as they, unlike clamped caps, exhibit a snapthrough behavior on loading to eversion and snapthrough in returning to their original shape. This latter phenomenon has apparently not been studied before. The use of a point load allows the basic behavior of the shell to be studied, without interference from stability effects associated with follower loads such as pressure. The reader is referred to References [21] and [70] for a comprehensive treatment of the singularity effects produced by the point load.

The spherical cap is not an inherently stable geometry under a point load, and may bifurcate into any of several asymmetric configurations. See Bushnell [10]. A general discussion of stability is beyond the scope of this thesis. The reader is referred to Koiter [38] and Thompson and Hunt [76] for a general discussion of stability. Suffice it to say, that care has been taken to ensure that the geometries considered here are within the range that has been shown experimentally [18] and numerically [10] to produce axisymmetric deformations.

Non-dimensional parameterization of the problem requires results presented in the next sections, in conjunction with analytical solutions.

5.2 GOVERNING EQUATIONS AND LINEAR SOLUTIONS

Consider the freely supported spherical cap in Figure 5.1. Its radius is a, its half angle ξ_o and its thickness h. The rise of the shell H and its base radius L are given by

$$H = a(1 - \cos \xi_o) \tag{5.1}$$

and

$$L = a \sin \xi_o \, . \tag{5.2}$$

An axial load P is applied at the apex of the cap and is taken as positive when in the direction shown.

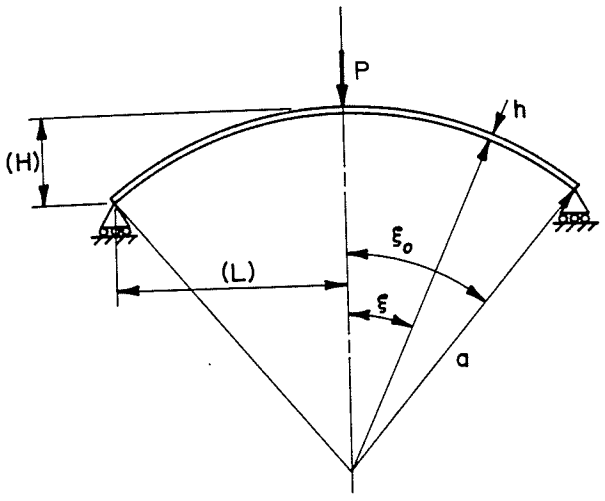

Figure 5.1 Spherical Cap

The response of a spherical cap is governed by Equations (2.107) to (2.109) subject to initial conditions.

$$K_1 = K_2 = a \tag{5.3}$$

Additional relationships

$$\xi = \left(\frac{S}{a}\right)$$

$$\Phi = -\left(\frac{S}{a}\right)$$

$$R = a \sin\left(\frac{S}{a}\right)$$

and

$$Z = a\left[1 - \cos\left(\frac{S}{a}\right)\right] \tag{5.4}$$

where, ξ is the angle to a generic point from the z axis, and Φ, R and Z give the angular, radial and axial position of the point in its undeformed configuration, can also be specified. For a free shell edge, the meridial edge moment M_1 at the edge of the shell ($\xi = \xi_o$) is zero

$$M_1\Big|_{\xi = \xi_o} = 0 \tag{5.5}$$

as is the radial component of the edge reaction force given by

$$-Q_1 \sin\phi + N_1 \cos\phi = 0 \tag{5.6}$$

See Figure 5.2. Note that Φ is measured in the deformed state. Application of the point load P is accomplished by use of a delta function at the apex as a special form of distributed axial load $q(r)$

$$q(r) = P\,\delta(r) \tag{5.7}$$

or by noting from free body considerations that

$$-2\pi r[Q_1 \cos\phi - N_1 \sin\phi] = P \tag{5.8}$$

not only at the shell edge but everywhere over the shell.

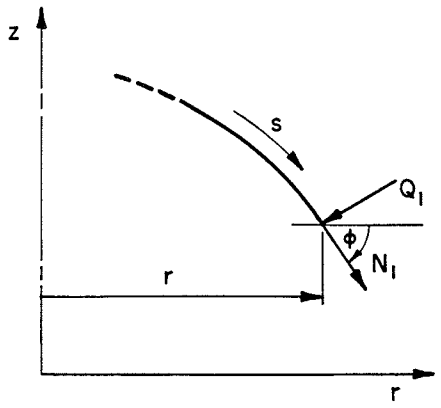

Figure 5.2 Load Resultants

A lucid derivation of the fourth order complex form differential equation governing the infinitesimal axisymmetric deformation of shells of revolution is given by Mollman [49, Section 2.2]. See also Novozhilov [55]. For the case of spherical caps, this equation reduces to the second order equation

$$\frac{d^2Q_1}{d\xi^2} + \frac{dQ_1}{d\xi}\cot\xi - Q_1\cot^2\xi + i\lambda^2 Q_1 = 0 \qquad (5.9)$$

where Q_1 is the shear in the meridian direction

i is $\sqrt{-1}$

ξ is the angle to a generic point from the shell apex (See Figure 5.1), and

$$\lambda^4 = 12(1 - \nu^2)\left(\frac{a}{h}\right)^2 - \nu^2 \ .$$

Equation (5.9) can be solved exactly for Q using hypergeometric functions. Other stress resultants and stresses are then determined [49, p. 74] from Q. Such solutions are however, quite difficult to obtain and alternate solutions are usually sought. It can be shown [11, Chapter 8] that load support in shells occurs by mutually interacting mechanisms of bending and in-plane stretching. For the plate discussed in the previous chapter, stretching or membrane effects

are not available to carry load until the plate is sufficiently deformed by the applied load that it is nonplanar. Since a shell is nonplanar even in its rest configuration, membrane effects can act immediately. This nonplanar requirement is typical of stretching mechanisms, since like the cable in a suspension bridge they are only effective in carrying the component of load which is tangent to the shell.

A cap which is sufficiently shallow that $L/(a/h)^{\frac{1}{2}} < 1$ carries load essentially like a plate. When the cap is simply supported, a point load produces deflections shear and moment resultants which are monotonic with respect to r. For deeper caps, bending effects are oscillatory and decay quickly away from the point load. This boundary layer effect is associated with interaction of the otherwise monotonic bending effects and membrane effects. The same effect can be seen in a beam with a transverse end load on an elastic foundation. While a similarly loaded free cantilever has a monotonic displacement, the addition of elastic support produces oscillatory displacements and stress resultants which decay away from the load. Indeed, Hetenyi [31, Section 49] shows that the shell equations are approximately analogous to those governing a beam of variable cross-section on an elastic foundation of variable stiffness. It has been shown [11, Section 9.7; 21], that bending effects are essentially confined to a region of radius $r \simeq 3(ah)^{\frac{1}{2}}$. Membrane stresses and deformation outside this region are also relatively insignificant. Consequently, provided the boundaries of the shell are sufficiently distant from the point load ($L > 3(ah)^{\frac{1}{2}}$), the apex deflection and maximum stress resultant values are independent of L, the radius of the cap base.

The above observations suggest possible simplifications to the governing equation (5.9). These approximations rely on simplifications which can be made

when the shell has certain geometric properties. See Donnell [17, Section 6.6] and Mollman [49, Section 2.3] for justification of these approaches. The shallow shell approach takes advantage of certain approximations which are valid when the slope of the shell is small. A variety of general solutions of this type for spherical caps are given by Hetenyi [31, Section 49], Mollman [49, Section 2.3], Timoshenko [79, Section 129-130], Flugge [20, Section 6.2.1], Seide [71, Section 6.5] and Reissner [63]. A historical treatment of the problem is given in Novozhilov [55, Section 50]. When slopes are small

$$\cot\xi \approx \frac{1}{\xi} \tag{5.10}$$

and Equation (5.9) simplifies to

$$\frac{d^2Q_1}{d\xi^2} + \frac{1}{\xi}\frac{dQ_1}{d\xi} - \frac{Q_1}{\xi^2} + i\lambda^2 Q_1 = 0 \ . \tag{5.11}$$

Specific solutions for a point load at the apex are given by Calladine [11, Section 9.7], Seide [71, Section 6.11], Flugge [20, Section 6.2.1.6], and Reissner [64].

An approach known as Geckeler's method [24] provides solutions in regions where the slope of the shell is high, and the governing equation (5.9) can be simplified to

$$\frac{d^2Q_1}{d\xi^2} + i\lambda^2 Q_1 = 0 \tag{5.12}$$

The method is useful for investigating the effects of loads or restraints at the edges of spherical caps. Since the caps of interest here have free edges, solutions of this type, such as those given by Mollman [49, Sections 2.3 and 2.6] and Calladine [11 Section 11.2.4] are only mentioned here for the sake of completeness. Deflections and stress resultants caused by edge loads also exhibit boundary layer behavior and are quickly damped out away from the shell edge. Calladine shows that all regions of a spherical cap are adequately described by either shallow

shell theory or Geckeler's method.

In addition to providing insight into the behavior of spherical caps, the linear solutions suggest suitable dimensionless parameters. See Taylor [75] for a discussion of dimensional analysis. One such parameter is

$$\lambda^4 = 12(1-\nu^2)\frac{a^2}{h^2} - \nu^2 \tag{5.13}$$

which occurs in the general governing equation (5.9) and in both simplified equations (5.11) and (5.12). Since

$$\nu^2 << 12(1-\nu^2)\left(\frac{a}{h}\right)^2 \tag{5.14}$$

the second term (ν^2) is usually ignored. However, the deflections predicted by linear analyses are confined to a region of radius $r \simeq 3(ah)^{\frac{1}{2}}$. Deformations associated with large deflections are not, as shown by the nonlinear solutions discussed in Sections 5.3 and 5.4. Hence, the geometric parameter

$$\lambda^2 = [12(1-\nu^2)]^{\frac{1}{2}}\frac{a}{h}\sin^2\xi_o \tag{5.15}$$

which also accounts for the base diameter of the shell has proved more suitable. For shallow shells this parameter is often [4,10,37, et cetera] defined as

$$\lambda^2 = [12(1-\nu^2)]^{\frac{1}{2}}\frac{a}{h}\xi_0^2 \tag{5.16}$$

A load parameter which is consistent with the solutions for a point loaded cap is $P^* = Pa/Eh$. The dimensionless deflection is frequently defined as w/h. This definition is consistent with the linear theory and provides deflection curves which in the small are almost solely dependent on the load P^*. Since we are interested in deflections to eversion where deflection is approximately twice the rise H of the shell, the dimensionless deflection w/H which provides similarity

in the large, is more suitable. We therefore assume the spherical cap to be described by geometric parameters

ξ_o = shell half angle, and

$\lambda^2 = [12(1 - \nu^2)]^{\frac{1}{2}} \frac{a}{h} \sin^2 \xi_o$;

material parameter

ν = Poisson's ratio;

and load and deflection parameters given respectively by

$P^* = \frac{Pa}{Eh^3}$ and

$\frac{w}{H}$ = center deflection/shell rise.

The load-deflection curve of a hemispherical cap is therefore given implicitly by

$$0 = \phi(\xi_0, \lambda^2, \nu, P^*, \frac{w}{H}) .$$

5.3 NONLINEAR SOLUTIONS AND EXPERIMENTAL RESULTS

The first nonlinear analysis of a freely supported spherical cap subjected to a point load at its apex was performed by Biezeno [9] in 1935. He derived a pair of coupled nonlinear equations for the radial and angular displacements u and ψ respectively of the shell middle surface. He then assumed the angular displacement ψ to take the form

$$\psi = C_1 \frac{r}{a} + C_2 \frac{r}{a} \ell n \frac{L}{r} \qquad (5.17)$$

and solved for u using one differential equation. A new function ψ^* results from substitution of functions ψ and u in the nonlinear and coupling terms of the other differential equation. Constants C_1 and C_2 were then found by equating the center deflection and edge rotation predicted by ψ and ψ^*.

In 1957 Chien and Hu [13] considered the more general case of a spherical cap with an axisymmetric ring load at radius αL. Coupled nonlinear equations in axial displacement w and meridial normal stress resultant N_1 were derived. By assuming the axial displacement in terms of center deflection w_o to take the form

$$w = w_o\left[1 - \left(\frac{r}{L}\right)^2\right]\cdot\left[1 - \frac{1+\nu}{5+\nu}\left(\frac{r}{L}\right)^2\right] , \qquad (5.18)$$

membrane stresses and total system energy $\bar{U}$ associated with the shell were obtained using one of the differential equations. A relationship between load P, α and w_o was then found by setting $d\bar{U}/dw_o=0$. For $\alpha=0$ the load is applied at the apex of the shell and results similar to Biezeno's are obtained.

In 1959 Ashwell [5] observed that point loaded caps exhibit two distinct regions: the outer region is essentially undeformed, and the inner region is a dimple where the shell is approximately everted. This observation is consistent with Love's concept of applicable surfaces, which states [44] in part, that the displacements of the middle surface of a shell may be of any order of magnitude, provided the shell is not over-strained.

> "This condition shows at once that, if the displacement is not very small, the strained middle surface must be, either exactly or very nearly, a surface applicable upon the unstrained middle surface."

(A surface which can be transformed from another surface without stretching or folding is said to be applicable on the first. Surfaces, such as cylinders and cones, which are applicable on a plane, are known as developable surfaces). Ashwell [5, p.44] recast Love's principle as

> " In the case of an initially curved shell, the middle surface must, after strains, be either a surface applicable on the unstrained surface, or derivable from such a surface by a displacement which is everywhere small."

On the strength of this principle, Ashwell described the displacement of the shell inside the dimple from an everted cap and from an undeformed spherical annulus in the outer region by two sets of Reissner's [63] linearized shallow shell equations. Radial displacements are ignored. Coefficients associated with the resulting Kelvin function terms are determined from equilibrium and compatibility considerations where the two solutions patch together at the edge of the dimple, and by the boundary conditions at the shell edge. The dimple radius is determined as a function of load using the assumption that the meridian tangent is normal to the z axis of the shell at this radius. The deflection is then calculated as the sum of the linearized deflections in the inner and outer regions and twice the dimple rise. His results are consistent with his own experiments on shallow aluminum alloy shells and with the earlier analytical work of Biezeno and Chien.

The first numerical analysis of the point loaded cap was done by Archer [4] in 1962. Like most of the numerical investigations mentioned here, Archer considers several different problems, including the point loaded cap. Reissner's nonlinear differential equations [66] for shells of arbitrary shape are solved for shallow shells using a finite difference scheme.

Evan-Iwanowski, Cheng and Loo published extensive experimental results for point loaded caps in 1962 [18] and 1964 [43]. Both metal and plastic specimens were studied. Their experiments are particularly valuable in verifying certian analytically predicted results. Of particular interest here: shells with $\lambda < 3.7$ exhibit monatonic load-deflection curves (cf. Biezeno, Chien and Ashwell who give values of 3.85, 3.64 and 3.56, respectively). Shells with $\lambda > 10.2$ buckle asymmetrically; the parameter H/L does not affect the critical load. Their conclusion that deep caps do not exhibit snapthrough does not agree with observations made herein.

Wilson and Spier [89] consider the deep spherical cap in their 1964 paper, which presents a general finite difference scheme for large axisymmetric deformations of thin shells. Load-deflection curves for inward and outward directed point loads, as well as selected stress and displacement contours, are given for loads less than the critical load.

Mescall [47,48] presents the first numerical analysis of load-deflection behavior in the post-buckling range for point loaded spherical caps. His load-deflection curves [47] include unstable equilibria, and for positive apex loads are in good qualitative agreement with the analytical results of Biezeno and the experimental results of Evan-Iwanowski et al. However, his load-deflection curves for negative post-buckled loads do not. The load-deflection curve given in [48] claims as many as nine (9) equilibrium states for a given load. Mescall notes from the experimental evidence [18] that real caps apparently ignore the bifurcation which his analysis shows can occur below P_{cr}. He notes that the axisymmetric contours at the bifurcation point are significantly different from each other. In view of the experimental and theoretical [85] evidence, it would appear that many of the equilibrium states Mescall predicts are not produced physically.

Bushnell [10] presents a finite difference analysis of spherical caps both for inward and outward directed point loads. His analysis shows that bifurcation occurs almost simultaneously with axisymmetric collapse for inward directed point loads when λ=9.54. He also shows that the pre-buckling load-deflection curves of simply supported caps approach those of a complete sphere as λ becomes large. Buckling loads are given for outward directed loads.

Ranjan and Steele [61] use Love's concept of applicable surfaces to solve the point loaded cap problem. Their approach is similar to Ashwell's [5] except

that: the meridian is assumed steep at the junction of inner and outer regions with the consequence that algebraic expressions, rather than Kelvin functions, result; dimple base radius is determined using an energy minimization principle; and nonlinear effects of pre-stress and moderate rotation are included.Loads as much as 20% less than Ashwell's,and in better agreement with experiments,result. Ranjan and Steele demonstrate their method on a cap with a clamped edge. Their results are, however, deemed pertinent to the problem at hand, since the shells are deep and since the results provide a valuable comparison with Ashwell's often quoted results.

In 1974 Kaplan [37] published an extensive survey on the buckling of spherical shells. While the survey did not discuss the point loaded cap in as much detail as the review given here, it does discuss a number of interesting related problems.

Vyrlan and Shil'krut [85] discuss a number of important current issues in stability of axisymmetric shells. In particular, they note that repeated snapping cannot occur and that "not more than two stable (at least in the small) axisymmetric equilibrium forms can correspond to the same value of the load parameter".

Parish [60], 1978 gives a finite element analysis of thin spherical caps with a point load for $\lambda^2 = 36$ and $\lambda^2 = 100$. Meridian contours are given for $\lambda^2 = 36$ and $\lambda^2 = 100$ through to eversion. The author gives the total computer time to calculate load-deflection for $\lambda^2 = 100$ as 20 minutes and states that 1/3 of this time is used passing through the snapthrough zone.

5.4 RESULTS AND DISCUSSION

Spherical caps with half angles $\xi_o = 5°$ and $22.5°$ are considered as representative of shallow caps, and a hemisphere is considered as an example

of a deep cap. It is noted in Section 5.3 that spherical caps with λ less than about 3.6 exhibit monotonic load-deflection curves similar to flat plates. Hence, discussion is limited to caps with higher λ values. Since the axisymmetric deformation of a spherical cap is not necessarily stable, it is necessary to also establish an upper limit of $\lambda \simeq 10$ on the caps analyzed here. This has been shown experimentally [18] and numerically [10] to be an approximate upper limit above which asymmetrical deformations can occur in shallow shells. The author's experimental results, discussed in part at the end of this section, indicate that this is also valid as an approximate limit for hemispheres.

Spherical caps with $\lambda^2 = 16, 36, 64$ and 100 were modelled numerically. Caps with $\xi_o = 5°$ and 22.5° are modelled accurately by 8 equal length elements. Sixteen similar elements are necessary to model a hemisphere ($\xi_o = 90°$), as the meridian extension λ_1 (not to be confused with the geometric parameter λ) varies considerably along the meridian and is not modelled well by elements over which λ_1 is constant. The refined model is particularly important for thin hemispheres ($\lambda^2 > 50$) where membrane effects governed by λ_1 predominate. Sample runs on shallow shells using 16 elements showed the 8 element model to be approximately 2% more rigid than its 16 element counterpart.

The analysis program is designed to start loading from either a rest or everted configuration. This facilitates modelling of the return path. The numerical scheme occasionally encounters difficulty following the snapping behavior. In these cases, it is convenient to begin at the everted configuration to calculate the return path. The return path of all shells with $\lambda^2 > 36$ is calculated to provide certainty as to whether snapping occurs or not. See, for example, shallow shells with $\lambda^2 = 64$.

By specifying apex displacement, rather than load, stable as well as unstable equilibrium states are observed and the mechanism of snapping is clearly

demonstrated.

Figure 5.3(a) shows the load center deflection curve of a cap with half angle $\xi_o = 22.5°$ and $\lambda^2 = 16$. The term deflection and corresponding symbol w will hereafter refer to the apex deflection, unless noted otherwise. Figure 5.3(b) shows the meridian contours, and loads associated with selected deflections. The correspondence between meridian contours and points on the load deflection curve is indicated by upper case letters. The rest state is at B . State A is a cap with an outward load and deflection. For inward deflections, the load is always inwards and reaches a relative maximum at D where $w/H \simeq 0.8$. This maximum of $Pa/Eh^2 = 1.33$ is known as the critical load P_{cr} . This local maximum is a critical load in the sense that if a load is specified, the displacement jumps from $w/H \simeq 0.8$ at D to $w/H \simeq 2.0$ between E and F as the load increases from P just less than, or equal to, P_{cr} to P slightly greater than P_{cr}. States from D to E are unstable as the load carrying capacity of the shell decreases with increasing displacement. These states can however be demonstrated experimentally by specifying displacement rather than load. From E to H load increases monotonically with load. The shell becomes nearly conical at large center displacements.

Figure 5.4 shows the load-deflection curve and meridial contours for a cap with $\lambda^2 = 36$. This identical to the cap in the previous figure, except that it is about half as thick. It is not surprising then, that they exhibit similar behavior. The thicker cap however, exhibits three configurations which are sustained by zero load. The two stable configurations are the rest state B and the everted state G . A self-equilibriating everted state is possible in a thin cap since membrane effects are sufficiently strong to overcome bending effects, which tend to roll the edges back down and restore the shell to its rest position. Two important features are visible at the edge of the meridial contour G : The

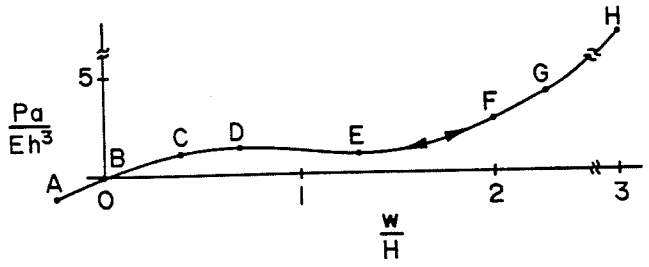

(a)

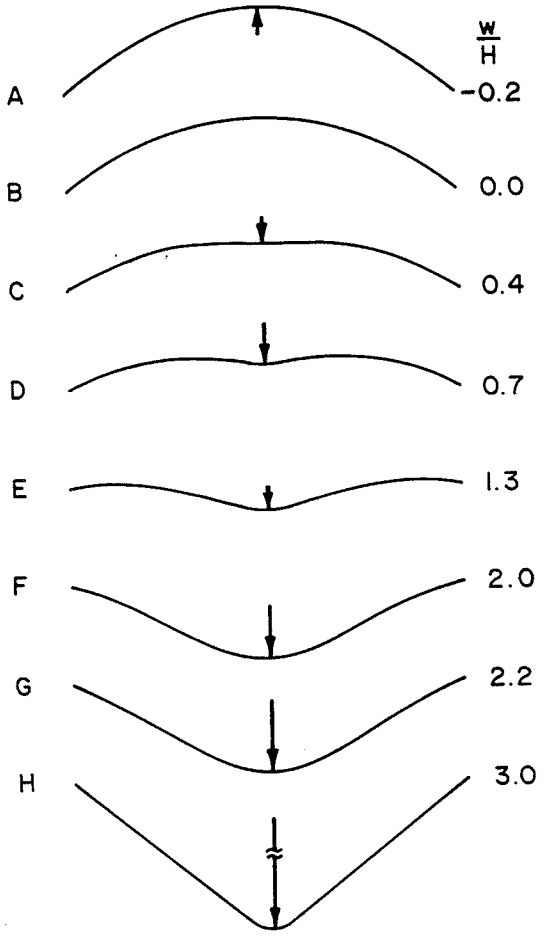

(b)

Figure 5.3 Load-Deflection and Meridian Contours for $\lambda^2 = 16$

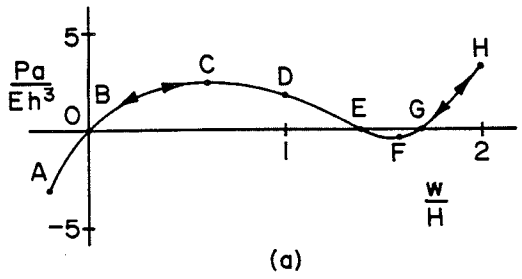

(a)

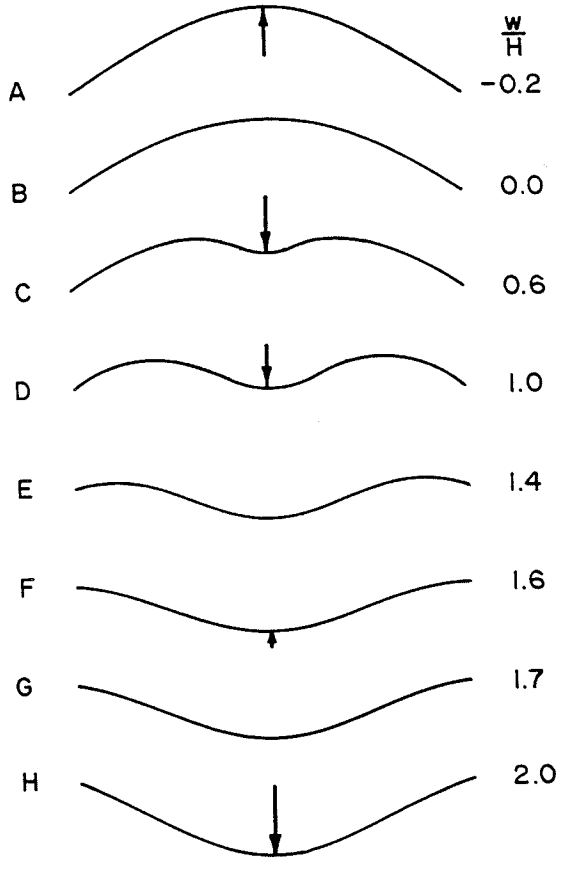

(b)

Figure 5.4 Load-Deflection and Meridian Contours for $\lambda^2 = 36$

meridian curvature has the same sign at the edge of the shell here and in every other configuration as it does in the rest state, as membrane effects must operate along a sufficient distance from the edge of the cap before sufficient force is developed to reverse the meridian curvature. Secondly, the edge slope is of opposite sign here compared to the rest configuration. This is clearly necessary if membrane effects which produce inward radial forces, are to prevent bending effects from rolling the edges down and returning the cap to its rest configuration. The everted state has been studied extensively by others [26, Section 2.20;3].

The load-deflection curves and contours shown in Figures 5.3 and 5.4 represent continuous deflection paths which are reversible at any point. The same states are produced by increasing the center deflection from w/H = 0 to w/H = 2 as are produced by reducing it from w/H = 2 to w/H = 0. This is not necessarily true for caps with higher values of λ^2.

Figure 5.5 shows the load-deflection curves and meridian contours produced by a cap with $\lambda^2 = 100$. Increasing deflection produces increasing load up to a critical load at point D followed by a decrease in load to zero at E . From E the shell snaps to a new configuration F . Rather than having a large dimple at E it has snapped to a new state of complete eversion, except for a small reverse dimple at the center. State F has the same center deflection as state E , but its strain energy is approximately 30% less. From F to G the reverse load required to maintain a particular deflection decreases. At G the cap is everted and is in equilibrium without external forces.

As the cap is returned to its rest state it again follows the curve H - G - F, but a new sequence of configurations is produced along F - J - K. At K the cap snaps to C and returns to B along the everting curve C-B. A cap with $\lambda^2 = 100$ is sufficiently thin that its bending resultants are relatively insignificant. Hence, it behaves essentially like a membrane structure. Since the behavior

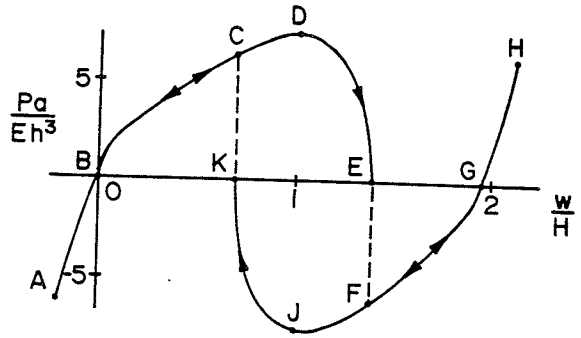

(a)

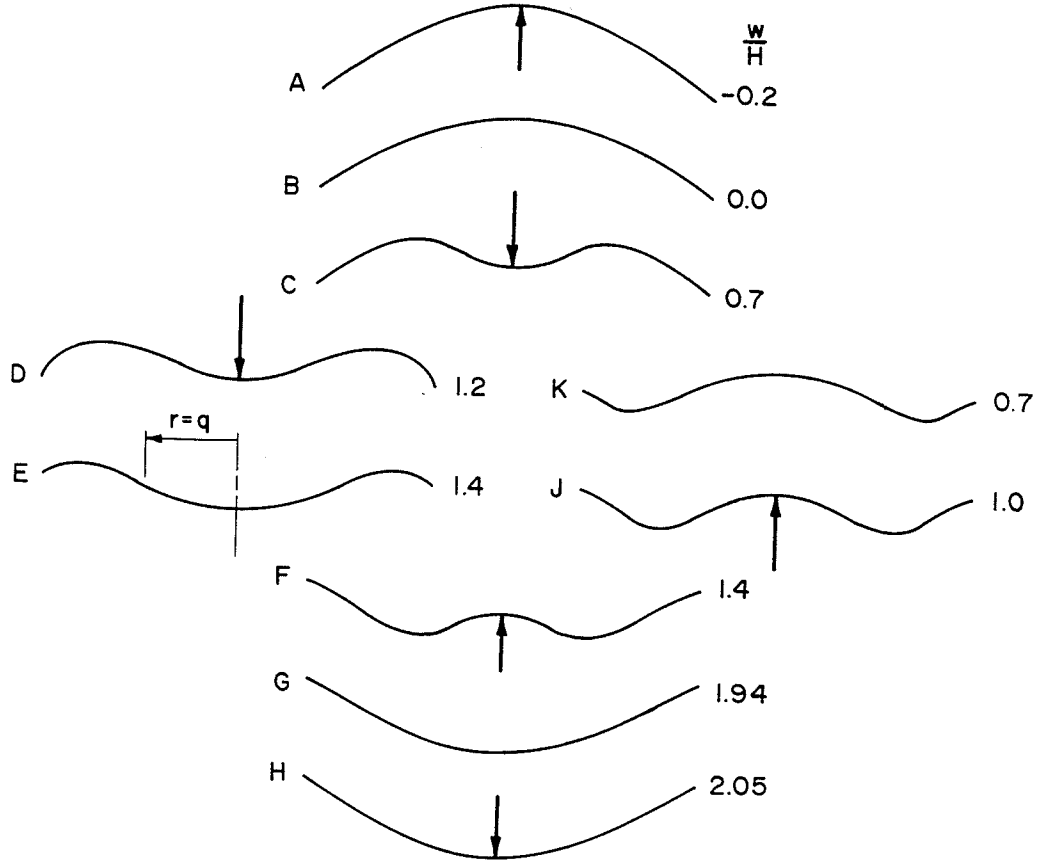

(b)

Figure 5.5 Load-Deflection and Meridian Contours for $\lambda^2 = 100$

of the rest and everted forms of a membrane structure are indistinguishable it is reasonable for the eversion and return paths of a very thin cap to be nearly identical (but rotated). Figures 5.4 to 5.7 and 5.10 show that load-deflection curves, meridians and snapping behavior become increasingly symmetrical with increasing λ^2.

It is reasonable to ask why some caps snap, while others which require a restraining force along the path to eversion, do not. Consider first, the cap shown in Figure 5.5 which exhibits snapping. Imagine the cap to be separated into two parts at radius $r = q$, the point of inflection along the meridian at state E . The inner region is nearly spherical and changes shape only slightly from state D to state E . The load curve from D to E is therefore due primarily to effects associated with the outer region. As a first approximation to the response of the outer region for deflections larger than at E , the load-deflection curve can be linearly extrapolated below zero force from E . The outer region then prefers to deflect more beyond E . The response of the inner region is similar to the curve through G since deflection of the everted sphere is governed by the response of the center dimple. Since the inner region is less stiff than the outer region, as shown by the lesser slope of its load-deflection curve (at G) compared with the outer region (at E), the outer region moves to the less stressed state F at the expense of the inner region becoming dimpled. It is clear that snapping begins at zero load, as this is the point at which the outer region is just able to provide the force to drive the inner region to its dimpled configuration. Static equilibrium states do not exist between E and F and a sudden snapping occurs as the shell goes from E to F .

The cap shown in Figure 5.4 is somewhat thicker than that shown in Figure 5.5. As a result, bending effects are more significant. Their presence causes the initial dimple to be smaller and less deep. The total deflection is due to

significant contributions from both inner and outer regions. The stiffness of the outer region at state E is approximately the slope of the load-deflection curve at E and the stiffness of the inner region, the slope at G. Since the inner region at state E (zero load) is stiffer than the outer region, snapping does not occur. For low λ^2, bending effects are prominent and cause a significant meridial curvature of the same sign as in the undeformed shell to occur at all times along the edge. It is this curvature which causes the outer region to be relatively less stiff and causes the edges to roll down on reverse loading, rather than for a significant reverse dimple to form.

Bending effects prevent shells with lower λ^2 values from everting to a more nearly spherical shape with $w/H \simeq 2.0$. Furthermore, bending effects acting in the direction of the cap parallels provide axisymmetric stability. These effects decrease with increasing λ^2 and above $\lambda^2 \simeq 100$ no longer provide sufficient stiffness in the parallel direction to ensure that deformations are axisymmetric. The experimental results of Evan-Iwanowski [18, Figs. 7.21 and 7.22] suggest that plastic caps may not maintain their stiffness in the parallel direction as the material deforms, as metal caps do; and that this may account at least in part, for their earlier collapse.

Figure 5.6 shows load deflection curves for $\lambda^2 = 16$, 36, 64 and 100, and cap half angles $\xi_o = 5°$ and 22.5°. These half angles correspond to caps having rise to base radius, ratios of $H/L = 0.044$ and $H/L = 0.20$, respectively, and represent shells ranging from very shallow to approximately the common limits of $H/L = 1/4 = 0.25$ [63] and $H/L = 1/6 \simeq 0.17$ [18] for shallow shells. From the figure it is clear that the response is largely independent of ξ_o when it is less than 22.5°. This is reasonable in view of the fact that the axial position of an undeformed hemispherical cap is given by

$$z = H - a\left(\frac{\xi^2}{2!} - \frac{\xi^4}{4!} + \frac{\xi^6}{6!} - \cdots\right) \tag{5.19}$$

which for a shallow shell simplifies to

$$z \simeq H\left(1 - \left(\frac{r}{L}\right)^2\right) \tag{5.20}$$

indicating that all shallow spherical caps have the same essentially parabolic shape and differ from one another only in rise H. Note that the curves for $\lambda^2 = 64$ are very similar to the loading curve for $\lambda^2 = 100$ which exhibits snapping.

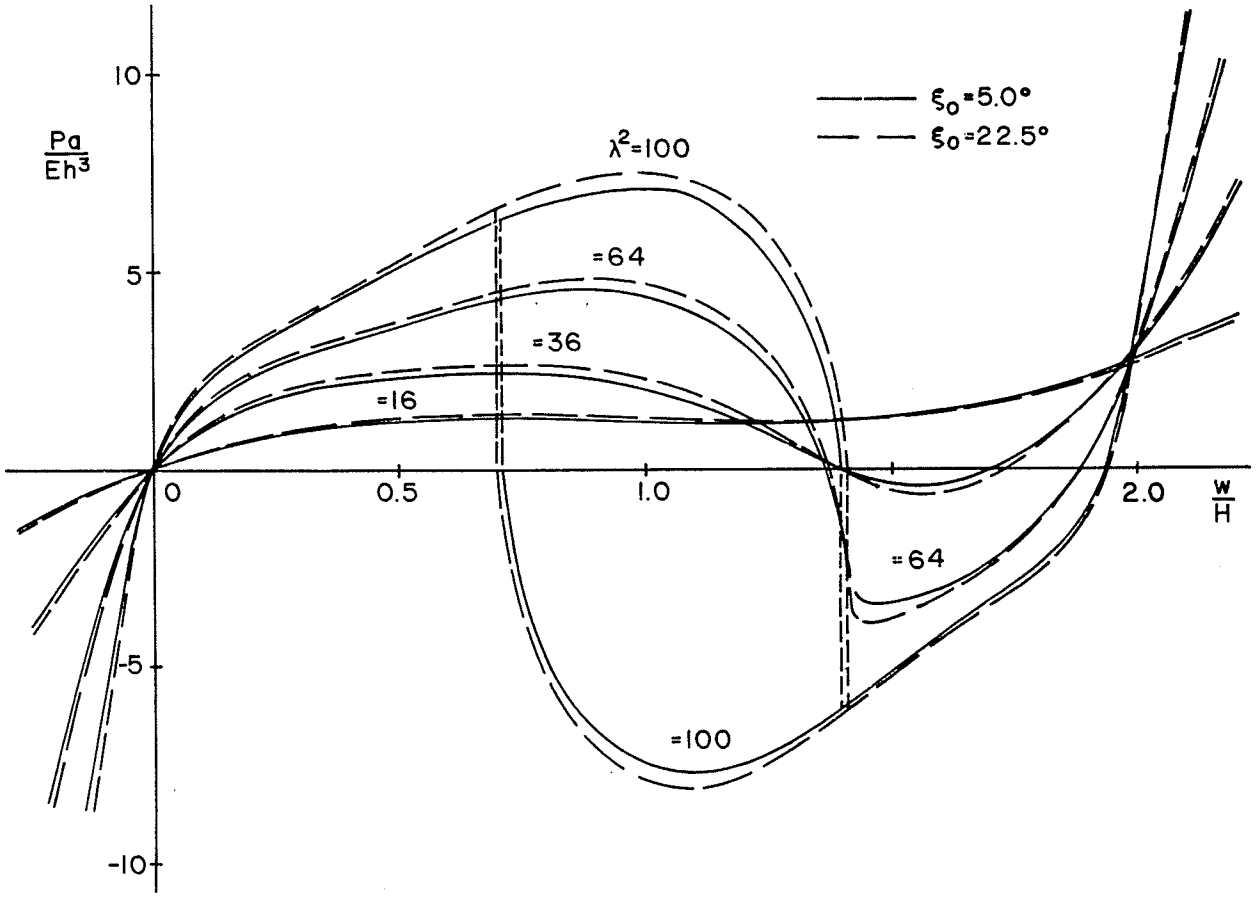

Figure 5.6 Load-Deflection Curves for Shallow Shells

Figure 5.7 shows load-deflection curves calculated by the author, Biezeno

[9] Mescall [47] and Parisch [60], and obtained experimentally by Evan-Iwanowski [18]. It appears that sufficient attention has not previously been paid to the mechanism of snapping, and the unique paths associated with eversion and return. While Mescall identifies a number of axisymmetric configurations for a given displacement, only those configurations corresponding to increasing loading from the rest position to the point of snapping, and part of the return path, appears to occur naturally.

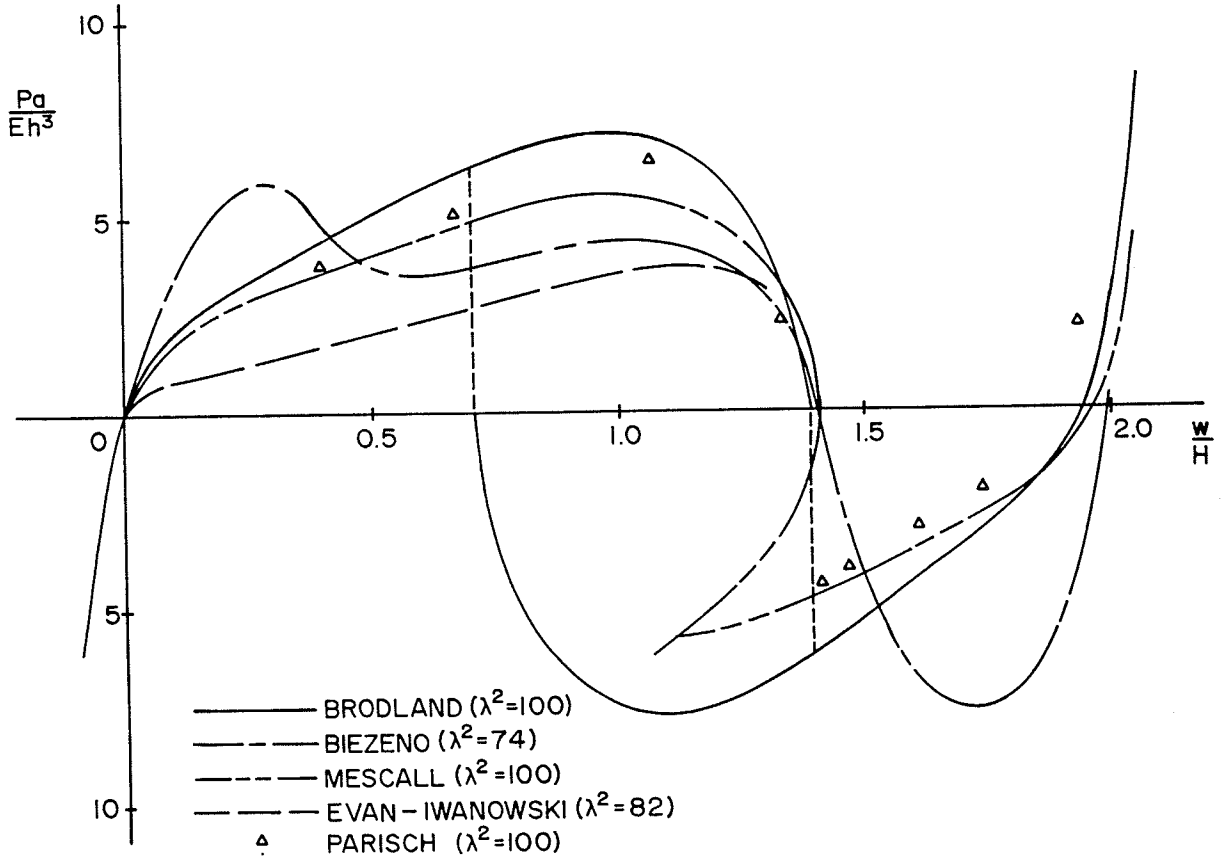

Figure 5.7 Comparative Load-Deflection Curves

For many practical applications, it is the critical load which is of primary interest. Figure 5.8 shows the critical load P_{cr} as a function of λ. Curves calculated by Biezeno [9], Chien [13], Ashwell [5], Archer [4] and Mescall [47] are also shown, as are the experimental values obtained by Ashwell [5] and Evan-Iwanowski [18]. The critical load calculated here is in good agreement with curves calculated by other researchers. Furthermore, the curve calculated here predicts slightly higher values of P_{cr} than have been obtained experimentally. Theoretical values of P_{cr} must necessarily be higher than those obtained

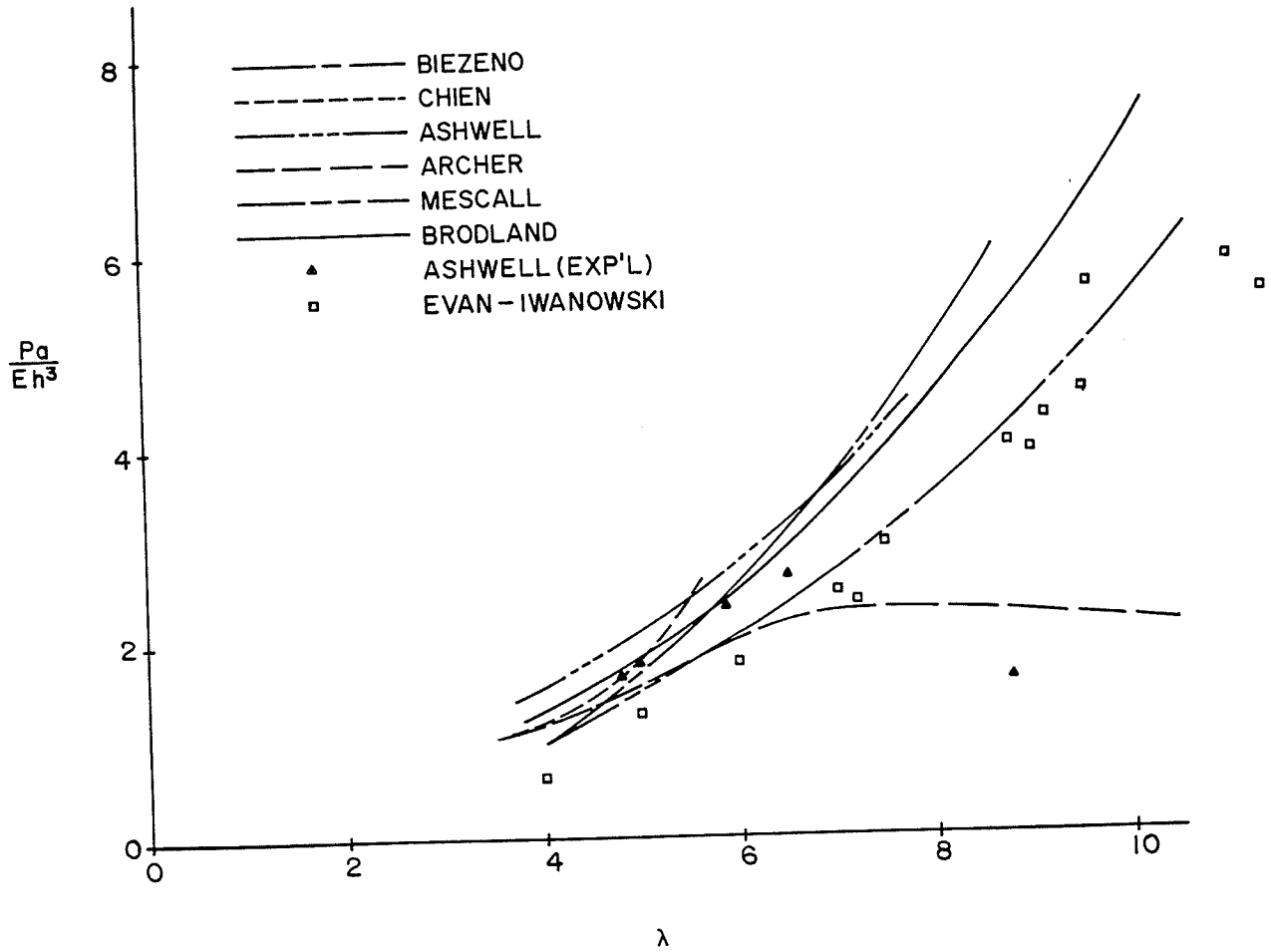

Figure 5.8 Critical Loads

experimentally, as even the small imperfections which are always present in specimens cause the shell to collapse at a lower load. Only the curve calculated here, and Ashwell's curve, predict P_{cr} values higher than any of the experimental values. The research of Ranjan and Steele [61] indicates that Ashwell's model is slightly too stiff and consequently predicts values for P_{cr} which are somewhat high.

The load deflection curves associated with hemispheres are shown in Figure 5.9. They are very similar in shape to those of shallow shells, except that the knee in the curve at the critical load is somewhat higher and much sharper. Snapping occurs in hemispheres for λ^2 values as low as 36, but does not occur in shallow shells unless $\lambda^2 > 64$. The deflection at which hemispheres snap through depends on the value of λ^2 and again, snapping occurs sooner on the return path.

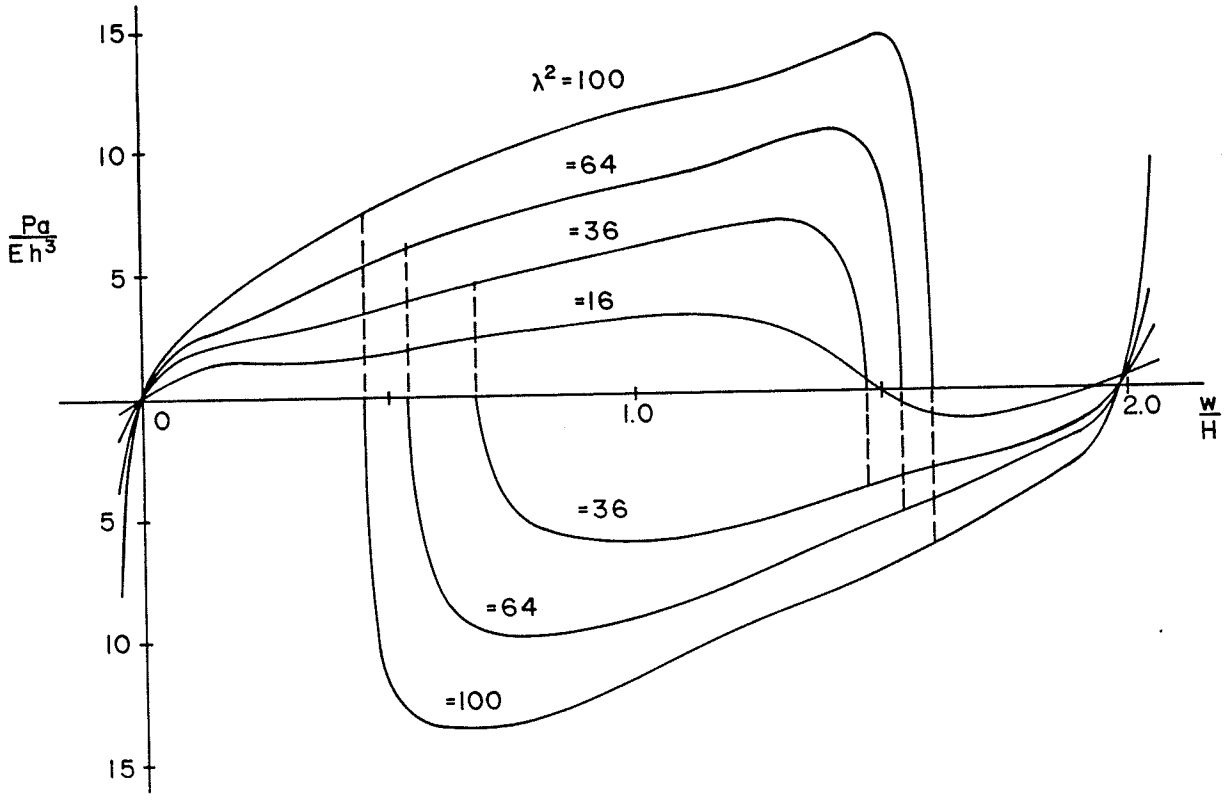

Figure 5.9 Load-Deflection Curves for a Hemisphere

The meridian contours of a hemisphere with $\lambda^2 = 36$ are shown in Figure 5.10. The general behavior is similar to that of shallow caps, although the radial displacements are more pronounced. Of particular interest are the significant radial edge displacements.

A number of spherical caps were cut from hollow rubber balls early in the research. These models provided considerable insight into the behavior of spherical caps. Since the load-deflection curves and snapping behavior obtained herein is significantly different from that published in the literature, it was decided to perform a supplementary experimental investigation.

The primary difficulty in modelling the caps is to support the edges against reversing axial loads while ensuring that radial forces and meridan moments are not present at this edge. This difficulty can be overcome by mounting the edges of the cap on cantilevered wires with bushings to prevent moment transfer. See Figure 5.11. A reversible load is applied through a radially restrained plunger, attached to the apex of the shell with a small screw. Since facilities were not available to the author to fabricate rubber specimens, a nearly hemispherical piece of rubber ball with $\lambda^2 = 95$ was used. The specimen had visible imperfections. Since the elastic properties of the rubber were not measured, the resulting load-deflection curves shown in Figure 5.12 are only qualitative. The deflection to snapping is symmetrical, but the configurations passed through during snapping are not. The specimen does not assume a symmetrical configuration immediately after snapping. It is not clear whether this is an inherent property of the geometry, a result of imperfections, or a result of material hysteresis. Clearly, however, the experimental curves exhibit the essential features predicted by the numerical scheme.

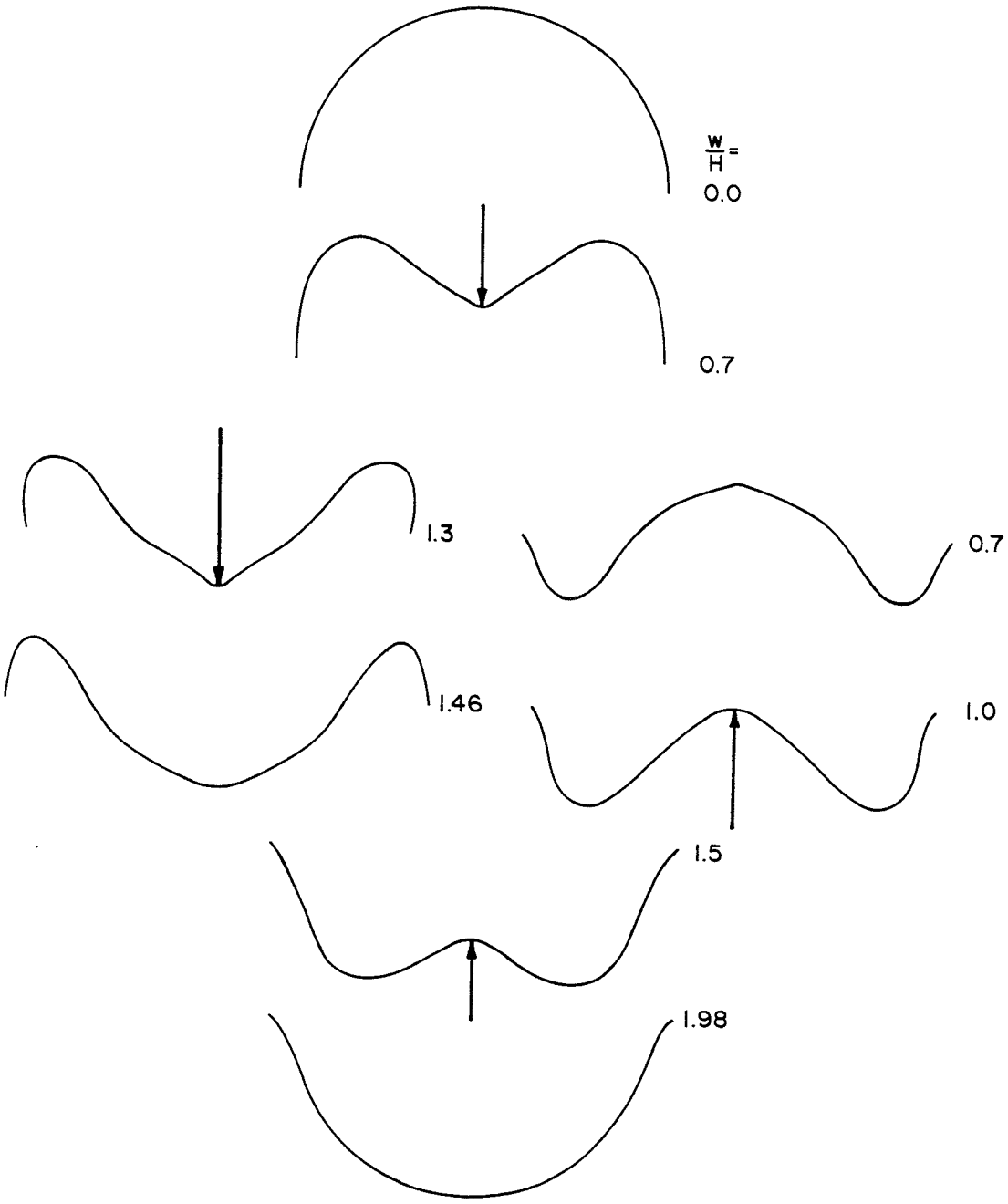

Figure 5.10 Meridian Contours for a Hemisphere

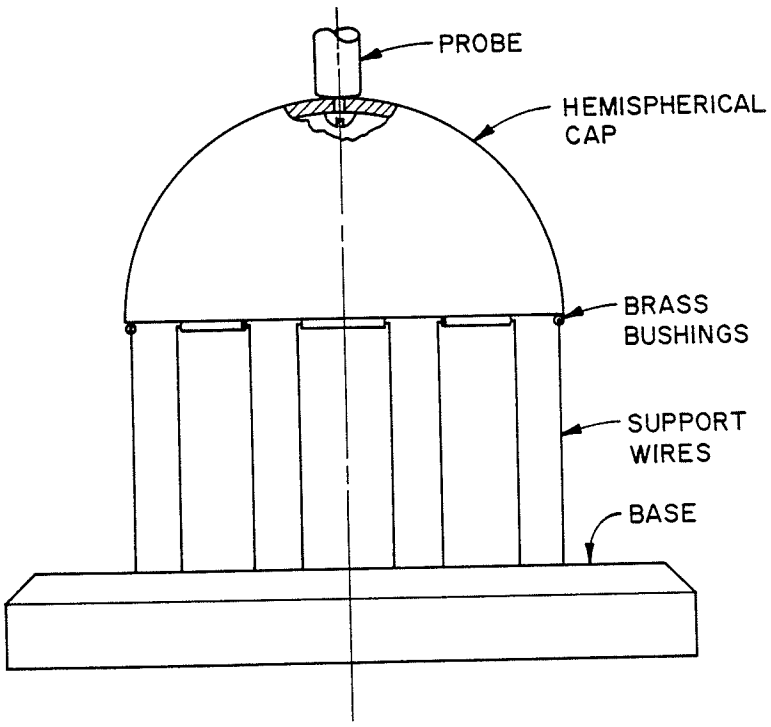

Figure 5.11 Experimental Apparatus

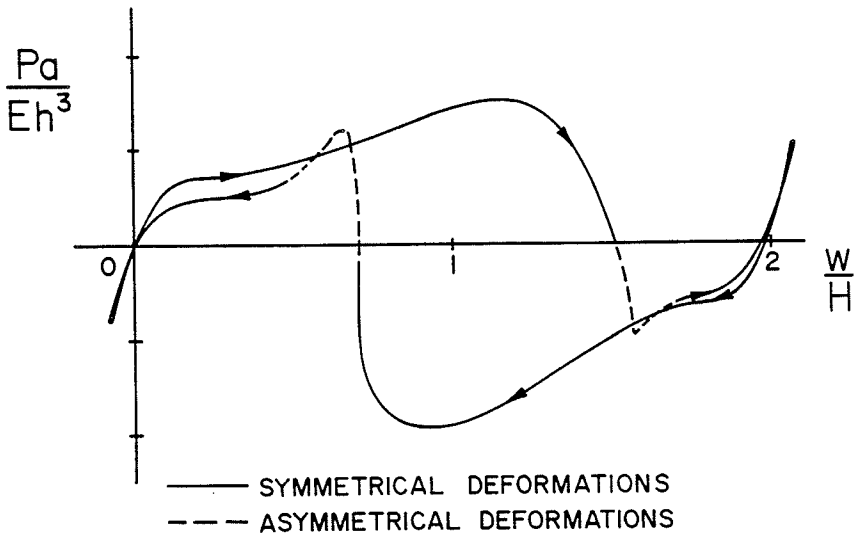

Figure 5.12 Experimental Load-Deflection Curve for $\lambda^2 = 95$

CHAPTER 6

EDGE LOADED CIRCULAR CYLINDER

6.1 INTRODUCTION

This chapter considers the behavior of a right circular cylinder clamped at one end and loaded with either an edge moment or a radial force distributed uniformly along the circumference of the other. Loads which do not include axial forces are used so that radial displacements are due to direct load effects and are not due in part to radial displacements induced through Poisson's ratio and axial strains caused by the axial components of the applied load. Compressive axial loads are particularly avoided as they give rise to asymmetric stability problems. A clamped end restraint is used so that short cylinders behave like cantilever elasticae. (See subsequent discussion, especially Section 6.3).

Analytical solutions exist [11,71,79] for the infinitesimal linear displacements and resulting stresses in cylinders subjected to arbitrary radial, axial and torque loads. While a few nonlinear cylinder solutions [16] do exist for particular load cases, the author is not aware of any nonlinear solutions to the problems of interest here. Even when such nonlinear solutions are known, they usually have a rather restricted range of applicability and may entirely miss the effect of certain parameters. This is seen for example in Chapter 4 where the nonlinear plate solutions apply only to deflections of the order of the plate thickness, and where the ratio of plate radius to plate thickness does not appear in any of the analytical solutions, despite the numerical solutions showing its considerable effect. We are interested in observing as many cylinder phenomena as possible, including those which are associated with highly nonlinear behavior.

Consider the cylinder shown in Figure 6.1. Its diameter is a, its length ℓ

and its wall thickness h. All cylinders exhibit one of three well known distinct types of response to load, depending on their relative proportions. These characteristic responses are associated with the three geometries represented in Figure 6.2.

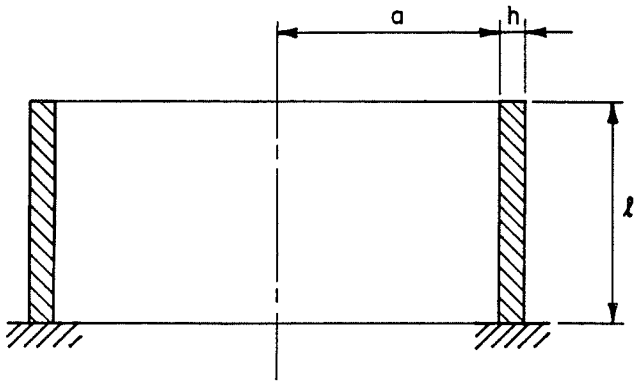

Figure 6.1 The Cylinder

We call a cylinder "short" when its proportions are such that the effects of hoop stress are negligible. In these cylinders, the meridian behaves like a wall; or with suitable adjustments for plane stress like a beam. Since a clamped end condition has been specified here, short cylinders will behave like cantilever walls. Short cylinders or shells which are not so severely restrained tend to deform so that their meridian shape remains unchanged [71, pp. 132,133]. When the length ℓ of a cylinder is sufficiently small or its wall thickness h is sufficiently large, the length over which hoop stresses can act is so small that their effect is obscured by meridian bending effects. Alternatively, it is possible to think of a cylinder as being made "short" by making its radius a large. Then, hoop effects become

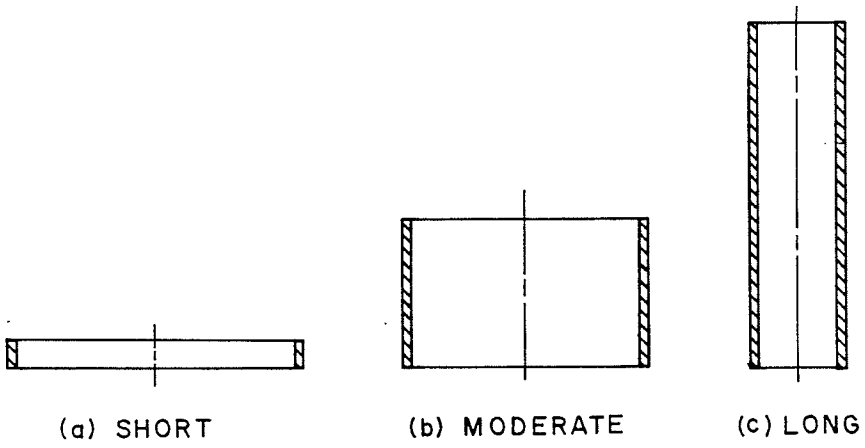

Figure 6.2 Cylinder Proportions

insignificant as the radius of curvature, given approximately by 1/a, becomes so large that any small segment appears as an insignificantly curved cantilever wall. From a different perspective, one may argue that the hoop stresses, being given approximately by δ /a, where δ is the radial displacement, become negligible for large a . Again, cantilever wall behavior is predicted.

A cylinder whose behavior is governed by the boundary conditions at both of its ends like a short cylinder, but whose behavior is also affected by hoop effects, is called intermediate. A so-called long cylinder is one in which transverse deflections are essentially confined to a region at the loaded end of the cylinder. Under this condition, it can be shown that the deformation at the loaded edge does not depend on the actual cylinder length, or on its actual boundary conditions. Such cylinders are for purposes of mathematical convenience, frequently modelled as being of semi-infinite length.

Dimensional analysis of the problem will be postponed to the next section since the most suitable dimensionless parameters cannot be easily determined without reference to the analytical solutions contained therein.

6.2 ANALYTICAL SOLUTIONS

The behavior of an axisymmetrically loaded cylinder is governed by the field equations given in Section 2.5, subject to the special conditions $K_1 \equiv 0$, $K_2 \equiv 1/a$. A governing fourth order differential equation can be derived [71, Section 4.1] from the field equations using the assumptions of both material and geometric linearity. For cases where no axial or pressure loads are present it takes the form,

$$\frac{d^4w}{dz^4} + 4\lambda^4 w = 0 \tag{6.1}$$

where

$$\lambda = \left[\frac{3(1-\nu^2)}{a^2h^2} \right]^{1/4} \tag{6.2}$$

A beam on a Winkler foundation [71, p. 121] is governed by the same equations. The general solution to this fourth order differential equation is

$$w = C_1 e^{-\lambda \ell} \sin(\lambda \ell) + C_2 e^{-\lambda \ell} \cos(\lambda \ell) + C_3 e^{\lambda \ell} \sin(\lambda \ell) + C_4 e^{\lambda \ell} \cos(\lambda \ell) \tag{6.3}$$

where constants C_i are found from the boundary conditions. See Calladine [11, Section 3.8] for a direct method to find the constants C_i. For the problems of interest here, the boundary conditions are:

$w(\ell) = w'(\ell) = 0$ at the clamped end, together with

$w''(0) = 0$, $w'''(0) = \frac{Q}{D}$ at applied shear Q, or

$W''(0) = \frac{M}{D}$, $w'''(0) = 0$ at applied moment M

where $D=\frac{Eh^3}{12(1-\nu^2)}$

and the resulting end deflections can be written respectively as

and $$\frac{wD\lambda^3}{Q} = f(\lambda\ell)$$

$$\frac{wD\lambda^2}{M} = g(\lambda\ell) \tag{6.4}$$

See for example, Hetenyi [31, p. 64] for the function $f(\lambda\ell)$. It has been found [31, p. 46; 71, Section 4.2(d)] from the linear solutions to Equation (6.1), that the product $\lambda\ell$ is an effective indicator of whether a cylinder is short, intermediate, or long. Delineating values of $\lambda\ell$ are discussed in Section 6.3.

When the cylinder is short, for example, $\lambda\ell$ is small and Equation (6.1) when written as

$$\frac{d^4w}{ds^4} + 4(\lambda\ell)^4 w = 0 \tag{6.5}$$

where $s = z/\ell$ clearly simplifies to the beam equation

$$\frac{d^4w}{dz^4} = 0 \quad \text{and} \quad \frac{d^4w}{ds^4} = 0 \tag{6.6}$$

Resulting end deflections for applied shear Q or moment M are according to linear beam theory,

$$w = \frac{Q\ell^3}{3D}$$

and

$$w = \frac{M\ell^2}{2D} \tag{6.7}$$

or

$$\frac{wD}{Q\ell^3} = \frac{1}{3}$$

and (6.8)

$$\frac{wD}{M\ell^2} = \frac{1}{2}$$

respectively.

When deflections are large, it is necessary to use equations describing the nonlinear deflection of a beam or so-called elastica. Fortunately, such solutions [22, Section 2.2] are known. End deflections predicted by these solutions take the form

$$\frac{wD}{Q\ell^3} = f\left(\frac{Q\ell^3}{D}\right)$$

$$\frac{wD}{M\ell^3} = g\left(\frac{M\ell}{D}\right) \tag{6.9}$$

for radial edge load Q and moment M respectively.

From dimensional analysis [75], we expect the deflection w/ℓ to be governed by two geometric ratios a/h and ℓ/h, and by a deformation parameter given as a ratio of applied load to material stiffness. In consideration of the analytical linear and elastica solutions, a/h and $\lambda\ell$ are suitable geometric parameters, ν is a suitable material parameter and a suitable choice of load and deflection parameters for applied radial loads Q and applied moments M are respectively $Q\ell^2/D$, $D/Q\ell^3$ and $M\ell/D$, $wD/M\ell^2$. It may seem surprising that the deflections do not take the form w/ℓ. However, the radial load and moment induced deflections can be written in terms of w/ℓ by using their corresponding load parameters, i.e.

$$\frac{wD}{Q\ell^3} = \left(\frac{Q\ell}{D}\right)^{-1} \frac{w}{\ell}$$

$$\frac{wD}{M\ell} = \left(\frac{M\ell}{D}\right) \frac{w}{\ell} \tag{6.10}$$

Hence, we have the implicit load-deflection relationships:

$$0 = \phi_Q\left(\frac{a}{h}, \lambda\ell, \nu, \frac{Q\ell^2}{D}, \frac{wD}{Q\ell^3}\right)$$

$$0 = \phi_M\left(\frac{a}{h}, \lambda\ell, \nu, \frac{M}{D}, \frac{wD}{M\ell^2}\right) \qquad (6.11)$$

for applied radial load Q and moment M, respectively. Note that the various analytical solutions can be easily expressed in terms of these parameters. Since the analytical solutions are all independent of the parameter a/h, the possible influence of this ratio must be determined numerically.

6.3 NUMERICAL SOLUTIONS AND DISCUSSION

In order to provide a comprehensive treatment of the cylinder problem, it is desirable to consider the deflection of cylinders for which the two geometric parameters a/h and $\lambda\ell$ and the appropriate load parameter $Q\ell^2/D$ or $M\ell/D$ are given a wide range of values. To this end, cylinders of constant length, thickness and applied load per unit of circumerential length, but varying radius are considered. This approach allows certain economies of solution, not the least of which are that the meridial dimensions of the numerical elements remain the same, and that the solution of one cylinder meridian can therefore be used as a starting configuration for the next if the radii of interest are considered in numerical order. Most runs were done using nine elements with $\ell = 4$ and $h = 0.1$, although values of ℓ from 2.6 to 12.6 and h values as small as 0.01 were also used. In all cases, the radius a took values ranging over five magnitudes from 1 to 100,000.

The non-dimensional radial deflection $wD/Q\ell^3$ of a cylinder subjected to a uniform radial load Q per unit of circumferential length is shown in Figure 6.3. There are several ways of interpreting this figure. The most natural way is to consider the cylinder length and thickness to remain constant. Curves of constant load $Q\ell^2/D$ then correspond to constant force Q per unit of circumferential length, and the ordinate $\lambda\ell$ varies inversely as the root of the

radius a . The load parameter $Q\ell^2/D$ corresponds numerically to the rotation of the free end of a cantilever, or short cylinder, as calculated from linear beam theory.

For sufficiently small loads, the deflection is described accurately by the linear differential Equation (6.1). The deformation predicted by this equation is shown in Figure 6.3 and is indistinguishable from the author's numerical solutions for various loads and geometric configurations with $Q\ell^2/D \leq 0.3$. Three distinct types of behavior are evident. For $\lambda\ell$ less than about 0.5, short cylinder behavior is exhibited. The deflection $wD/Q\ell^3$ is independent of $\lambda\ell$ as the radial restraint provided by hoop stresses is insignificant and the cylinder meridian responds like a cantilever wall. Its end deflection agrees within 1/2% with the non-dimensional deflection of 1/3 predicted by beam theory. For $0.5 < \lambda\ell < 1.5$, intermediate cylinder behavior is exhibited, in which the deflection is reduced with increasing $\lambda\ell$ as hoop effects become increasingly important. The mechanism of load carrying changes for intermediate length cylinders from effects associated with the clamped end at $\lambda\ell \simeq 0.5$ to hoop effects at $\lambda\ell \simeq 1.5$. For $\lambda\ell$ greater than about 1.5, long cylinder behavior is evident in that the radial end deflection is independent of the cylinder length. The deflection curve appears as a straight line of slope -3, and corresponds to a deflection of constant

$$\frac{wD\lambda^3}{Q} = \frac{wD}{Q\ell^3} \cdot (\lambda\ell)^3 \qquad (6.12)$$

This behavior occurs because the load is supported entirely by hoop and local bending effects, which are essentially damped out within a portion of cylinder of length $1.5/\lambda$.

Figure 6.3 also shows the deflections which occur from application of loads sufficient to cause geometrically nonlinear behavior. Loads corresponding to load $Q\ell^2/D$ values of 1.69, 8.68, 30.0, 100. and 300. are shown. The first two loads

correspond to elasticae whose end rotations are 40° and 80°. The other three are arbitrary high loads.

Since short cylinders are more flexible than long ones, nonlinear behavior first becomes evident at small $\lambda\ell$ values. For moderate loads, such as $Q\ell^2/D$ = 1.69, shown in Figure 6.3, nonlinear behavior begins nearly concurrently with intermediate length behavior, as shown by deviation of the deflection from the analytical solution. For small $\lambda\ell$, the deflection agrees within $\frac{1}{2}$% with the elastica deflections calculated using the methods of Frish-Fay [22] and Wang [86], and shown on the figure. For $\lambda\ell \geq 1.7$ the cylinder is sufficiently long that hoop effects reduce the deflection to within the applicable range of linear equations. For any finite value of $Q\ell^2/D$, the deflection will always become small enough that it will agree with the linear solution as the product $\lambda\ell$ is made sufficiently large (radius a made sufficiently small).

It is possible for cylinders to exhibit long cylinder behavior before they become sufficiently stiff to make deflections linear. For example, the dashed line in Figure 6.3 passes through a series of heavily loaded cylinders with $Q\ell^2/D$ = 30,100 and 300, which may be thought of as differing only in length. In absolute or dimensional terms their end deflections are identical as are their meridian contours near the loaded ends. This contour is shown in Figure 6.4 and corresponds to $\lambda\ell$ = 2.8 for $Q\ell^2/D$ = 30. The radial deflection, however, is only 70 percent of that predicted by linear theory, indicating the influence of the nonlinear effects. The deflection of these heavily loaded cylinders agrees well with their corresponding elastica solutions for small $\lambda\ell$ and agrees with the linear solution for large $\lambda\ell$.

Figure 6.4 shows the approximate load - $(\lambda\ell)$ domains within which short, intermediate and long cylinder behavior occur under radial loading, and also shows the domain of linear and nonlinear radial deflection. This figure shows that for loads of $Q\ell^2/D \leq 0.3$, short, intermediate and long cylinder behavior are all linear.

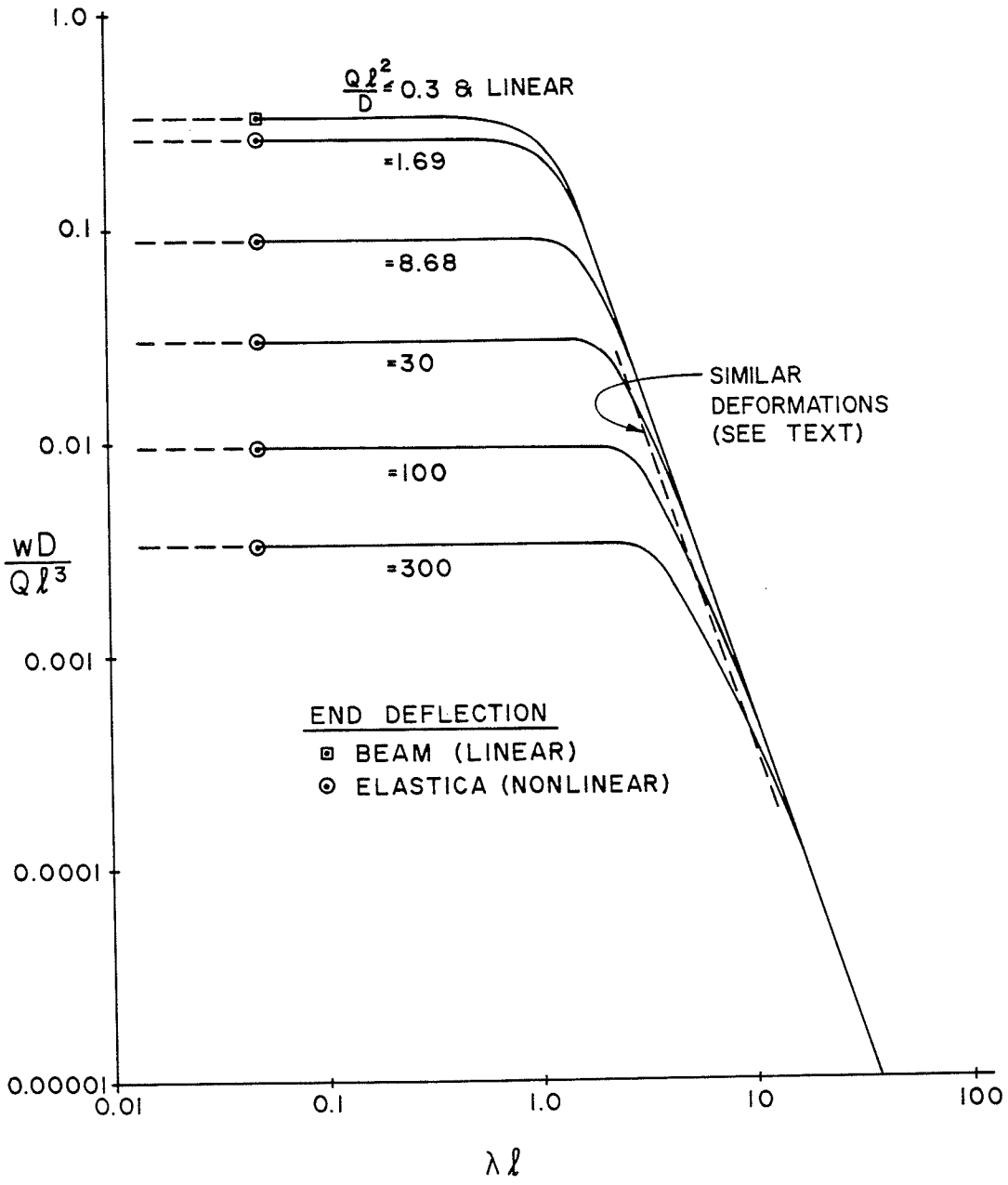

Figure 6.3 Radial Edge Deflection Due to Radial Load

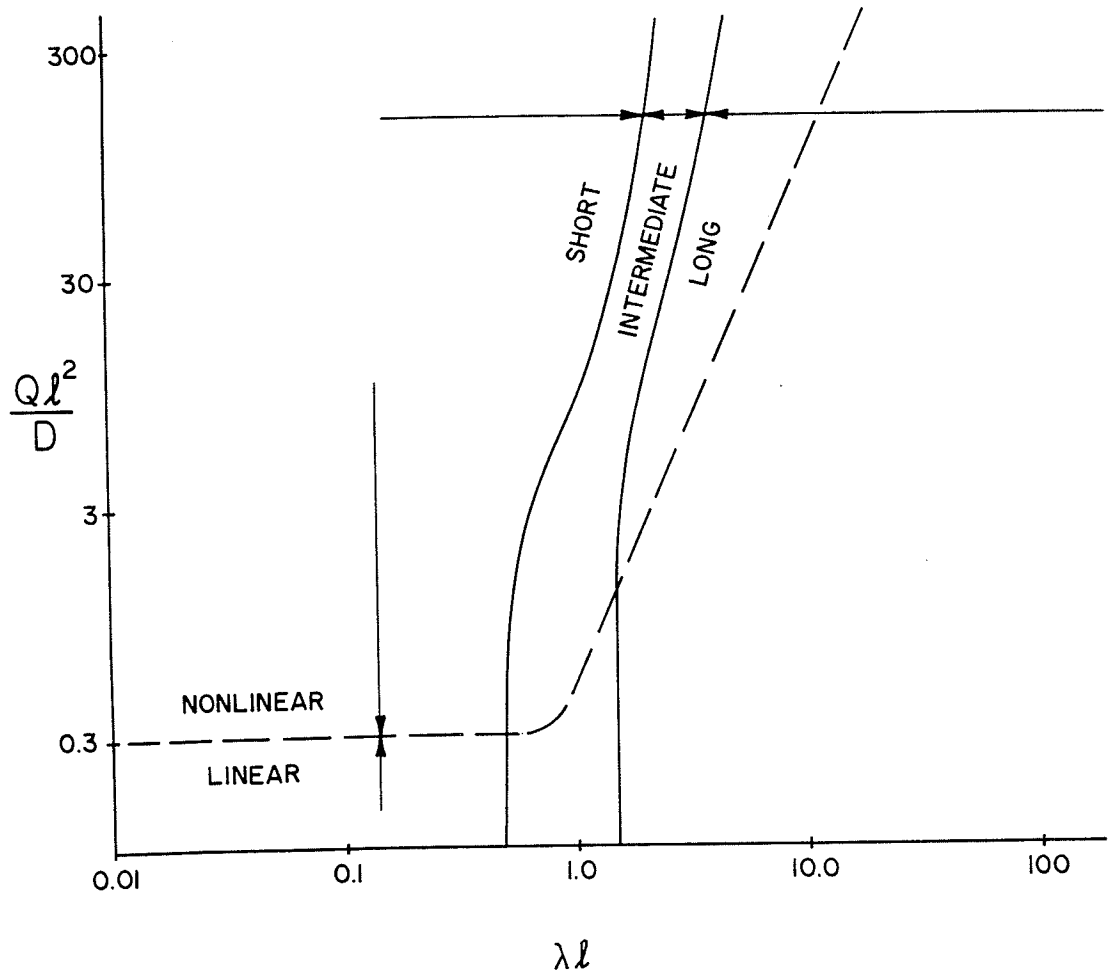

Figure 6.4 Behavior Domains (Radial Load)

For $0.3 < Q\ell^2/D < 1.3$, short behavior is nonlinear, intermediate behavior may be nonlinear or linear, and long behavior is linear. Finally, for $Q\ell^2/D > 1.3$, nonlinear short, intermediate and long behavior are followed by linear long behavior with increasing $\lambda\ell$. The upper bound of $\lambda\ell \simeq 0.5$ on short behavior for $Q\ell^2/D < 0.3$ is the same as the bound given by Seide [71, Section 4.2(d)] and is similar to the value $\pi/4$ given by Hetenyi [31, p. 46] for the mathematically equivalent problem of a beam on an elastic foundation. Their lower bounds of 3 and π respectively are much more stringent than the bound of $\lambda\ell \simeq 1.5$ indicated in Figure 6.4.

Figure 6.5 shows meridial contours for a cylinder loaded radially such that its load parameter $Q\ell^2/D$ is 30. For $\lambda\ell = 2.8$, long cylinder behavior is evident in that significant meridial deformations are limited to a region which does not extend to the fixed end. When $\lambda\ell > 7$, deformations are small enough to be modelled accurately by linear theory, as shown by comparison with the contour predicted by linear theory. When deformations are large, such as for $\lambda\ell = 4.9$, nonlinear effects become important. Intermediate cylinder behavior is evident for $\lambda\ell = 2.2$ since the deflection contour is significant close to the fixed end, but is dependent on the value of $\lambda\ell$. For $\lambda\ell < 0.5$ short cylinder behavior or elastica behavior is evident as the deflection is independent of $\lambda\ell$. The cylinder contour is nearly indistinguishable from the elastica contour calculated by the method of Wang [86]. Loads are not sufficient to cause discernable extension. For loads in excess of $Q\ell^2/D = 30$ the meridial curvature at the base of the elastica slightly exceeds the limits of thin shell theory.

Figure 6.6 shows the radial deflection of a cylinder loaded with a couple uniformly distributed along its free edge. Radial end deflection is plotted rather than end rotation, since the former is not monotonic for large loads and the latter is predicted correctly by beam theory for large rotations, even though its derivation is such that in general it should not. For loads small enough that $M\ell/D < 0.3$

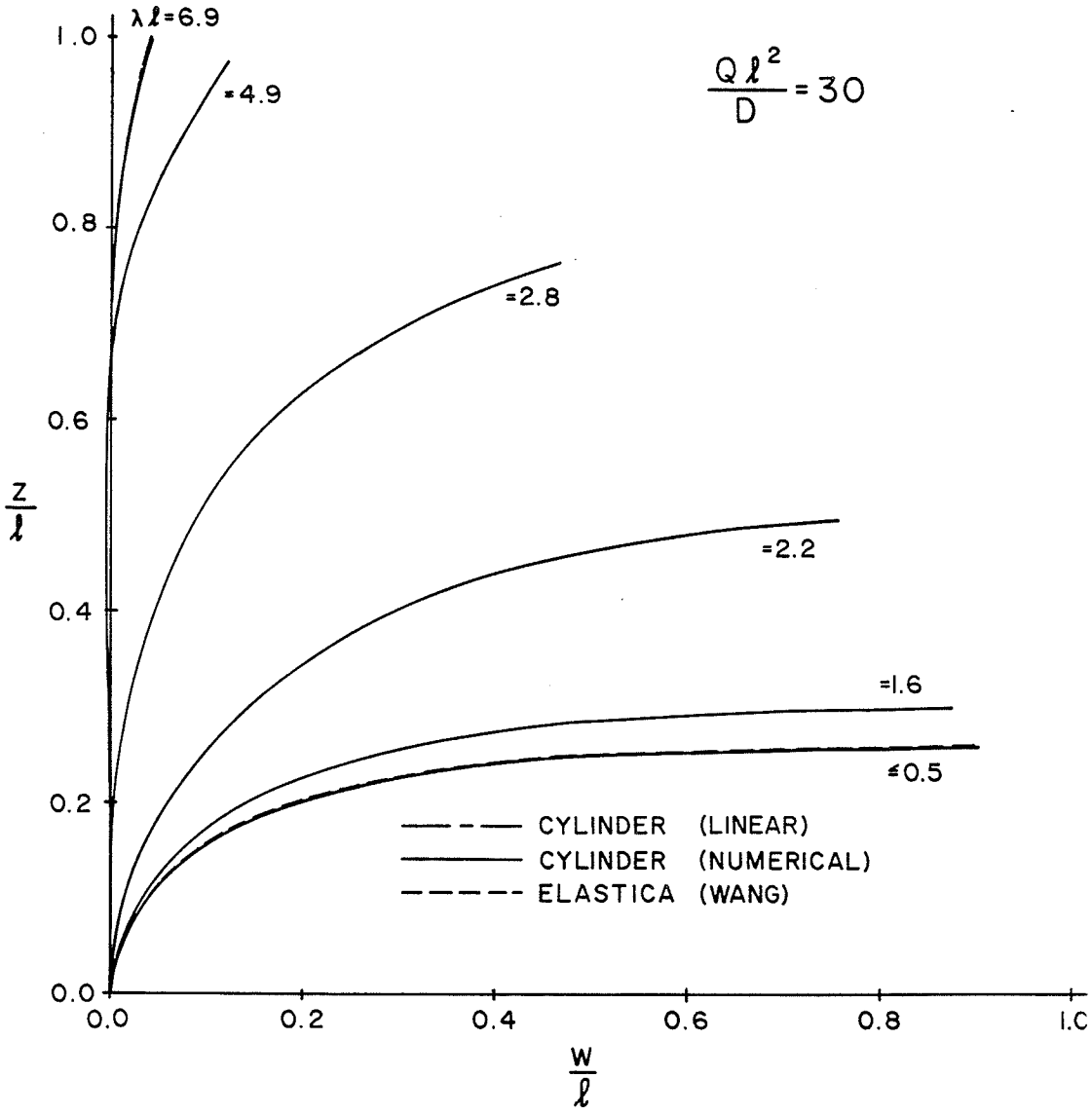

Figure 6.5 Meridian Contours (Radial Load)

deflections are accurately described by linear theory. The radial deflections calculated from linear theory are indistinguishable from those calculated numerically with $M\ell/D \leq 0.3$. Long, intermediate, and short cylinder behavior is evident from the graph.

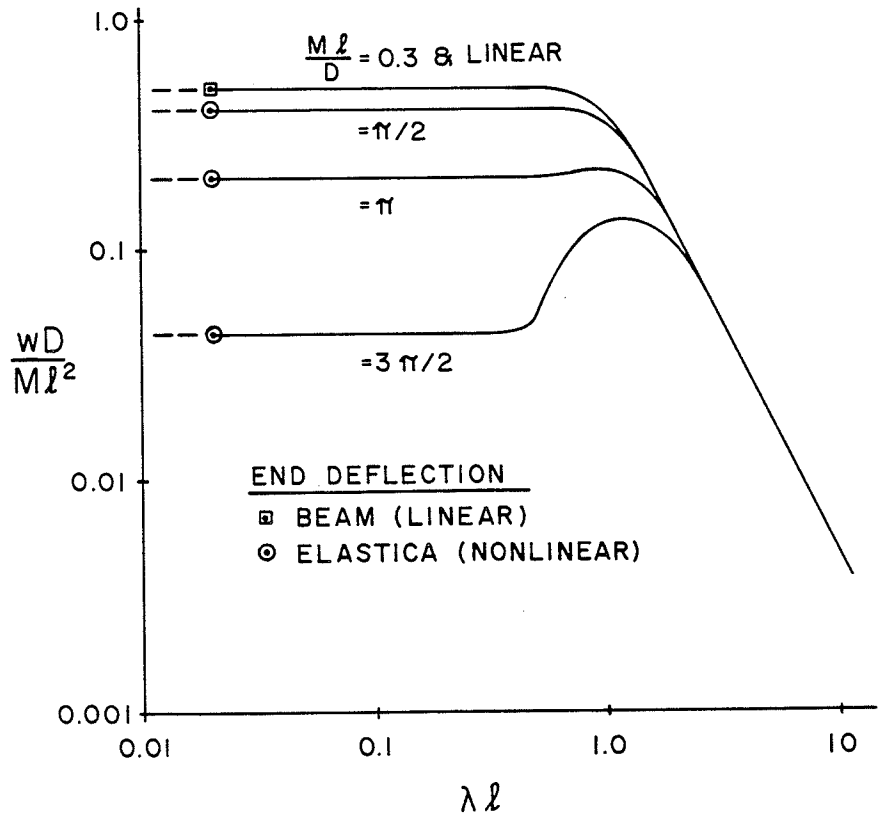

Figure 6.6 Radial Edge Deflection Due to Edge Moment

For larger values of the deflection parameter $M\ell/D$, nonlinear behavior is apparent. The deflection parameter corresponds numerically to the rotation of the free end of an elastica. See Equations (1.2) and (1.3) and their associated discussion in Section 1.1. Hence short cylinders with $M\ell/D$ equal to $\pi/2$, π and $3\pi/2$ deform respectively to a quarter circle, semi-circle and 3/4 of a circle. The deflection of the most heavily loaded cylinders is not monotonic with respect to $\lambda\ell$, since the radial component of the deflection decreases as the meridian wraps around, (see also Figure 6.6). For small $\lambda\ell$ the dimensionless deflections agree with the beam and elastica solutions shown within 0.16% of the undeformed length ℓ and for large $\lambda\ell$ they are indistinguishable from the linear solutions.

Figure 6.7 shows the approximate load - $(\lambda\ell)$ domains of short, intermediate and long cylinder behavior under edge moment loading, and the domain within which radial deflections are accurately described by linear theory. For loads $M\ell/D < 0.3$, the bounds on short and long behavior are the same as for a radial load.

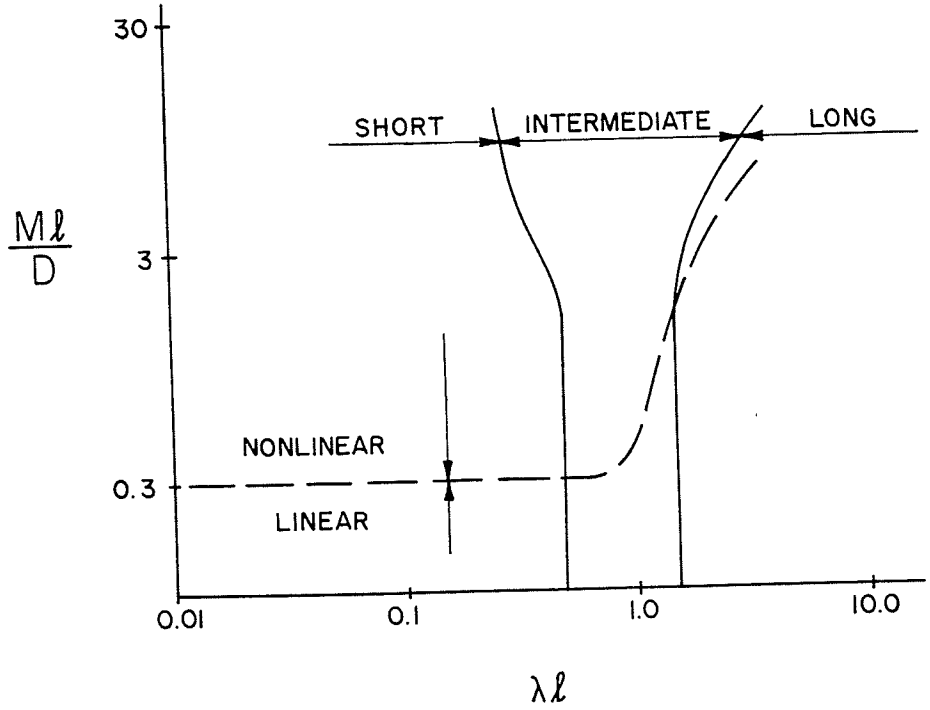

Figure 6.7 Behavior Domains (Edge Moment)

Figure 6.8 shows the meridian contour of a cylinder loaded such that $M\ell/D = 3\pi/2$. Long, intermediate and short cylinder behavior are evident. For $\lambda\ell = 4.9$ the transverse deflections of the numerical and linear solutions agree within $\frac{1}{2}\%$. The difference in meridian contours is due to the axial displacement which is not predicted by the linear solution. The short cylinder contour is nearly indistinguishable from the circular contour calculated from elastica theory. The curvature limits of thin shell theory are reached in this deformed state.

It was noted earlier, that a sequence of cylinders of increasing radius a was used to produce the graphs. The author has observed that if the radius of certain short cylinders, such as those with $\lambda\ell = 0.69$ and 0.35 in Figure 6.8 have their respective radii reduced, that new equilibrium states are produced. These new states correspond to cylinders in which the meridian bending is not sufficient to overcome the hoop stresses and push the end of the elastica outward so the meridian can straighten out. The new meridians are similar in shape to their precursors, except that their radial displacement component is reduced. These contours are not shown as it is not clear where this phenomenon would occur naturally and their inclusion would unnecessarily complicate the figure.

Linear theory is generally restricted to problems where slopes are less than 0.1. The foregoing examples have illustrated that linear theory may be able to accurately predict the radial displacement component of cylinders with rotations as large as 0.3, but it does not predict the sometimes significant axial displacement components which occur with these end rotations.

Dimensions within the bounds of thin shell theory were chosen to give the ratio a/h a wide range of values while holding all other parameters fixed. The ratio a/h had no discernable effect on either contours or radial end deflections even under nonlinear conditions.

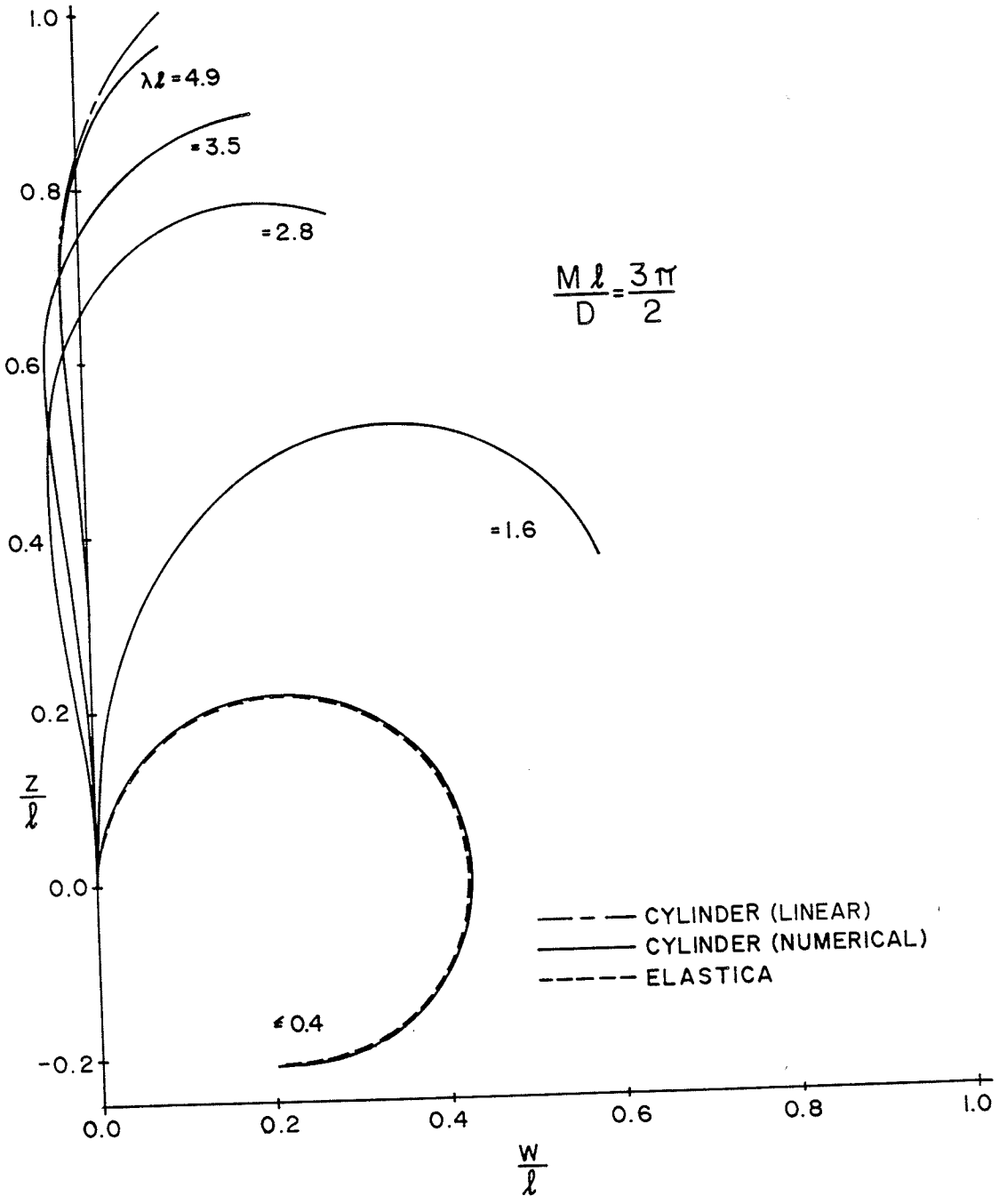

Figure 6.8 Meridian Contours (Edge Moment)

REFERENCES

1. Alexander, H., "A Constitutive Relation for Rubber-Like Materials," Int. J. Eng. Sci., Vol. 6, 1968, pp. 549-563.

2. Antman, S.S., "Existence and Nonuniqueness of Axisymmetric Equilibrium States of Nonlinearly Elastic Shells," Arch. Ration. Mech. Anal., Vol. 40, 1971, pp. 329-371.

3. Antman, S.S., "The Eversion of Thick Spherical Shells," Arch. Ration. Mech. Anal., Vol. 70, 1979, pp. 113-123.

4. Archer, R.R., "On the Numerical Solution of the Nonlinear Equations for Shells of Revolution," J. Math. Phys., Vol. 41, 1962, pp. 165-178.

5. Ashwell, D.G., "On the Large Deflection of a Spherical Shell with an Inward Point Load," Proc. IUTAM Symp. Theory of Thin Elastic Shells, Delft, The Netherlands, 1959, pp. 43-63.

6. Ashwell, D.G., "Nonlinear Problems," Handbook of Engineering Mechanics, ed. W.Flugge, McGraw-Hill, N.Y., 1962.

7. Berger,H.M., "A New Approach to an Analysis of Large Deflection of Plates," J. Appl. Mech., Vol. 22, 1955, pp. 465-472.

8. Bernadou, M. and J.M. Boisserie, The Finite Element Method in Thin Shell Theory: Applications to Arch Dam Simulations, Birkhauser, Boston, 1982.

9. Biezeno, C.B., "Uber die Bestimmung der "Durchschlagkraft" einer schwachgekrummten, kreisformigen Platte," Z. Angew. Math. Mech., Vol. 15, 1935, pp. 10-22.

10. Bushnell, D., "Bifurcation Phenomena in Sperhical Shells Under Concentrated and Ring Loads," AIAA J., Vol. 5, No. 11, Nov. 1967, pp. 2034-2040.

11. Calladine, C.R., Theory of Shell Structures, Cambridge University Press, Cambridge, 1983.

12. Chein, W.Z.,"The Intrinsic Theory of Thin Shells and Plates," Q. Appl. Math., Vol. 1944, pp. 297-327; Vol. 2, 1944, pp. 43-59; Vol. 2, 1944, pp. 120-135.

13. Chein, W.Z. and H.C. Hu, "On the Snapping of a Thin Spherical Cap," 9th. Int. Congr. Appl. Mech., Vol. 6, University of Brussels, 1957.

14. Cosserat, E., and F. Cosserat, Theorie des Corps Deformables, Herman, Paris, 1909.

15. de Veubeke, B.F., "A New Variational Principle for Finite Elastic Displacements," Int. J. Eng. Sci., Vol. 10, 1972, pp. 745-763.

16. Donnell, L.H., "Stability of Thin-walled Tubes Under Torsion," N.A.C.A. TR 479, 1934.

17. Donnell, L.H., Beams, Plates and Shells, McGraw-Hill, New York, 1976.

18. Evan-Iwanowski, R.M., H.S. Cheng and T.C. Loo, "Experimental Investigations of Deformations and Stability of Spherical Shells Subjected to Concentrated Load at the Apex," Proc. Fourth U.S. Nat. Congr. Appl. Mech., Berkeley, June 1962, pp. 563-575.

19. Federhofer, K., "Uber Die Berechnung Der Dunnen Kreisplatte Mit Grosser Ausbiegung," Der Eisenbau, Vol. 9, 1918.

20. Flugge, W., Stresses in Shells, 2nd. ed., Springer-Verlag, New York, 1973.

21. Flugge, W. and Elling, R.E., "Singular Solutions for Shallow Shells," Int. J. Solids Struct., Vol. 8, 1972, pp. 227-247.

22. Frisch-Fay, R., Flexible Bars, Butterworths, London, 1962.

23. Fung, Y.C., Foundations of Solid Mechanics, Prentice-Hall, New Jersey, 1965.

24. Geckeler, J.W., "Uber die Festigkeit achsen-symmetrischer Schalen," Forschungsarbeiten auf dem Gebiete des Ingenieurwesens, Heft 276.

25. Goldberg, M.A., "A Modified Large Deflection Theory of Plates," Proc. Fourth U.S. Nat. Congr. Appl. Mech., Berkeley, June 1962, pp. 611-618.

26. Green, A.E. and J.E. Adkins, Large Elastic Deformations, 2nd. ed., Clarendon Press, Oxford, 1970.

27. Green, A.E. and R.T. Shield, "Finite Elastic Deformations of Incompressible Isotropic Bodies," Proc. Roy. Soc. London, Vol. A202, 1950, pp. 407-419.

28. Green, A.E. and W. Zerna, Theoretical Elasticity, 2nd. ed., Clarendon Press, Oxford, 1968.

29. Gurtin, M.E., An Introduction to Continuum Mechanics, Academic Press, N.Y., 1981.

30. Hencky, H., "Uber den Spannungszustand in kreisrunden Platten mit verschwindender Biegungssteifigkeit," Zeitschrift fur Mathematik und Physik, Vol. 63, 1915, pp. 311-317.

31. Hetenyi, M., Beams on Elastic Foundation, University of Michigan Press, 1946.

32. Hughes, T.J.R. and W.K. Liu, "Nonlinear Finite Element Analysis of Shells: Part I. Three Dimensional Shells," Comput. Methods Appl. Mech. Eng., Vol. 26, 1981, pp. 331-362.

33. Hughes, T.J.R. and W.K. Liu, "Nonlinear Finite element Analysis of Shells: Part II. Two Dimensional Shells," Comput. Methods Appl. Mech. Eng., Vol. 27, 1981, pp. 167-181.

34. Irons, B.M., "The Patch Test for Engineers," Proceedings of the Finite Element Symposium Atlas Computer Laboratory, Chilton, Didcot, England, March 26-28, 1974, pp. 171-192.

35. Irons, B.M., "The Superpatch Theorem and Other Propositions Relating to the Patch Test," Proceedings of the Fifth Canadian Congress on Applied Mechanics, University of New Brunswick, May 26-30, 1975, pp. 651-652.

36. Irons, B. and S. Ahmad, Techniques of Finite Elements, John Wiley and Sons, N.Y., 1980.

37. Kaplan, A., "Buckling of Spherical Shells," Thin-Shell Structures: Theory, Experiment and Design, ed. C. Fung and E.E. Sechler, Prentice-Hall Inc., New Jersey, 1974, pp. 247-288.

38. Koiter, W.T., "On the Stability of Elastic Equilibrium," Dissertation, Delft, Holland, 1945. Also: NASA Tech. Tran., Vol. F10, 1967.

39. Koiter, W.T., "On the Principle of Stationary Complementary Energy in the Nonlinear Theory of Elasticity," SIAM J. App. Math., Vol. 25, No. 3, Nov. 1973, pp. 424-434.

40. Leigh, D.C., Nonlinear Continuum Mechanics, McGraw-Hill, New York, 1968.

41. Libai, A. and J.G. Simmonds, "Large-Strain Constitutive Laws for the Cylindrical Deformation of Shells," Int. J. Non-Linear Mech., Vol. 16, No. 2, 1981, pp. 91-103.

42. Libai, A. and J.G. Simmonds, "Highly Non-Linear Cylindrical Deformations of Rings and Shells," Int. J. Non-Linear Mech., Vol. 18, No. 3, 1983, pp. 181-197.

43. Loo, T.C. and R.M. Evan-Iwanowski, "Experiments on Stability on Spherical Caps," Proc. ASCE, Vol. EM3, June 1964, pp. 255-270.

44. Love, A.E.H., The Mathematical Theory of Elasticity, 4th ed., Cambridge University Press, 1927, p. 553.

45. Malvern, L.E., Introduction to the Mechanics of a Continuous Medium, Prentice-Hall, New Jersey, 1969.

46. Mallett, R.H. and L.A. Schmit, Jr., "Nonlinear Structural Analysis by Energy Search," Journal of the Structural Division ASCE, Vol. ST3, June 1967, pp. 221-234.

47. Mescall, J., "Large Deflections of Spherical Shells Under Concentrated Loads," J. Appl. Mech., Vol. 32, 1965, pp. 936-938.

48. Mescall, J., "Numerical Solutions of Nonlinear Equations for Shells of Revolution," AIAA J., Vol. 4, No. 11, Nov. 1966, pp. 2041-2043.

49. Mollmann, H., Introduction to the Theory of Thin Shells, John Wiley and Sons, Chichester, 1981.

50. Mooney, M., "A Theory of Large Elastic Deformation," J. Appl. Phys., Vol. 11, 1940, pp. 582-592.

51. Nadai, A., Die Elastische Platten, Springer, Berlin, 1925.

52. Naghdi, P.M. and R.P. Nordgren, "On the Nonlinear Theory of Elastic Shells Under the Kirchoff Hypothesis," Q. Appl. Math., Vol. 21, 1963, pp. 49-59.

53. Naghdi, P.M., "The Theory of Shells and Plates," Handbuch der Physik, Vol. VI a-2, Springer-Verlag, Berlin, 1972, pp. 425-640.

54. Norrie, D.H. and G. deVries, An Introduction to Finite Element Analysis, Academic Press, New York, 1978.

55. Novozhilov, V.V., Thin Shell Theory, 2nd. ed., transl. P.G. Lowe, P. Noordhoff Ltd., Groningen, 1964.

56. Oden, J.T., Finite Elements of Nonlinear Continua, McGraw-Hill, N.Y., 1972.

57. Ogden, R.W., "Large Deformation Isotropic Elasticity: On the Correlation of Theory and Experiment for Incompressible Rubber-like Solids,"Proc. R. Soc. London, Vol. A326, 1972, pp. 565-584.

58. Oliviera, E.R. de Arantes e, "Theoretical Foundations of the Finite element Method," Int. J. Solids Sturct., Vol. 4, 1968, pp. 929-952.

59. Parish, H., Large Displacements of Shells Including Material Nonlinearities," Comput. Methods Appl. Mech. Eng., Vol. 27, 1981, pp. 183-214.

60. Parisch, H., "Geometrically Nonlinear Analysis of Shells," Comput. Methods Appl. Mech. Eng., Vol. 14, 1978, pp. 159-178.

61. Ranjan, G.V. and C.R. Steele, "Large Deflection of Deep Spherical Shells Under Concentrated Load," Proceedings, 18th Structures, Structural Dynamics and Materials Conference, San Diego, March 1969.

62. Rao, S.S., Optimization: Theory and Applications, 2nd. ed., John Wiley and Sons, New York, 1984.

63. Reissner, E., "Stresses and Small Displacements of Shallow Spherical Shells, I," J. Math. Phys., Vol. 25, 1946, pp. 80-85.

64. Reissner, E., "Stresses and Small Displacements of Shallow Spherical Shells, II", J. Math. Phys., Vol. 25, 1946, pp. 279-300, also Vol. 27, 1948, p. 240.

65. Reissner, E., "On Finite Deflections of Circular Plates," Proc. Symp. in Appl. Math., Vol. 1, Aug. 2-4, 1947, pp. 213-219.

66. Reissner, E., "On Axisymmetric Deformation of Thin Shells of Revolution," Proc. Symp. in Appl. Math., Vol. 3, 1950, pp. 27-52.

67. Rektorys, K., Variational Methods in Mathematics, Science and Engineering, 2nd. ed., Reidel, Dordrecht, 1980.

68. Saada, A.S., Elasticity: Theory and Applications, Pergamon Prress, New York, 1974.

69. Sanders, J.L., "Nonlinear Theories for Thin Shells," Q. Appl. Math., Vol. 21, No. 1, 1963, pp. 21-36.

70. Sanders, J.L., "Singular Solutions to the Shallow Shell Equations," J. Appl. Mech., Vol. 37, 1970, pp. 361-364.

71. Seide, P., Small Elastic Deformations of Thin Shells, Noordhoff Publishing, The Netherlands, 1975.

72. Synge, J.L., and W.Z. Chein, "The Intrinsic Theory of Elastic Shells and Plates," Theodore Von Karman Anniversary Volume, 1941, pp. 103-120.

73. Spang, H.A., "A Review of Minimization Techniques for Nonlinear Functions," SIAM Review, Vol. 4, No. 4, 1962, pp. 343-365.

74. Strang, G., "Variational Crimes in the Finite Element Method," in The Mathematical Foundations of the Finite Element Method, ed. A.K. Aziz, Academic Press, New York, 1972, pp. 689-710.

75. Taylor, E.S., Dimensional Analysis for Engineers, Clarendon Press, Oxford, 1974.

76. Thompson, J.M.T. and G.W. Hunt, A General Theory of Elastic Stability, John Wiley and Sons, London, 1973.

77. Timoshenko, S., Vibration Problems in Engineering, D. Van Nostrand Co., N.Y., 1928, p. 317.

78. Timoshenko, S.P. and J.M. Gere, Theory of Elastic Stability, 2nd ed., McGraw-Hill, New York, 1961.

79. Timoshenko, S. and S. Woinowsky-Krieger, Theory of Plates and Shells, McGraw-Hill, New York, 1959.

80. Treloar, L.R.G., The Physics of Rubber Elasticity, 3rd. ed., Clarendon Press, Oxford, 1975.

81. Truesdell, C. and R.A. Toupin, "The Classical Field Theories," Handbuch der Physik, Vol. III, Springer-Verlag, Berlin, 1960, pp. 226-793.

82. Valanis, K.C. and R.F. Landel, "The Strain-Energy Function of a Hyperelastic Material in Terms of the Extension Ratios," J. Appl. Phys., Vol. 38, 1967, pp. 2997-3002.

83. Volterra, E. and J.H. Gaines, Advanced Strength of Materials, Prentice-Hall, Englewood Cliffs, N.J., 1971.

84. von Karman, T., "Festigkeitsprobleme im Maschinenbau," Enzyklopaedie der mathematischen Wissenschaften, Teubner-Verlag, Leipzig, Germany, Vol. 4, 1910, pp. 348-352.

85. Vyrlan, P.M. and D.I. Shil'krut, "Stability of Equilibrium Forms of Geometrically Nonlinear Spherical Shells," Mech. Solids, Vol. 13, No. 4, 1978, pp. 153-159.

86. Wang, C.Y., "Large Deflections of an Inclined Cantilever with an End Load," Int. J. Non-Linear Mech., Vol. 16, No. 2, 1981, pp. 155-164.

87. Way, S., "Bending of Circular Plates with Large Deflection," Transactions, A.S.M.E., Vol. 56, 1934, pp. 627-636.

88. Williams, J.G., Stress Analysis of Polymers, 2nd. ed., Ellis Horwood Ltd., Chichester, 1980.

89. Wilson, P. and E.E. Spier, "Numerical Analysis of Large Axisymmetric Deformations of Thin Spherical Shells," Proc. First AIAA Annual Meeting, 1964, pp. 1716-1725.

90. Zienkiewicz, O.C., The Finite Element Method, 3rd ed., McGraw-Hill, London, 1977.